

# **Unravelling the Toolbox of Mussel Underwater Adhesion**

DISSERTATION

Zur Erlangung des akademischen Grades

**Doktor der Naturwissenschaften**

(Dr. rer. nat.)

im Promotionsprogramm „Polymer Science“ der Bayreuther  
Graduiertenschule für Mathematik und Naturwissenschaften (BayNAT),  
Universität Bayreuth

vorgelegt von

**Jia Wang**

aus Jinan, V. R. *China*

Bayreuth, 2019

This doctoral thesis was prepared at the department of (*department*) at the University of Bayreuth from (09/2014) until (07/2019) and was supervised by Prof. Dr. Thomas Scheibel.

This is a full reprint of the dissertation submitted to obtain the academic degree of Doctor of Natural Sciences (Dr. rer. nat.) and approved by the Bayreuth Graduate School of Mathematical and Natural Sciences (BayNAT) of the University of Bayreuth.

Date of submission: 11/07/2019

Date of defence: 18/12/2019

Acting director: Prof. Dr. Markus Lippitz

Doctoral committee:

Prof. Dr. Thomas Scheibel	(reviewer)
Prof. Dr. Dirk Schüler	(reviewer)
Prof. Dr. Hans-Werner Schmidt	(chairman)
Prof. Dr. Birte Höcker	

# Table of Contents

Summary .....	i
Zusammenfassung .....	iii
List of symbols and abbreviations .....	v
1. Introduction - mussel underwater adhesion .....	1
1.1 Byssus structure .....	1
1.1.1 Byssus architecture .....	1
1.1.2 Molecular structure .....	4
1.2 Byssus assembly .....	5
1.2.1 pH and ionic strength .....	5
1.2.2 Coacervation .....	5
1.2.3 Redox control .....	8
1.3 Interfacial adhesion .....	9
1.3.1 Surface drying property .....	9
1.3.2 H-bonds vs coordinative bonds .....	11
1.3.3 Other interactions .....	12
1.4 Bridging cohesion .....	13
1.4.1 Metal-mediated coordination .....	13
1.4.2 Covalent cross-linking .....	15
1.4.2.1 Dopa oxidation .....	15
1.4.2.2 Fe <sup>3+</sup> -mediated Dopa oxidation .....	17
1.4.2.3 Dopaquinone reaction pathways .....	18
1.4.3 Cation- $\pi$ interactions .....	18
2. Aims .....	21
3. Synopsis .....	22
3.1 Recombinant production of mussel inspired proteins .....	22
3.2 Mussel foot protein-3b (mfp-3b) shows coacervation behavior .....	23
3.3 Mussel polyphenol oxidase-like protein (PPOL) shows antioxidant activity .....	24
4. References .....	26
5. Publication list .....	34
6. Individual contribution to joined publications .....	35
Publications .....	36
Publication I .....	36
Recombinant production of mussel byssus inspired proteins .....	36
Publication II .....	49
Coacervation of the recombinant <i>Mytilus galloprovincialis</i> foot protein-3b .....	49
Publication III .....	63
A mussel polyphenol oxidase-like protein shows thiol-mediated antioxidant activity .....	63
Acknowledgements .....	81
(Eidesstattliche) Versicherungen und Erklärungen .....	82

## Summary

Over the past decades, biomimetics of novel advanced materials have been developed by replication of natural systems. With respect to tissue adhesives, marine mussel is an ideal model due to its exceptional attachment to substrates in seawater. Mussel-inspired materials are expected to bring about improvements in adhesive technology. A prerequisite for successful biomimetics is to scrutinize the natural system and get fundamental understandings of the adhesion.

The attachment of several marine mussels is mediated by a particular holdfast system, the mussel byssus, which is composed of ~96 % (w/w) of proteins by dry weight. The byssus consists of dozens of byssal threads, which are anchored to the substratum by an adhesive plaque. Mussel foot proteins in plaques are directly contacting the substrates and are, therefore, vital for achieving strong byssus attachment. In this work, mussel foot protein 3b (mfp-3b), one of the predominant proteins in plaques from *Mytilus galloprovincialis* (*M. galloprovincialis*) has been recombinantly produced and characterized.

rmfp-3b possesses 18 positively and 2 negatively charged residues, which give rise to a soluble state at low pH (pH 3.0-4.0). In the presence of citrate, rmfp-3b showed upper critical solution temperature (UCST) mediated complex coacervation at pH 3.0. Upon decreased temperature, the rmfp-3b solution changed from transparent ( $T > T_{cp}$ , cloud point temperature) to turbid ( $T < T_{cp}$ ), and this behavior was reversible. Low temperatures probably can reduce the surrounding water shell of rmfp-3b but increase the hydrogen bonding as well as the amount of deprotonated citrate, which results in increased molecular interactions. Small amounts of multivalent anions gave rise to prominent coacervation, reminiscing that mfp-3b is probably secreted in the form of a condensed coacervate with multivalent anions, e.g. sulfate, in secretory granules. Upon elevation of pH from secretion level (pH 3.0) to seawater level (pH 8.0), mfp-3b coacervate was formed likely due to the deprotonation of acidic residues yielding increased intermolecular interactions, suggesting seawater could be a natural regulator of this process. By means of coacervation, secretion and spreading on wet substrates are beneficial due to the specific properties, such as shear-thinning behavior and low interfacial energy. Thereby, mfp-3b can adhere to wet substrates without dispersion in the surrounding seawater.

The high content of 3,4-dihydroxyphenylalanine (Dopa) in byssus indicates the existence of polyphenol oxidases for post-translational modification of Tyr residues, which is pivotal for underwater adhesion. The gene sequence of a polyphenol oxidase like protein (PPOL) was identified after screening of a foot cDNA library of *M. galloprovincialis*. Recombinant production of PPOL (rPPOL) and the short variant rP319 have been established. The catalytic activity of rPPOL and rP319 have not been identified, which might be due to the poor copper coordination of His residues at acidic pH. rPPOL (rP319) is composed of 15 (5) Cys residues, and ~13 (~3) thereof show free thiols and ~2 (~2) are disulfide bonded. rPPOL and rP319 were capable of inhibiting Dopa oxidation, whereas alkylated variants showed weaker inhibition, suggesting that PPOL is probably a free thiol-based antioxidant. rPPOL (rP319-NEM) with the most (least) thiols showed maximum (minimum) antiradical power. One molecule rPPOL can reduce ~38 DPPH radicals, indicating that other reactive groups might exist besides the ~13 free thiols devoting to the antioxidant activity. Considering the antioxidant property, PPOL probably locates at the plaque-substrate interface to protect Dopa from oxidation, like mfp-6; however, verification of the location of PPOL will need further investigations.

## Summary

---

This work provides novel insights into the molecular behavior of mfp-3b and PPOL involved in underwater adhesion of marine mussels, which enrich the mechanisms of mussel underwater adhesion and advances future development of tissue adhesives.

## Zusammenfassung

In den letzten Jahrzehnten wurden in der Biomimetik neuartige Materialien durch Identifizierung und Replikation biologischer Systeme entwickelt. Ein ideales Vorbild für Untersuchung von Gewebeklebstoffen ist die Miesmuschel. Da sie sich hervorragend auf dem Meeresgrund anhaftet, stellt sie ein interessantes Modellsystem in der Klebstofftechnologie dar. Die Voraussetzung für ein erfolgreiches biomimetisches System ist, das natürliche Adhäsionssystem zu verstehen und grundlegende Erkenntnisse darüber zu gewinnen.

Die Anhaftung von Miesmuscheln wird durch ein Haftsystem, den sogenannten Muschelbyssus, vermittelt, der bezogen auf sein Trockengewicht zu ~ 96% (w / w) aus Proteinen besteht. Der Byssus setzt sich aus Dutzenden von Byssusfäden zusammen, welche über adhäsive Plaques auf dem Meeresgrund verankert sind. Die in den adhäsiven Plaques enthaltenen Muschelfußproteine können mit vielen Substraten in direkten Kontakt treten und sind daher für eine starke Byssushaftung von entscheidender Bedeutung. In dieser Arbeit wurde das Muschelfußprotein 3b (mfp-3b), eines der vorherrschenden Proteine in adhäsiven Plaques von *Mytilus galloprovincialis* (*M. galloprovincialis*), rekombinant hergestellt und charakterisiert.

mfp-3b besitzt 18 positiv und 2 negativ geladene Reste, die bei niedrigem pH-Wert (pH 3,0-4,0) die Löslichkeit erhöhen. In Gegenwart von Citrat (pH 3,0) zeigt mfp-3b eine durch die obere kritische Lösungstemperatur (UCST) vermittelte Komplexkoazervation. Bei Senken der Temperatur ändert sich die Transmission der mfp-3b-Lösung reversibel von transparent ( $T > T_{cp}$ , Trübungspunkttemperatur) zu trüb ( $T < T_{cp}$ ). Niedrige Temperaturen können höchstwahrscheinlich die umgebende Hydrathülle von mfp-3b verkleinern, jedoch die Zahl der Wasserstoffbindungen, sowie die Menge an deprotoniertem Citrat erhöhen. Dies führt zu erhöhten molekularen Wechselwirkungen. Geringe Mengen mehrwertiger Anionen führen zu einer deutlichen Koazervation, was darauf hinweist, dass mfp-3b wahrscheinlich in Form eines kondensierten Koazervats mit mehrwertigen Anionen, z.B. Sulfat, im Sekretgranulat abgesondert wird. Bei Erhöhung des pH-Werts vom Sekretionsniveau (pH 3,0) auf das Meerwasserniveau (pH 8,0) bildet sich aufgrund der Deprotonierung von sauren Resten ein Koazervat, was auf erhöhten intermolekularen Wechselwirkungen basiert und darauf schließen lässt, dass Meerwasser ein natürlicher Regulator dieses Prozesses sein könnte. Die Koazervation, Sekretion und Ausbreitung auf feuchten Substraten ist durch die spezifischen Eigenschaften, wie z.B. Scherverdünnungsverhalten und geringe Grenzflächenenergie, vorteilhaft. Dadurch kann mfp-3b an feuchten Oberflächen haften, ohne sich im umgebenden Meerwasser zu verteilen.

Der hohe Gehalt an 3,4-Dihydroxyphenylalanin (Dopa) im Byssus weist auf die Existenz von Polyphenoloxidasen zur posttranslationalen Modifikation von Tyr-Resten hin, die entscheidend für die Unterwasseradhäsion sind. Nach Überprüfung einer cDNA-Datenbank aus Muschelfüßen der Muschel *M. galloprovincialis*, wurde die Gensequenz eines Polyphenoloxidase-ähnlichen Proteins (PPOL) identifiziert. Die rekombinante Produktion von PPOL (rPPOL) und einer verkürzten Variante rP319 wurde etabliert. Eine katalytische Aktivität von rPPOL und rP319 wurde nicht gefunden, was möglicherweise auf die schlechte Kupferkoordination von His-Resten bei saurem pH zurückzuführen ist. rPPOL (rP319) enthält 15 (5) Cys-Reste, wovon ~13 (~3) als freie Thiole und ~2 (~2) disulfidgebunden vorliegen. rPPOL und rP319 konnten die Oxidation von Dopa hemmen, während die alkylierten Varianten eine schwächere Hemmung zeigten, was darauf hindeutet, dass PPOL wahrscheinlich ein freies Antioxidans auf Thiolbasis ist. rPPOL (rP319-NEM) mit

den meisten (wenigsten) Thiolen zeigte maximale (minimale) antiradikale Wirkung. Ein rPPOL-Molekül kann ~38 DPPH-Radikale reduzieren, was darauf hindeutet, dass neben den ~13 freien Thiolen möglicherweise andere reaktive Gruppen existieren, die für die antioxidative Aktivität verantwortlich sind. In Anbetracht der antioxidativen Eigenschaften befindet sich PPOL, wie mfp-6, wahrscheinlich an der Grenzfläche zwischen adhäsive Plaque und Substrat, um Dopa vor Oxidation zu schützen. Die Überprüfung der Lokalisierung von PPOL im Muschelfuß erfordert jedoch weitere Untersuchungen.

Diese Arbeit lieferte neue Einblicke in das molekulare Verhalten von mfp-3b und PPOL bei der Unterwasseradhäsion von Miesmuscheln. Die Erkenntnis über Mechanismen der Adhäsion, von Muscheln im Wasser ist wichtig für die zukünftige Entwicklung von Gewebeklebstoffen.

## List of symbols and abbreviations

Ach	Acetylcholine
AFM	Atomic force microscopy
APR	Antiradical power (1/EC <sub>50</sub> )
cm / mm / μm/ nm	Centimeter / millimeter / micrometer / Nanometer
CM-mfp-6	Thiol-blocked mfp-6
CuA	Copper-binding site A
CuB	Copper-binding site B
Dopa	3,4-Dihydroxyphenylalanine
DPPH	2,2-Diphenyl-1-picrylhydrazyl
EC <sub>50</sub>	Half-maximal effective concentration
<i>E. coli</i>	<i>Escherichia coli</i>
EGF	Epidermal growth factor
EPR	Electron paramagnetic resonance
GSH	Reduced glutathione
HA	Hyaluronic acid
H-bond	Hydrogen bond
H <sub>2</sub> O <sub>2</sub>	Hydrogen peroxide
kDa	Kilodalton
K <sub>ox</sub>	Dopa oxidation rate
K <sub>dis</sub>	Dopaquinone dismutation rate,
M / mM / μM	Molar / millimolar / micromolar concentration
MADQUAT	poly(2-(trimethylamino)ethylmethacrylate)
Man7OHTrp	C <sub>2</sub> -mannosyl-7-hydroxytryptophan
mfp-1, -2, -3, -3b, 3S, -4, -5, -6	Mussel foot protein -1, -2, -3, -3b, 3S, -4, -5, -6
mfp-131, -151, -151-RGD, -3S-pep	Engineered mussel foot protein -131, -151, -151-RGD, -3S-pep
mfp-3S-pep-random #1, #2, #3	Three randomized mfp-3S-pep sequence #1, #2, #3
<i>M. galloprovincialis</i>	<i>Mytilus galloprovincialis</i>
MSM	Mushroom-shaped microstructure
NEM	N-Ethylmaleimide
NTA	Nature-derived tissue adhesive
O <sub>2</sub>	Oxygen
O <sub>2</sub> <sup>•-</sup>	Superoxide anion radical
OH <sup>•</sup>	Hydroxyl radical
PEG	Polyethylene glycol
pI	Isoelectric point
PPOL	Polyphenol oxidase like protein from <i>Mytilus galloprovincialis</i>
PS	Polystyrene
PLL	Poly-L-lysine
pTyr	Poly-L-tyrosine

## List of symbols and abbreviations

---

PTrp	Poly-L-tryptophan
<i>P. viridis</i>	<i>Perna viridis</i>
pvfp-1	Mussel foot protein -1 from <i>Perna viridis</i>
ROS	Reactive oxygen species
rPPOL	Recombinant polyphenol oxidase like protein
rP319	Short variant of rPPOL
rPPOL-NEM	Alkylated rPPOL using N-Ethylmaleimide
rP319-NEM	Alkylated rP319 using N-Ethylmaleimide
SEM	Scanning electron microscopy
SFA	Surface forces apparatus
SIMS	Secondary ion mass spectroscopy
STA	Synthetic tissue adhesive
T <sub>cp</sub>	Cloud point temperature
TC	Tren-Cam
TDC	Tren-Dab-Cam
TEA	Tetraethylammonium
TLACC	Tren-LysAC-Cam
TLB	Tren-Lys-Bam
TLC	Tren-Lys-Cam
TLP	Tren-Lys-Pam
UCST	Upper critical solution temperature

# 1. Introduction - mussel underwater adhesion

Ocean creatures are able to achieve strong wet adhesion and exhibit strong attachment resistance to violent waves.<sup>1-5</sup> In particular, marine mussels have drawn widespread attention due to their strong underwater adhesion by means of a particular holdfast system, the mussel byssus.<sup>6</sup> The involved proteins are modified with 3,4-dihydroxyphenylalanine (Dopa), and Dopa chemistry is the key feature of the byssus, thereby considering Dopa as a pivotal contributor for wet adhesion.<sup>6-9</sup> A substantial amount of mussel-mimetic investigations by means of Dopa, therefore, were already used for developing novel tissue adhesives.<sup>2, 10</sup>

However, Dopa-based materials are challenged due to auto-oxidation.<sup>1, 11</sup> Increasing pH from acidic to physiological values results in abortion of interfacial adhesion, which differs from the strong wet adhesion in nature.<sup>12-14</sup> Likewise, the interfacial adhesion mediated by mussel foot protein -3, and -5 (mfp-3, -5) are not as high as that of natural byssus.<sup>13, 15, 16</sup>

To get a more comprehensive understanding of mussel underwater adhesion, four sections are scrutinized including byssus structure (Fig. 1B; [section 1.1](#)), byssus assembly (Fig. 1C; [section 1.2](#)), interfacial adhesion (Fig. 1B; [section 1.3](#)) and bridging cohesion (Fig. 1B; [section 1.4](#)).

## 1.1 Byssus structure

### 1.1.1 Byssus architecture

The mussel byssus consists of a bundle of collagenous threads with a mechanical gradient: the elastic portion approaches to the soft mussel foot and the stiff portion approaches to the substratum (Fig. 1A).<sup>17-20</sup> The byssus is covered by a thin protective cuticle (2-5  $\mu\text{m}$ ), which consists of densely packed granules with diameters in the sub-micrometer range in a homogenous matrix (Fig. 1B).<sup>21-23</sup> The cuticle possesses one exclusive protein, mfp-1, and the granules therein show a condensed complex with reversible  $\text{Fe}^{3+}$ -Dopa coordination compared to the loose matrix ([section 1.4.1](#)).<sup>23-25</sup> It is proposed that the condensed granules contribute to the hardness (fivefold harder than the collagenous core), whereas the matrix with less cross-linking provides extensibility (up to > 100 % strain).<sup>23</sup> At high strain (> 30 %), the granules are capable of resisting large deformation via sacrificing the matrix with micro-crack formation; elongation of the granules is reversible at once when removing strain, whereas the micro-cracks are not.<sup>23</sup>

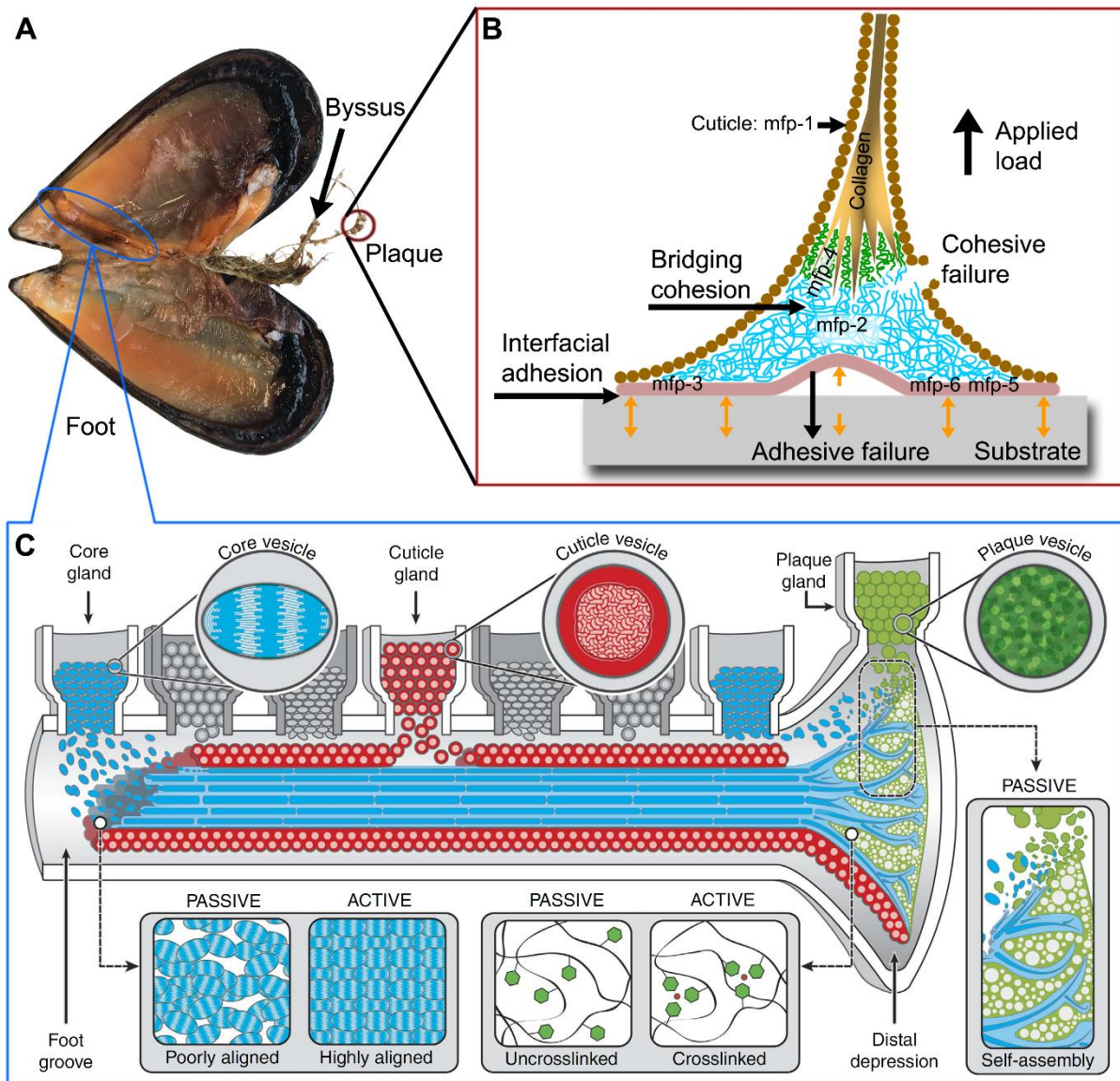


**Figure 1.** Mussel byssus structure (A) An open mussel showing the byssus and foot. The byssus comprises a bundle of threads and adhesive plaques at the end, which is further illustrated in (B). The mussel attachment includes interfacial adhesion between the interfacial proteins (mfp-3, -5, -6) and substrate as well as the interior bridging cohesion; adhesion and/or cohesion failure give rise to byssus detachment. (C) An illustrative model showing the byssus assembly process divided in passive and active aspects. A ventral groove is located along the topside of the foot, surrounded with interdigitated core glands and cuticle glands, and terminated at the distal depression at the tip of the foot with plaque glands nearby. Each gland has particular protein precursors pre-organized within secretory vesicles, which are released into the ventral groove followed by spontaneously coalescence and organization into native-like structures. Collagenous proteins in the oval core vesicles are well organized in a smectic phase of liquid crystals, facilitating the organization during assembly. Cuticle protein precursors in the cuticle vesicles coalesce and spread over the collagenous core, creating a protective granular coating. Likewise, plaque vesicle proteins are prepared in a dense phase, which is released into the distal depression to form a foam-like structure by means of coalesce. Additional mechanical forces as well as metal additives are required to get highly aligned collagenous core and metal-mediated coordinative cross-links, respectively. The porous plaque might stem from phase inversion. (C) is reprinted and adapted from Ref.<sup>26</sup>, under a Creative Commons license.

The collagenous core extends into plaques via a root-like penetration (Fig. 1B).<sup>17, 20, 27</sup> The mature plaque shows a foam-like structure with interconnected pores.<sup>20, 27, 28</sup> Two length scales of pore dimension are observed with interpenetrating large pores ( $\sim 1 \mu\text{m}$ ) in a dense meshwork ( $\sim 100 \text{ nm}$ ).<sup>27</sup> The overall byssus exhibits a mushroom-shaped microstructure (MSM), which is widely distributed in natural adhesive systems, e.g. mussels,<sup>20, 27</sup> sea stars,<sup>29, 30</sup> *Caulobacter crescentus*,<sup>31, 32</sup> and some algae,<sup>33</sup> indicating an optimal solution in the case of wet adhesion.<sup>34</sup> By means of MSM, enhanced adhesive performance with high tolerance to substrate irregularities was confirmed compared to other microstructures, such as flat punch.<sup>35-38</sup> Compared to the short-term dynamic adhesion via spatula shaped elements, e.g. geckos, MSM gives rise to long-term adhesion as shown in mussels.<sup>34, 37</sup> Additionally, an artificial MSM model showed higher underwater adhesion ( $\sim 25 \%$ ) than in air, whereas the flat punch showed a significant reduction ( $\sim 88 \%$ ) (Fig. 2A).<sup>39</sup> In air, there was no obvious difference in detachment force on both hydrophobic and hydrophilic substrates, which was mainly attributed to van der Waals force as the main binding force (Fig. 2A).<sup>39</sup> The increased underwater adhesion by means of MSM implicates that additional mechanism(s) should be involved.<sup>39</sup> Inspired by beetles, it is proposed that entrapped air between individual MSMs probably contributes to this process.<sup>40, 41</sup> During pulling off, the space of entrapped air increases, thereby giving rise to pressure reduction and a consequent suction effect (Fig. 2B).<sup>40</sup> In the case of mussels, entrapped air inside the open foam-like microstructures, might provide similar consequence contributing to incredible underwater adhesion.

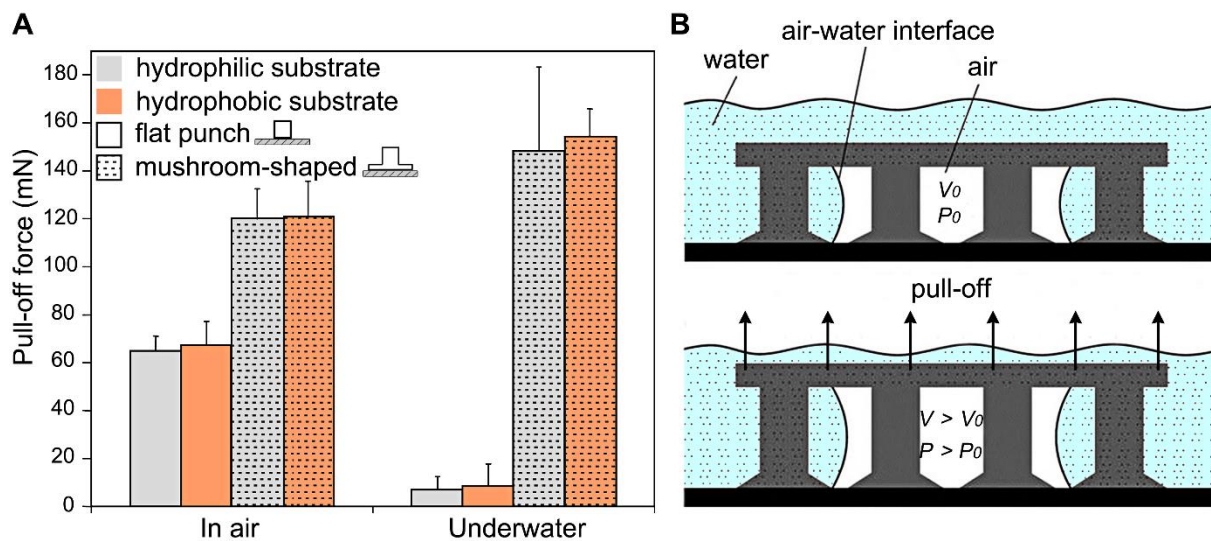


**Figure 2.** (A) Pull-off forces of mushroom-shaped microstructures (MSMs) on hydrophilic and hydrophobic substrates with smooth flat punches as control, measured in both air and underwater. Reprinted and adapted with permission from Ref.<sup>39</sup>, Copyright 2004, Royal Society, (B) Entrapped air in MSMs underwater in equilibrium (top) and during pull-off (bottom). Abbreviations:  $V_0$ , initial entrapped air volume;  $V$ , volume during pull-off;  $P_0$ , initial pressure in the entrapped air space;  $P$ , pressure during pull-off. Reprinted and adapted with permission from Ref.<sup>40</sup>, Copyright 2012, Royal Society of Chemistry.

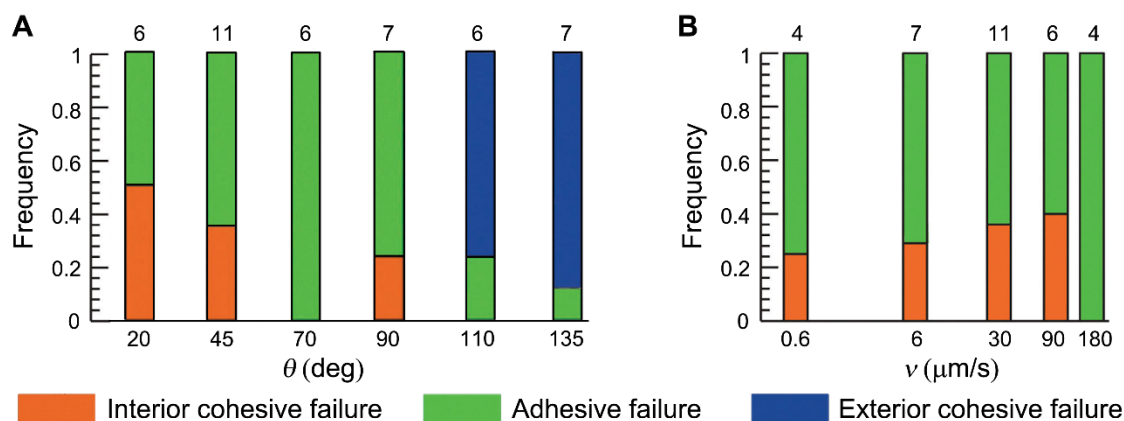


**Figure 3.** Effects of pull angle (A) and rate (B) on the failure mode of mussel detachment. Pull rate in (A) as well as pull angle in (B) were fixed at  $30 \mu\text{m/s}$  and  $45^\circ\text{C}$ , respectively. The tested numbers are placed above each bar. The failure mode is indicated by distinctive bar colors and the probability is represented by bar length. Reprinted and adapted with permission from Ref. <sup>15</sup>, Copyright 2015, Royal Society of Chemistry.

Recently, Desmond, K.W. et al have characterized mussel detachment dynamics by measuring the detachment force as well as deformation locations.<sup>15</sup> The mussel plaque reveals two kinds of failures: the adhesive failure via crack initiation on the thread-plaque junction and subsequent propagation radically toward the surrounding area of the surficial plaque, as well as the cohesion failure via plaque deformation, including interior or/and exterior cohesive failures (Fig. 1B, 3A).<sup>15</sup> The probability of failure mode is highly dependent on the pull angle (Fig. 3A). At natural angles of  $5\text{--}45^\circ\text{C}$ , adhesive failure and interior cohesive failure were mostly associated with the detachment, and the fraction of adhesive failure increased with increasing pull angle (Fig. 3A).<sup>15</sup> At pull angles  $\geq 90^\circ\text{C}$ , which are unlikely to occur in natural settings, the exterior cohesive failure dominated (Fig. 3A).<sup>15</sup> The average detachment force decreased with the increasing pull angle.<sup>15</sup> Comparably, the pull rate showed almost no influence on failure mode and detachment force (Fig. 3B).<sup>15</sup>

### 1.1.2 Molecular structure

The byssus is characterized by a high amount of Dopa-containing proteins, and more than 20 have been identified with various locations and functions.<sup>1, 42, 43</sup> Mussel foot proteins (mfps) in plaques, including mfp-2, -3, -4, -5, -6, as well as one additional protein in cuticle, mfp-1, have been extensively studied.<sup>1, 43</sup> All the identified mfps are quite basic.<sup>1, 44</sup> mfp-1 is primarily located in the protective cuticle, extending from the byssal thread to plaque (Fig. 1B).<sup>24, 25</sup> mfp-1 ( $\sim 115$  kDa, 10-15 % of Dopa) consists of repetitive decapeptide (AKP<sup>1</sup>SYP<sup>2</sup>P<sup>3</sup>TYK in 71 units, P<sup>1</sup> is Pro, P<sup>2</sup> is trans-4-2,3-cis-3,4-dihydroxyproline, P<sup>3</sup> is trans-4-hydroxy-L-proline and Y is Dopa) and hexapeptide (AKPTYK in 12 units, Y is Dopa) motifs.<sup>24, 25</sup> mfp-2, the most abundant plaque protein, is the primary component of the foam-like plaque matrix (Fig. 1B).<sup>24, 45</sup> mfp-2 ( $\sim 40$  kDa, 3-5 % of Dopa) is composed of 11 repetitive epidermal growth factor (EGF)-like motifs, which are stabilized by three disulfide bonds.<sup>24, 45</sup> A  $\text{Ca}^{2+}$  binding motif is revealed at least in one of the EGF-like motifs.<sup>45</sup> mfp-4 is located at the junction between collagenous threads and plaque matrix (Fig. 1B).<sup>46</sup> mfp-4 (70-93 kDa, 2-5 % of Dopa) contains one repetitive decapeptide motif (in 35 units) with high amounts of His, which probably contributes to the interconnection.<sup>46, 47</sup> Non-repetitive mfp-3 and mfp-5, as two of the smallest mussel proteins (5-9.5 kDa, 20-30 % of Dopa), are both located at the plaque-substrate interface and are considered as major contributors to the interfacial adhesion (Fig. 1B).<sup>8, 46, 48-50</sup> Likewise, mfp-6 (11 kDa, 2-3 % of Dopa) also resides at the

plaque-substrate interface (Fig. 1B).<sup>49</sup> The exceptional high amount of Cys residues (11 %) in mfp-6 is dedicated to the reducing reservoir, thereby controlling the redox chemistry of Dopa.<sup>16, 51</sup>

## **1.2 Byssus assembly**

Mussel byssus is rooted and generated in a specific organ, the mussel foot, which is equipped with several glands beneath the top ventral groove as well as a distal depression connected to the destination of the groove (Fig. 1C).<sup>26, 52, 53</sup> Each gland, containing distinctive secretory vesicles, is responsible for synthesizing and pre-packing different precursor proteins, which are prerequisites for byssus construction.<sup>26, 53</sup> The core glands with oval vesicles (long axis, 1-2  $\mu\text{m}$ ) are located along the ventral groove to produce a smectic phase of liquid crystals, subsequently assembling into the collagenous core of the thread (Fig. 1C).<sup>26, 52, 53</sup> Interlaced with core glands, the cuticle glands with spherical vesicles (0.5-1  $\mu\text{m}$  diameter) produce the protective cuticle precursors of mfp-1, which are not as well aligned as the collagenous precursors (Fig. 1C).<sup>26, 53</sup> Located near the distal depression at the foot tip, the plaque glands with spherical vesicles (1-2  $\mu\text{m}$  diameter), particularly secrete plaque precursors (Fig. 1C).<sup>26, 53</sup> The byssus assembly is reminiscent of a microfluidic system with precise control of fluids. A model of byssus assembly is proposed in which protein precursors are pre-packed in their corresponding glands and delivered to the ventral groove as well as distal depression where they coalesce spontaneously and self-assemble into exquisite 3D nano- and micro-architectures (Fig. 1C).<sup>1, 26</sup> Despite the achievements concerning byssus assembly, there are still some open questions: How do mussel proteins get deposited on wet substrate without dispersion in the surrounding seawater? How can Dopa be kept from auto-oxidation upon equilibration in seawater before adhering to substrate?

### **1.2.1 pH and ionic strength**

The ambient conditions within the ventral groove, such as pH, ionic strength and redox state, as well as subsequent mechanical post-treatment are necessary for regulation of byssus assembly. It has been determined that the secretion pH is around pH 3.0 and the ionic strength around 100 mM, which is significantly different to that of seawater where final maturation is taking place.<sup>16, 54</sup>

### **1.2.2 Coacervation**

Complex coacervation refers to a liquid-liquid phase separation within oppositely charged polyelectrolytes in aqueous solution, by means of electrostatic interactions, H-bonds, hydrophobic and/or van der Waals interactions.<sup>55, 56</sup> The phase separation gives rise to an upper polyelectrolyte-depleted phase and a settled polyelectrolyte-enriched phase, which is coacervate.<sup>56</sup> In some cases, coacervation occurs with one single polyelectrolyte, which is regarded to as self-coacervation or simple coacervation.<sup>56</sup>

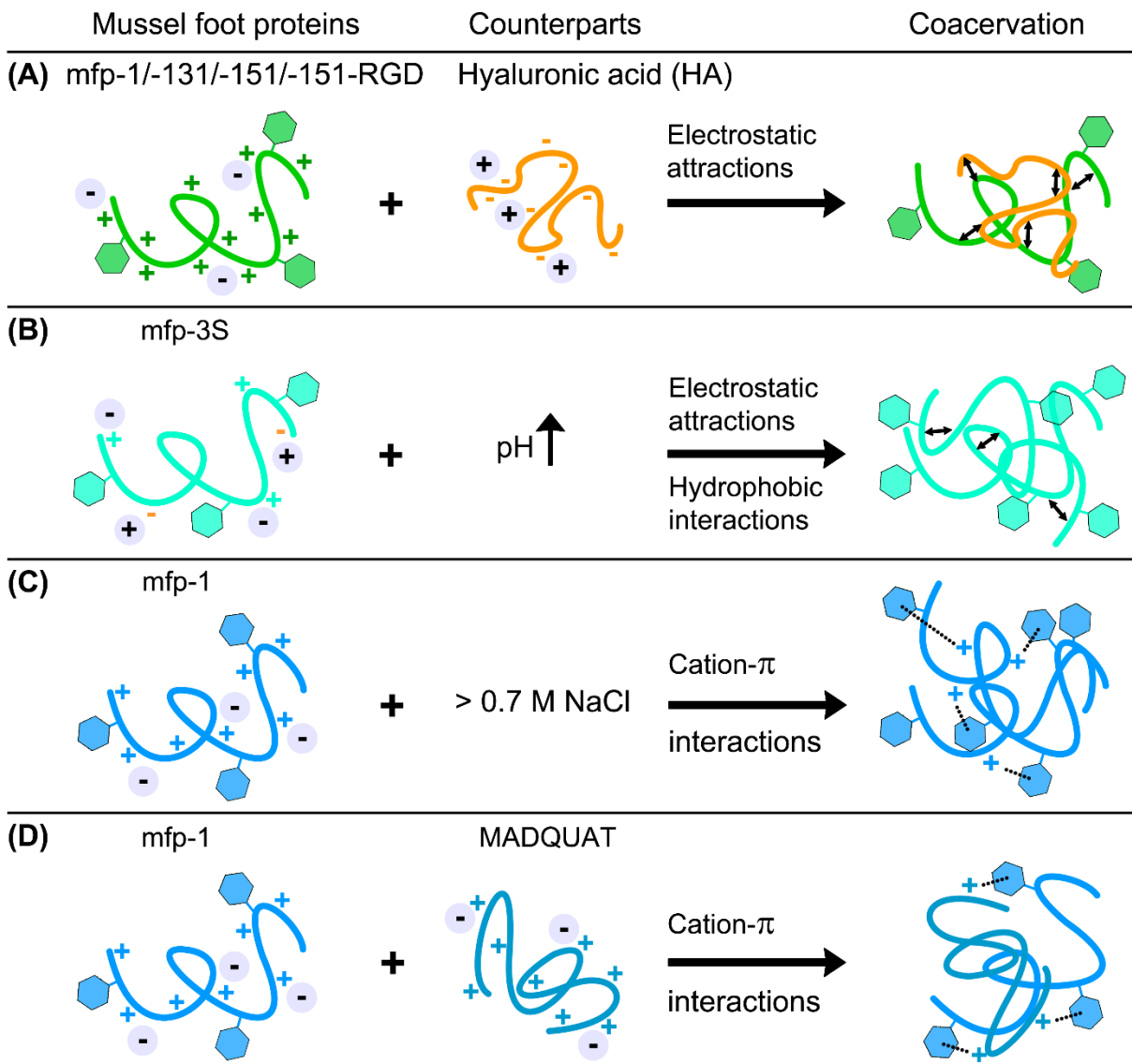


**Figure 4.** Schematic illustrations on coacervation of mussel protein analogues. (A) In the presence of anionic hyaluronic acid (HA), cationic mfp-1/-131/-151/-151-RGD can form coacervate mainly via electrostatic attractions. (B) Self coacervation of mfp-3S is driven by electrostatic attractions as well as hydrophobic interactions upon increasing pH, which results in a zwitterion with deprotonated acidic groups. (C) In the absence of a counterpart, cationic mfp-1 exhibits coacervation via strong cation- $\pi$  interactions upon addition of sea level salt (> 0.7 M NaCl), screening the electrostatic repulsions. (D) Strong cation- $\pi$  interactions are able to overcome the electrostatic repulsions and induce coacervation between cationic mfp-1 and cationic poly(2-(trimethylamino)ethylmethacrylate) (MADQUAT). The  $\leftrightarrow$  and ..... denote the electrostatic attractions and cation- $\pi$  interactions, respectively.

Phase separation within biomacromolecules plays an important role in assembly and construction of cellular structures, such as forming membraneless compartments, signaling complexes, and fibrous structures.<sup>57, 58</sup> Recent investigations reveal that coacervation also participates and contributes to natural underwater adhesion, e.g. in mussels,<sup>59-61</sup> sandcastle worms,<sup>3, 62</sup> squids<sup>4</sup> and sea urchins<sup>63</sup>. To build up a tubular protector by adhering sand grains, sandcastle worms are used to secrete complex coacervation based adhesives, consisting of several oppositely charged proteins.<sup>50, 51</sup> Raman spectral analysis revealed that the ambient environment of Tyr residues in plaque vesicles transitioned from hydrophobic to hydrophilic during assembly with a proposed conformational change of proteins, suggestive of the probably existence of coacervation during

assembly.<sup>26</sup> In the case of mussels, the identified mfps are enriched in basic Lys and Arg residues, showing positive charge under seawater pH.<sup>44</sup> No acidic components have been identified until now. Acidic hyaluronic acid (HA), existing in extracellular matrix, is considered as a potential anionic counterpart of mfps. Complex coacervation has been revealed between HA and mfp analogues, e.g. mfp-1,<sup>64</sup> mfp-131,<sup>65</sup> mfp-151<sup>65</sup> and mfp-151-RGD,<sup>66</sup> at a low ionic strength within pH values ranging from 3.0 to 4.6 (Fig. 4A). The incorporation of Dopa in mfps has no remarkable effect on complex coacervation.<sup>65</sup>

mfp-3S, possessing three positively charged residues as well as two negatively charged residues, underwent self-coacervation in the absence of anionic counterparts under secretion conditions (acidic pH and 0.1 M ionic strength), via hypothetical electrostatic and hydrophobic interactions (Fig. 4B).<sup>61</sup> The peculiar contributions of negatively charged residues and the primary amino acid sequence to coacervation are not clear. Therefore, a novel analogue mfp3S-pep was designed, corresponding to mfp-3S's pI but only half the length.<sup>67</sup> mfp-3S-pep exhibited similar coacervation behavior as mfp-3S.<sup>67</sup> The acidic version of mfp-3S-pep, substituting one Asp for Arg and giving a pI of 4.2, was still able to coacervate, suggesting Arg is not essential for self-coacervation.<sup>67</sup> To better unravel the contributions of charge, more comprehensive studies on additional mfp-3S-pep analogues are necessary with all charged residues depleted. The randomization of mfp-3S-pep sequence gave rise to three additional new analogues: mfp-3S-pep-random #1, #2, #3. Only random #2 exhibited similar random coil structure as well as coacervation behavior as mfp-3S-pep, suggesting the significance of the primary amino acid sequence for coacervation.<sup>67</sup>

Strong cation- $\pi$  interactions are present between cationic residues and aromatic groups in mfps as discussed below in [section 1.4.3](#), which contribute to the cohesion.<sup>68-71</sup> Given that high molarity of NaCl showing neglectable effect on cation- $\pi$  interactions as well as the ability to screen electrostatic repulsions, mfp-1 alone underwent coacervation via cation- $\pi$  interactions at sea-level salt concentration (> 0.7 M NaCl) (Fig. 4C).<sup>60</sup> Kim, S. et al revealed that strong short-ranged cation- $\pi$  interactions were capable of triggering coacervation even within two positively charged polyelectrolytes, (mfp-1 and poly(2-(trimethylamino)ethylmethacrylate) (MADQUAT)) by overcoming the long-range electrostatic repulsions (Fig. 4D).<sup>72</sup>

Coacervation gives rise to high condensation of proteins, thereby facilitating a thick coating on substrates without dispersion into the surrounding seawater. In addition, coacervate with low interfacial energy (< 1 mJ/m<sup>2</sup>) as well as low friction coefficient allows an easy spreading on large contact areas.<sup>60, 61</sup> The shear-thinning behavior of coacervate makes it possible to flow through the narrow conduit without blocking.<sup>60, 61</sup> The revealed coacervation of mfp-3S,<sup>61</sup> possessing only three positively charged residues, as well as mfp-1, locating within the cuticle, cannot represent that of the other interfacial proteins. To get better understandings of coacervation, investigations on other types of interfacial proteins are necessary.

### 1.2.3 Redox control

Molecular oxygen ( $O_2$ ) is essential for aerobic organisms by supporting metabolism, whereas it gives rise to undesirable deleterious bi-products, namely reactive oxygen species (ROS), including hydroxyl radical ( $OH^\bullet$ ), superoxide anion radical ( $O_2^{\bullet-}$ ) and hydrogen peroxide ( $H_2O_2$ ).<sup>73, 74</sup> A protective mechanism based on antioxidants has been evolved in organisms, including enzymatic antioxidants (e.g. peroxidase, catalase and glutathione peroxidases) and non-enzymatic antioxidants (e.g. vitamin C, E, and reduced glutathione (GSH)), which are capable of scavenging free radicals.<sup>73, 74</sup> Abnormal augmentation of ROS due to *in vivo* production or environmental uptake gives rise to oxidative stress, resulting in impairment of biological functions or even death of organisms.<sup>73, 75</sup>

In the case of mussels, acidic secretion is able to keep Dopa in a reduced state before adhering to substrate.<sup>16, 54</sup> However, Dopa shows high tendency toward auto-oxidation after exposure to surrounding  $O_2$ -saturated seawater. A forceful adhesion comprises moderately reduced (mainly mediating adhesion) and oxidized (mainly mediating cohesion) Dopa (Fig. 1B). Either adhesion or cohesion failure results in a vulnerable attachment (Fig. 1B), suggesting the necessity of a rigorous redox control for mussel attachment. The thiol-enriched mfp-6, which is co-secreted with mfp-3 into distal depression (Fig. 5), exhibits poor adhesion but can recover mfp-3's adhesion significantly (Fig. 6A).<sup>16</sup> mfp-3 exhibited pH-dependent adhesion, which was almost aborted at pH 5.5.<sup>16</sup> Addition of mfp-6 yielded the recovery of substantial adhesion of mfp-3 at pH 5.5. (Fig. 6A).<sup>16</sup> Thiol-blocked mfp-6 (CM-mfp-6) failed to rescue the loss adhesion, indicating the contribution of free thiols to the reducing activity.<sup>16</sup> By means of 2,2-diphenyl-1-picrylhydrazyl (DPPH) assay, the reducing capacity was determined to be about 17 electrons per molecule of mfp-6, 9 of which come from Cys thiols and 8 of which come from hostage Dopa residues (Fig. 6B).<sup>51</sup> Considering the different reactivity between protonated (RSH) and deprotonated (thiolate,  $RS^-$ ) thiol groups, the thiol  $pK_a$  is influencing the antioxidant activity.<sup>76</sup> mfp-6 showed high antioxidant activity even at pH 3.0, suggesting an unusual low thiol  $pK_a$  compared to the typical value of around 8-9.<sup>16</sup> A low thiol  $pK_a$  endows mfp-6 with notably reducing activity at a broad pH range.<sup>16</sup> DPPH assay on mussel plaque extractions revealed that about 50 % Dopa as well as 30 % antioxidant activity still remained after 20 days, indicating that the involved antioxidant works not only during foot deposition but also in mature plaque.<sup>77</sup> The question is how much mfp-6 contributes to this high and long-term antioxidant activity and are there other contributors?

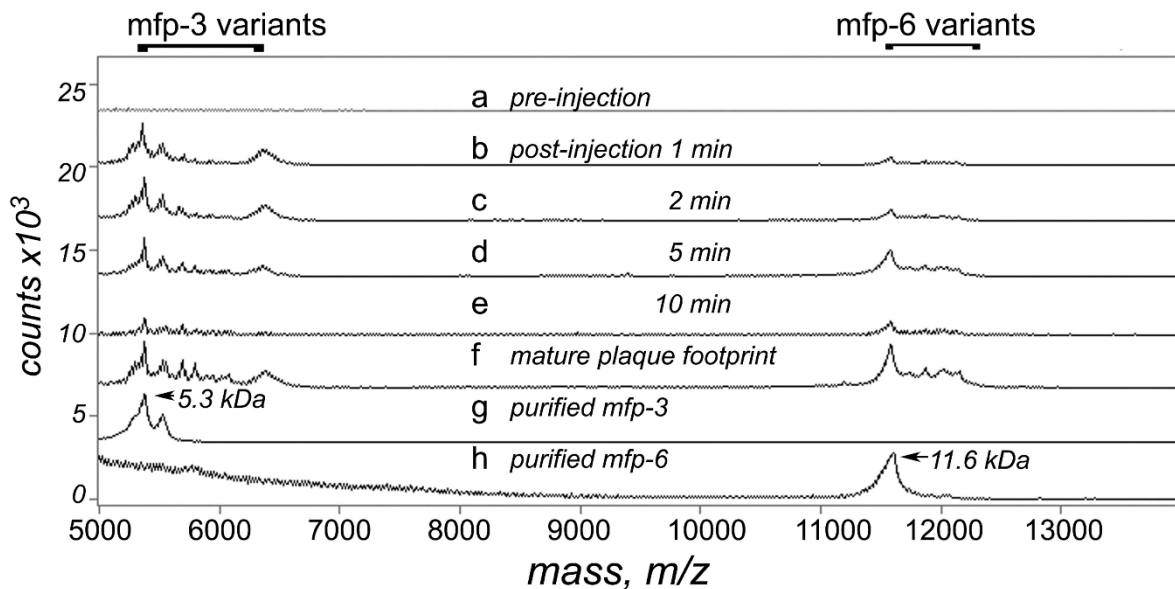


**Figure 5.** Mass analysis of secreted proteins in distal depression before (a) and after (b-e) injection KCl into the pedal nerve. Purified mfp-3 (5.3 kDa), mfp-6 (11.6 kDa) and mature plaque footprint were taken as control. Reprinted and adapted with permission from Ref. <sup>16</sup>, Copyright 2011, Springer Nature.

### 1.3 Interfacial adhesion

Adhesion or cohesion failure results in plaque peeling off (Fig. 1B),<sup>15</sup> suggesting the importance of both adhesion and cohesion. The interfacial adhesion in mussel byssus is conducted by interfacial mfp-3 and -5 via directly contacting with underlying substrates, which are associated with surface drying property, H-bonds, coordination bonds, hydrophobic interactions, and van der Waals forces.

#### 1.3.1 Surface drying property

Mica and other mineral oxides are frequently used for adhesion measurements, since they are representative surfaces of rocks in the mussel's intertidal habitat. With respect to mica, water and cations get attracted to the negatively charged surface to form a hydration layer in general, which is a substantial barrier to impede initial adhesion. However, mussels are capable of adhering to that kind of hydrated saline surfaces, suggesting that one underlying adaptation to remove the hydration layer is involved in the natural system. Recently, mfp-3S has been revealed to be a "molecular vanguard" to break through the hydration layer.<sup>67, 78</sup> In particular, the hydrophobic residues of mfp-3S play a critical role for the adaption.<sup>78</sup> Only Dopa-bearing analogues showed eviction of interfacial water, and faster eviction was demonstrated with coacervation, suggesting an eviction synergy between Dopa and coacervation.<sup>67</sup>

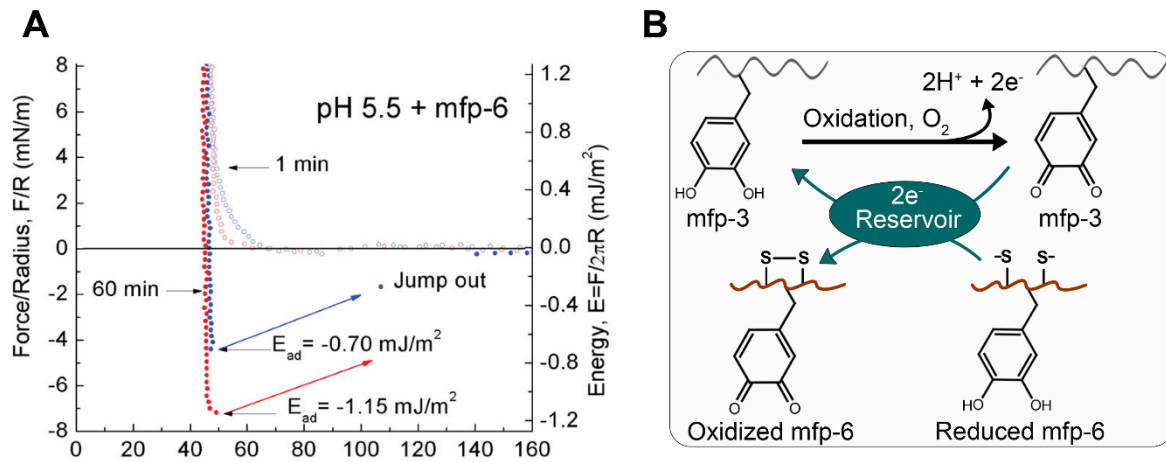


**Figure 6.** Antioxidant property of mfp-6. (A) Adhesion abortion of mfp-3 was identified at pH 5.5, whereas addition of mfp-6 rescued the adhesion loss. With more contact time (from 1 min to 60 min) of two surfaces, the adhesion energy increased. Reprinted and adapted with permission from Ref.<sup>16</sup>, Copyright 2011, Springer Nature. (B) A model of redox modulation by means of mfp-6. With increasing pH or additional oxidants, it shows high tendency from Dopa to Dopaquinone. One molecule reduced mfp-6 is capable of dedicating  $\sim 17$  electrons to the reducing reservoir,  $\sim 9$  of which come from thiolates and  $\sim 8$  of which come from Dopa, which provides electrons to reduce Dopaquinone back to Dopa.<sup>16, 51</sup>

Besides Dopa residues, mfp-3 and -5 are rich in Lys residues as well.<sup>44</sup> Due to the abundant Dopa residues, it is not so easy to ascertain the specific contributions of Lys residues to adhesion. Siderophore, comprising a paired catechol (the functional group of DOPA) and Lys, is a simple platform to explore molecular contributions to adhesion. Three Tren-based siderophore analogues have been synthesized with/without catechol and amine functionalities (Fig. 7A).<sup>79</sup> Group I with both catechol and amine functionalities (Tren-Lys-Cam (TLC), Tren-Dab-Cam (TDC) with short amine chain) was capable of displacing salt ions from a mica surface and showed high adhesion energies (Fig. 7).<sup>79</sup> The length of amine chain (TDC) did not influence the adhesion property.<sup>79</sup> Group II with amine functionality (Tren-Lys-Pam (TLP) with one hydroxyl group, Tren-Lys-Bam (TLB) without hydroxyl groups) exhibited low adhesion (Fig. 7).<sup>79</sup> TLB required a higher concentration to adsorb to the mica surface. Group III with catechol functionality (Tren-Cam (TC) without amine, Tren-Lys<sup>AC</sup>-Cam (TL<sup>AC</sup>C) with amine acetylated) showed no adhesion in the presence of high molarity of salt (200 mM) (Fig. 7).<sup>79</sup> Therefore, catechol as well as Lys are prerequisites for wet adhesion by means of displacing surface salts and hydration layers synergistically.<sup>79</sup>

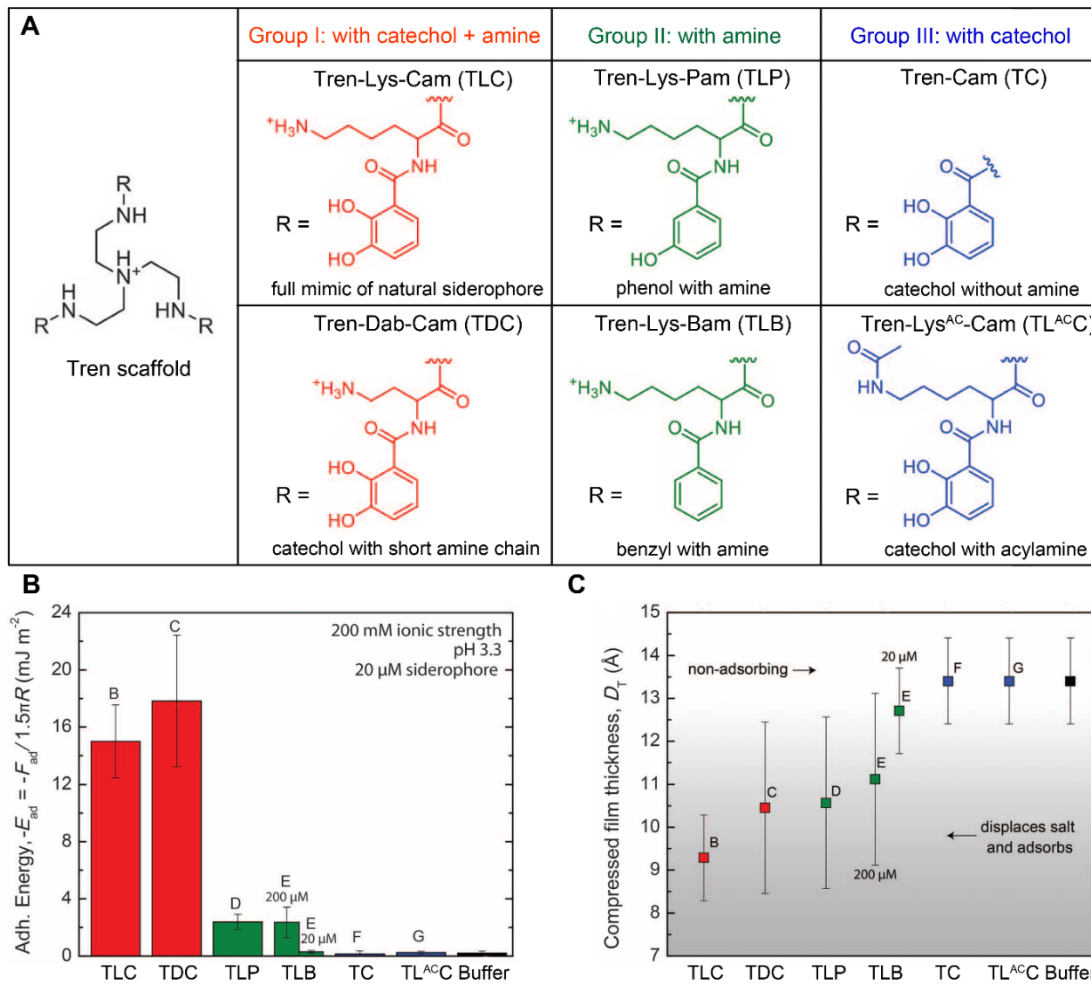


**Figure 7.** The synergy of Lys and catechol functionalities in adhesion. (A) Structure of Tren scaffold with different R groups (Group I, II, III). (B) The adhesion energy in the presence of 20  $\mu\text{M}$  siderophore analogs (TLB with both 20  $\mu\text{M}$  and 200  $\mu\text{M}$ ) at pH 3.3. (C) Monolayer thickness between two mica surfaces in the presence of siderophore analogs. The decreased film thickness is in accordance with high adhesion energy, suggestive of successful dehydration at the mica surface. Reprinted and adapted with permission from Ref. <sup>79</sup>, Copyright 2015, The American Association for the Advancement of Science.

### 1.3.2 H-bonds vs coordinative bonds

During acidic secretion, both hydroxyl groups of Dopa are protonated and prefer to form bidentate H-bonds with O atoms on polar surfaces, e.g. silica and mica, which are regarded as primary contributor to interfacial adhesion (Fig. 8A).<sup>13, 80</sup> The bonding lifetime of bidentate H-bonds on mica ( $E = \sim 28 \text{ kT}$ ) is predicted to be  $\sim 10^6$  times longer than the monodentate form ( $E = \sim 14 \text{ kT}$ ) according to Bell theory ( $\tau = \tau_0 e^{-E/kT}$ ,  $\tau$  is bonding lifetime,  $\tau_0$  is the average time of molecular vibrations,  $E$  is bonding-dissociation energy,  $k$  is Boltzmann's constant and  $T$  is temperature).<sup>12, 16, 81</sup> The extra-prolonged lifetime of bidentate H-bonds provides a basis for adhesion. Dopa-incorporated polymers as well as mfps, e.g. mfp-3 and -5, exhibit promising adhesion.<sup>12-14, 82, 83</sup> Dopa substitution or oxidation leads to adhesion loss, suggesting the importance of Dopa to adhesion.<sup>12-14, 82, 83</sup>

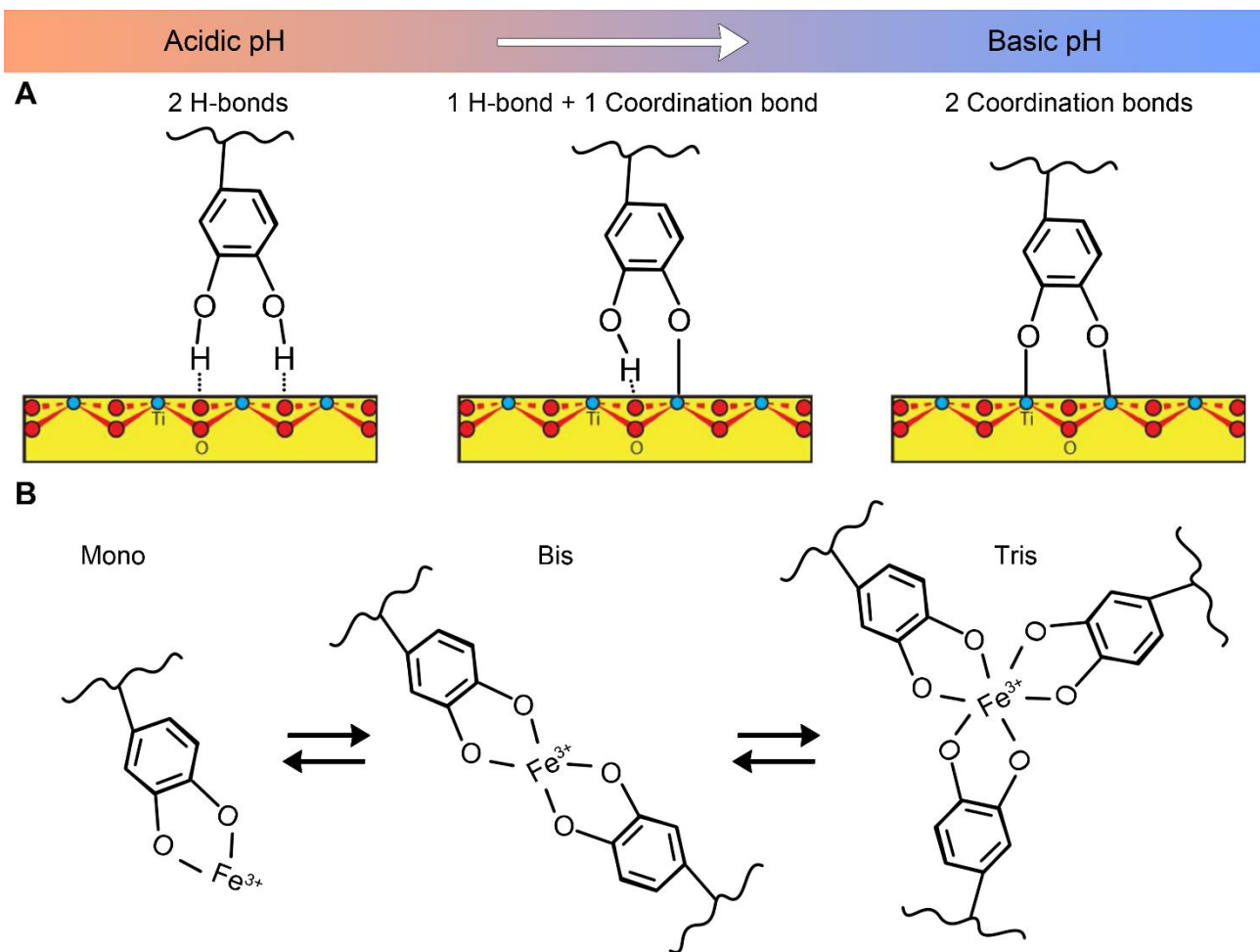


**Figure 8.** pH-dependent metal binding chemistry of catechol. (A) Interfacial catechol bonding to metal oxide surfaces turns from bidentate H-bonds at acidic pH to bidentate coordination at basic pH. Reprinted and adapted with permission from Ref.<sup>80</sup>, Copyright 2013, American Chemical Society. (B) Interior Fe<sup>3+</sup>-catechol coordination turns from mono-complex at acidic pH to tris-complex at basic pH, which is reversible.

Upon equilibration to slightly basic seawater, both hydroxyl groups of Dopa deprotonate to some extent and form bidentate coordination subsequently on TiO<sub>2</sub> surfaces, which gives rise to increased adhesion (Fig. 8A).<sup>80</sup> At intermediate pH, a combination of one H-bond and one coordination is possible (Fig. 8A).<sup>80</sup> Meanwhile, increasing pH makes Dopa more susceptible to auto-oxidation, thereby decreasing the adhesion. The dissociation energy of the bidentate Ti-Dopa coordination bond is around 4 times higher than that of the Dopaquinone to TiO<sub>2</sub> surface.<sup>82</sup> Under these two opposing effects, the adhesion force at pH 7.5 was higher than at pH 5.5.<sup>80</sup> To get maximal interfacial adhesion, a redox regulation is necessary to protect Dopa from auto-oxidation.

### 1.3.3 Other interactions

The adhesion of mfp-1, -3, -5 to methyl (CH<sub>3</sub>)- terminated hydrophobic and alcohol (OH)- terminated hydrophilic surfaces were investigated.<sup>84</sup> Higher adhesion on hydrophobic surfaces than hydrophilic surfaces was revealed due to the hydrophobic interactions between aromatic moieties and surficial (CH<sub>3</sub>)- groups.<sup>14, 84</sup> In addition, electrostatic interactions and van der Waals forces are also associated with interfacial adhesion.<sup>85,</sup>

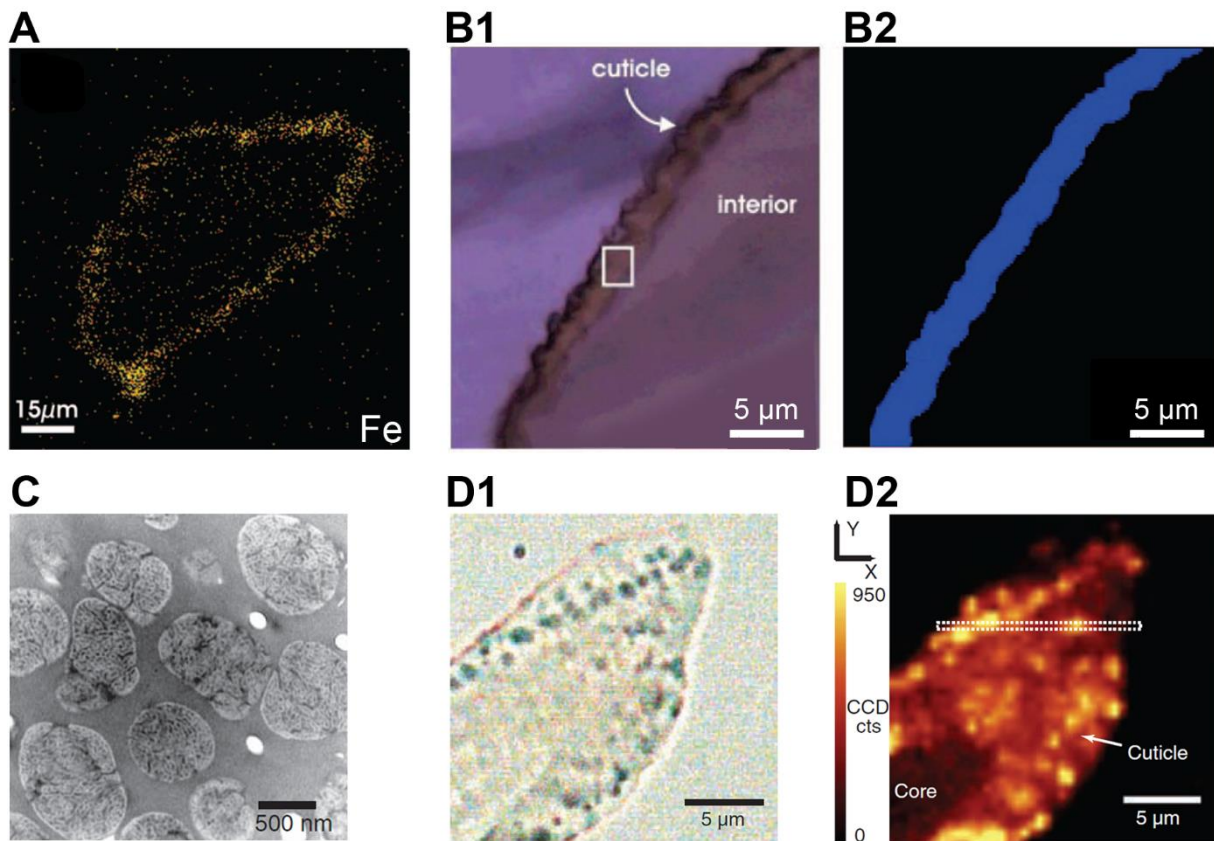


**Figure 9.** Imaging of the byssal thread of *M. galloprovincialis*. (A) Distribution of Fe in a sectioned byssal thread generated by secondary ion mass spectroscopy (SIMS). The thread in transverse section was viewed under bright-field microscopy (B1) or under 330-385 nm UV light (B2) Strong blue auto fluorescence was shown in the cuticle, in accordance with the presence of Dopa. A, B1, and B2 are reprinted and adapted with permission from Ref.<sup>22</sup>, Copyright 2009, American Chemical Society. (C) Transmission electron microscopy (TEM) image of the granular structure of cuticle. (D1) Light microscopy of a thin cuticle section ( $\sim 3 \mu\text{m}$ ) showing granules as dark spots. (D2) 2D Raman image with integration of  $\text{Fe}^{3+}$ -Dopa peak ( $490$  to  $696 \text{ cm}^{-1}$ ) gave high intensity on granules than surrounding matrix. C, D1, and D2 are reprinted and adapted with permission from Ref.<sup>23</sup>, Copyright 2010, The American Association for the Advancement of Science.

## 1.4 Bridging cohesion

Bridging cohesion is mainly mediated by foam-structured mfp-2 and give rise to hardness of the byssus, thereby increasing the overall attachment strength.<sup>24, 87</sup> Metal-mediated coordination, covalent cross-linking and cation- $\pi$  interactions are mainly involved in the bridging cohesion.

### 1.4.1 Metal-mediated coordination

Marine mussels are able to accumulate metals *in vivo* from surrounding seawater, e.g. Fe, Zn, Cu and Mn, with concentrations which are up to 100 000 times higher than in seawater.<sup>88-91</sup> A majority of the absorbed Fe transported to the byssus, suggesting the participation of Fe during byssus assembly.<sup>88</sup> Wilker, J.J. group revealed that addition of  $\text{Fe}^{3+}$  gave rise to curing of mussel adhesive precursors.<sup>92, 93</sup> The existence of  $\text{Fe}^{3+}$  in mature plaques was later confirmed directly by electron paramagnetic resonance (EPR).<sup>94</sup> Dopa as well as  $\text{Fe}^{3+}$  were precisely identified within the cuticle (Fig. 9A, 9B1, 9B2).<sup>22, 23</sup> Removal of  $\text{Fe}^{3+}$  from byssus by chelation resulted in a hardness reduction by 50 %, suggesting that  $\text{Fe}^{3+}$  plays a significant role in advancing the mechanical property thereof.<sup>22</sup>

The cuticle of intertidal *Mytilus galloprovincialis* (*M. galloprovincialis*) consists of numbers of granules interspersed in the homogeneous matrix (Fig. 9C).<sup>21, 22</sup> Compared to the matrix, the granules show a higher density of tris  $\text{Fe}^{3+}$ -Dopa complexes as shown by confocal Raman spectroscopy (Fig. 9D1, 9D2).<sup>23</sup> The high density of tris  $\text{Fe}^{3+}$ -Dopa complexes in granules might be due to high concentrations of mfp-1.<sup>23</sup> The highly cross-linked granules as well as the less cross-linked matrix are believed to provide hardness and extensibility to the cuticle, respectively, which makes it ideal for coating.<sup>21-23</sup> At high deformation, the granules can protect the cuticle from crack propagation at the expense of microcracks in the matrix.<sup>21-23</sup> mfp-1 showed poor bridging properties in the absence of  $\text{Fe}^{3+}$ .<sup>95</sup> Upon addition of  $\text{Fe}^{3+}$  to mfp-1, strong and reversible bridging was revealed due to formation of tris  $\text{Fe}^{3+}$ -Dopa complexes,<sup>95-97</sup> which is consistent with the analysis of the natural byssus.<sup>21-23</sup> By means of tris  $\text{Fe}^{3+}$ -Dopa coordination hydrogels based on natural mfps or Dopa-incorporated polymers have been processed with deformable and self-healing properties.<sup>98</sup>

In plaques,  $\text{Fe}^{3+}$ -Dopa complexes exhibit a high intensity in the cuticle (mfp-1), moderate intensity in the foam (mfp-2), and low intensity at the interface (mfp-3, -5) (Figure 10).<sup>87</sup> Addition of  $\text{Fe}^{3+}$  to mfp-2 improved the adhesion by 5 to 7 times, and the precipitations thereof exhibited strong Raman signals, suggestive of  $\text{Fe}^{3+}$ -Dopa complexes.<sup>87</sup> Furthermore, mfp-2 is capable of interacting with interfacial mfp-5 as well.<sup>87</sup> In the case of plaques, the complexation of mfp-2 with  $\text{Fe}^{3+}$  as well as mfp-5 contributes to forming a plump structure, inducing strong cohesion.<sup>87</sup>

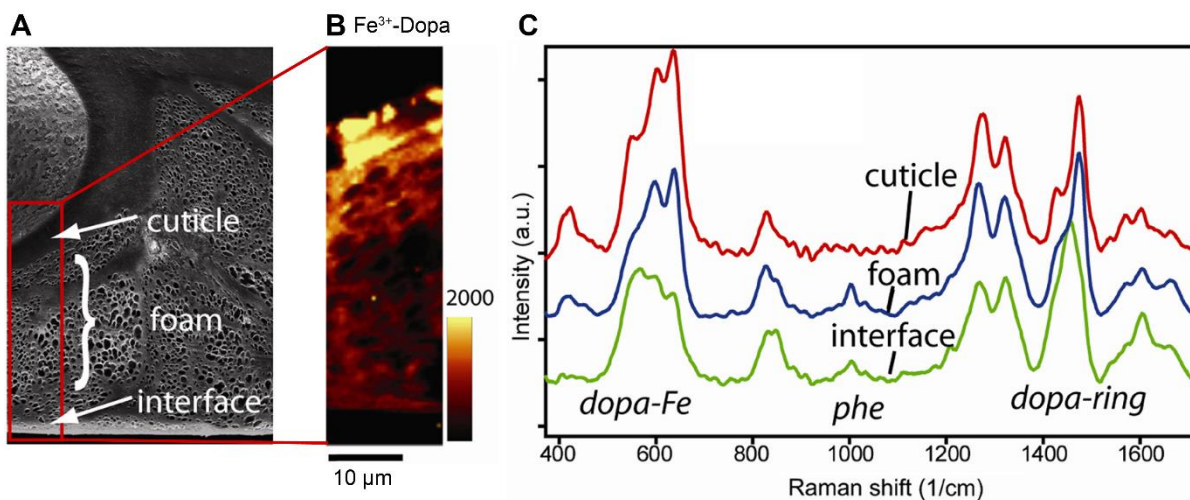


**Figure 10.** Analysis of  $\text{Fe}^{3+}$ -Dopa complex in the adhesive plaque of *M. galloprovincialis*. (A) Scanning electron microscopy (SEM) image of a sectioned plaque. (B) Raman microscopy image of the boxed region in (A) was integrated for  $\text{Fe}^{3+}$ -Dopa ( $490$  to  $696$   $\text{cm}^{-1}$ ), which revealed the highest intensity in the cuticle. (C) Average Raman spectra of the cuticle, foam and interface. Reprinted and adapted with permission from Ref.<sup>87</sup>, under a Creative Commons license.

Considering the typical octahedral geometry of  $\text{Fe}^{3+}$  as well as the bidentate property of catechol,  $\text{Fe}^{3+}$  is able to bind one, two, or three catechol ligands.<sup>99</sup> Therefore, complexes of  $\text{Fe}^{3+}$ -catechol exist in three different stoichiometries, e.g. mono-, bis-, tris-complex, which can be regulated by pH,  $\text{Fe}^{3+}$  to catechol ratio, and the nature of the catechol analogues (Fig. 8B).<sup>95, 97, 100</sup> With respect to a Dopa-modified PEG polymer, the mono-complex of  $\text{Fe}^{3+}$ -Dopa dominated at  $\text{pH} < 5.6$ , the bis-complex at  $5.6 < \text{pH} < 9.1$ , and the tris-complex at  $\text{pH} > 9.1$ , depending on the deprotonation of catecholic hydroxyls.<sup>100</sup> In general, the substituents of the phenolic ring affect the  $\text{pK}_a$  of catechol analogues. The electron-withdrawing substituents, e.g.  $-\text{NO}_2$ , can increase the stability of the deprotonated catechol moiety, resulting in a lower  $\text{pK}_a$ ; whereas electron-donating substituents, e.g.  $-\text{NH}_2$ , can decrease the stability accordingly, resulting in a higher  $\text{pK}_a$ .<sup>101, 102</sup> Therefore, the catechol analogues with lower  $\text{pK}_a$ , e.g. carbonyl-substituted chrysobactin, can form tris coordination with  $\text{Fe}^{3+}$  at relative low pH ( $\text{pH} > 6.1$ ).<sup>103</sup> Regarding Dopa-incorporated proteins, the sequence may influence the  $\text{pK}_a$ .<sup>1</sup>

The  $\text{Fe}^{3+}$  to catechol ratio is also critical for complex formation.<sup>97</sup> Different ratios of  $\text{Fe}^{3+}$  to catechol (mfp-1) at pH 7.0 resulted in two different coordination complexes: a purple one (548 nm) at high ratios and a pink one (500 nm) at low ratios.<sup>97</sup> Analysis revealed that bis- as well as tris-complexes were involved in the purple and pink complex, respectively.<sup>97</sup> Another study showed similar result that tris-complex was formed with strong and reversible bridging interactions at low  $\text{Fe}^{3+}$  concentrations (10  $\mu\text{M}$ ), whereas non-bridging mono-complexes were formed with cohesion loss at high  $\text{Fe}^{3+}$  concentrations (100  $\mu\text{M}$ ).<sup>95</sup> The solubility of  $\text{Fe}^{3+}$  is low at basic pH, which makes  $\text{Fe}^{3+}$ -mediated cross-linking unpractical.<sup>100, 104</sup> Pre-binding  $\text{Fe}^{3+}$  to catechol in mono-complex at acidic pH, and then increasing the pH to induce tris-complexes can avoid  $\text{Fe}^{3+}$  precipitation and overcome this obstruction accordingly.<sup>100</sup>

## 1.4.2 Covalent cross-linking

### 1.4.2.1 Dopa oxidation

The oxidation of Dopa to Dopaoquinone, either spontaneously at mild to alkaline pH (auto-oxidation)<sup>105, 106</sup> or upon addition of transition metallic (e.g.  $\text{Fe}^{3+}$ ),<sup>107, 108</sup> nonmetallic (e.g.  $\text{IO}_4^-$ )<sup>109</sup> or enzymatic (e.g. catechol oxidase) oxidants<sup>110</sup>, plays a vital role for byssus curing with covalent cross-linking (Fig. 11).<sup>102</sup> Catechol oxidase (EC 1.10.3.1), catalyzing Dopa to Dopaoquinone, has been identified and extracted from mussel byssus.<sup>110, 111</sup> The catechol oxidase works at pH 8.0 and probably works together with Dopa auto-oxidation at seawater conditions.<sup>110</sup>

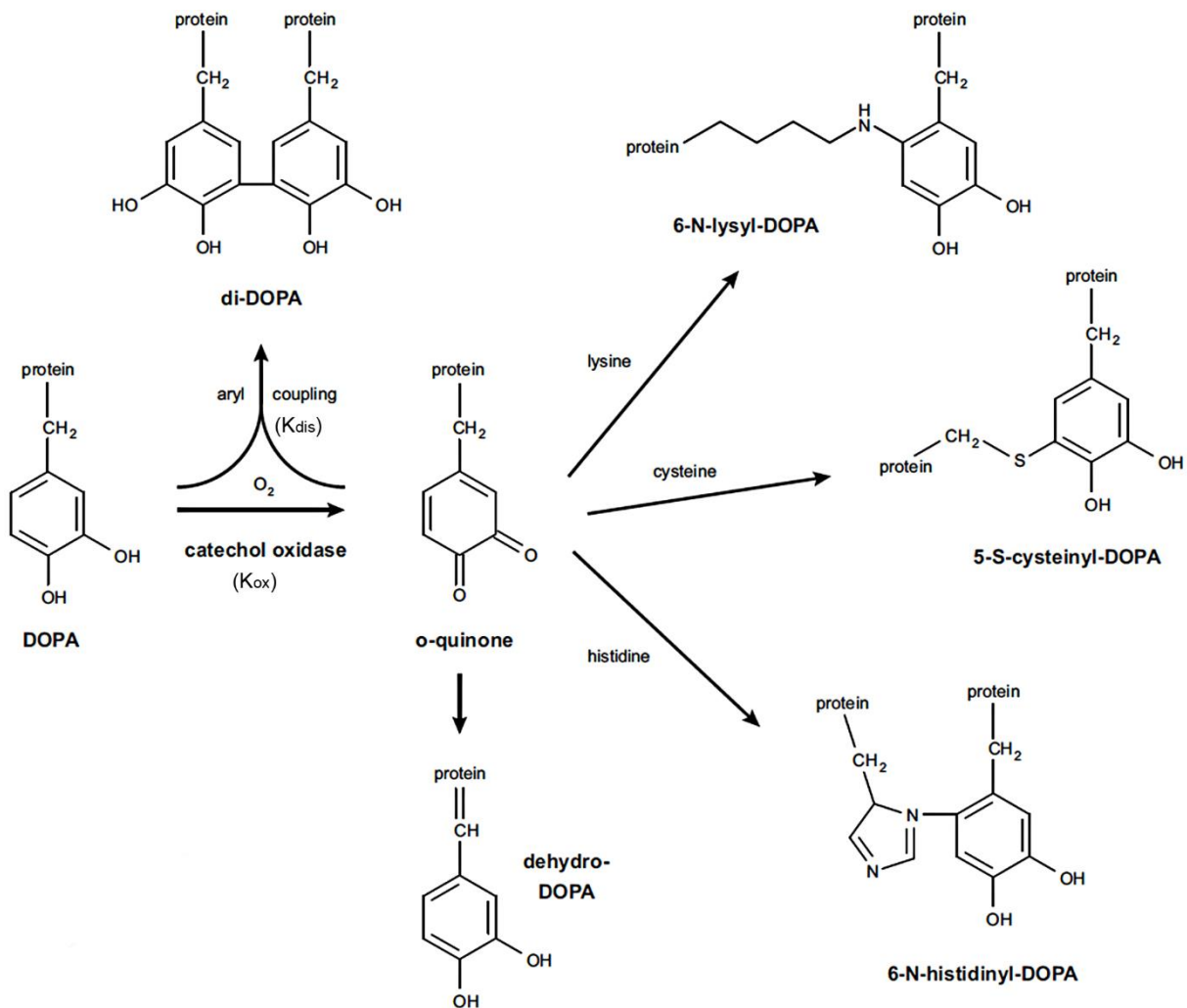


**Figure 11.** Reaction pathways of Dopa in mussels. Dopa is oxidized into the intermediate product Dopaoquinone (oxidation rate,  $K_{ox}$ ) automatically or triggered by additional oxidants, e.g. catechol oxidase and periodate. Dopaoquinone is quite reactive to undergo a variety of reactions yielding covalent cross-linking. Aryl-coupling of the generated Dopaoquinone and another Dopa (Dopaoquinone dismutation rate,  $K_{dis}$ ) gives rise to di-Dopa and subsequent polymerization. Tautomerization of Dopaoquinone to dehydro-Dopa results in polymerization as well. Furthermore, Dopaoquinone can react with a variety of nucleophiles in Michael-type additions, e.g. lysyl, histidyl and cysteinyl groups. Reprinted and adapted with permission from Ref. <sup>42</sup>, Copyright 2014, Elsevier.

Multiple factors can affect Dopa oxidation, such as pH, redox potential (e.g. the type and concentration of oxidant), nature of Dopa and the substituent groups thereof. In general, Dopa oxidation is more susceptible with increasing pH, especially with basic pH, due to the reduced reduction potential.<sup>12, 105</sup> The type of oxidant has apparent influence on the oxidation rate, e.g. the rate of enzyme-mediated oxidation is proportional to the enzyme concentration, whereas periodate-induced oxidation shows maximal rate at a Dopa to periodate molar ratio between 1 and 2.<sup>12, 112</sup> In addition, Dopa gets oxidized easily with electron-donating substituents, (e.g. -NH<sub>2</sub>),<sup>113</sup> whereas a contrary effect on oxidation exists with electron-withdrawing substituents (e.g. -NO<sub>2</sub>).<sup>114, 115</sup> van der Leeden, M.C. found an interesting oxidation behavior of mfp-1, which inversely corresponded with osmotic pressure.<sup>116</sup> Increasing osmotic pressure gave rise to conformational changes of mfp-1, and, therefore, altered the reactivity of mfp-1 toward oxidation, which might be protection approach for mussels during the storage of proteins in granules.<sup>116</sup>

### 1.4.2.2 $Fe^{3+}$ -mediated Dopa oxidation

At acidic pH, Dopa gets oxidized by  $Fe^{3+}$  generating Dopamine and  $Fe^{2+}$ .<sup>107, 108, 117</sup> Besides the above-mentioned  $Fe^{3+}$ -Dopa coordination in mussels,  $Fe^{3+}$  is also speculatively involved in redox reactions with Dopa at acidic pH (Fig. 12). Addition of  $Fe^{3+}$  to Dopa-containing mfp-1 and mfp-2 resulted in immediate precipitation at acidic pH.<sup>94, 118</sup> Electron paramagnetic resonance (EPR) of the precipitated solid confirmed the presence of  $Fe^{3+}$  and an organic radical, likely due to  $Fe^{3+}$  mediated Dopa oxidation.<sup>94</sup> Further investigations on small catechol-containing molecules confirmed the formation of *o*-quinone upon reduction of  $Fe^{3+}$  to  $Fe^{2+}$ , which was favored at acidic pH (pH 2.0-3.0) and almost undetectable at basic pH.<sup>118</sup>

During byssus assembly, a pH regulation takes place.<sup>16, 54</sup> The byssus precursors are initially stored at acidic pH (pH  $\approx$  3.0) and exposed and equilibrated to seawater (pH  $\approx$  8.4) after release.<sup>54</sup> The  $Fe^{3+}$ -Dopa interactions, including coordination as well as covalent interactions, are clearly pH dependent, which might be related to the pH switch during assembly (Fig. 12). However, the characteristic  $Fe^{3+}$ -Dopa complexes have not been identified in artificially induced byssus or mussel foot glands.<sup>26</sup> The storage and processing specifics of byssal precursors with  $Fe^{3+}$ , e.g. the blended stages thereof, are not well known. Partial Dopa might form covalent cross-links with  $Fe^{3+}$  at acidic conditions and the others coordinate with  $Fe^{3+}$  after exposure to seawater (Fig. 12).<sup>118, 119</sup>

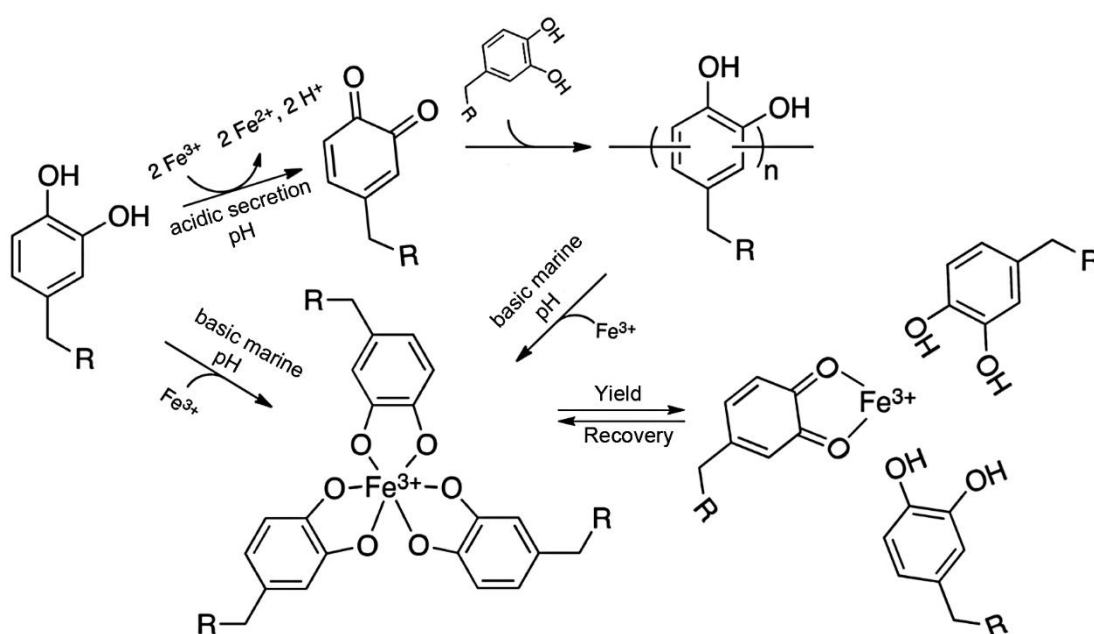


**Figure 12.** A proposed model for pH-dependent Fe-Dopa interactions in mussel byssus. At acidic pH, parts of Dopa are oxidized into Dopamine upon reduction of  $Fe^{3+}$  to  $Fe^{2+}$ , resulting in covalent polymerization via aryl-coupling. Upon exposure to basic pH, Dopa coordinates with  $Fe^{3+}$ , which is reversible. To achieve maximal mechanical properties, there should be a precise balance in pH regulating covalent vs coordination reactions during byssus assembly. Reprinted and adapted with permission from Ref.<sup>118</sup>, Copyright 2014, RSC Publishing.

A catechol-terminated branched PEG was inspired to form hydrogels in the presence of  $\text{Fe}^{3+}$  at pH 3.0, which was augmented with increasing pH (pH 9.0).<sup>119</sup> The covalent cross-linking (pH 3.0) endows hydrogels with a high toughness, whereas the coordination (pH 9.0) works in a sacrificial way to dissipate energy under applied force owing to the reversible rupture and re-forming ability.<sup>119</sup> For optimal mechanical performance, the amount of covalent vs coordinative cross-linking needs to be accurately modulated, and further investigations are required to find out how mussels regulate the curing process with  $\text{Fe}^{3+}$ .

#### 1.4.2.3 Dopaquinone reaction pathways

Dopaquinone is a quite reactive intermediate, which can be attacked by various biological sourced nucleophiles by the Michael addition, e.g.  $-\text{NH}_2$ ,  $-\text{SH}$  and imidazole (Fig. 11).<sup>102, 120</sup> Michael addition is highly dependent on the nature of nucleophile groups, e.g.  $\text{pK}_a$ ,<sup>121</sup> which further affects the cross-linking efficiency. In general, the thiol addition to Dopaquinone appears more efficient compared to other nucleophiles,<sup>122</sup> getting significant attention for biomedical applications.<sup>123</sup> Aryl-coupling of Dopaquinone with another unoxidized Dopa leads to two highly reactive semiquinones, further giving rise to diDopa cross-links.<sup>83, 124-126</sup> Tautomerization of Dopaquinone yields  $\alpha, \beta$ -dehydro-Dopa, which might further participate in forming cross-links (Fig. 11).<sup>127, 128</sup>

At present, cross-linking by means of diDopa<sup>83</sup> and cysteinylDopa<sup>49, 129</sup> has been detected in mussel byssus. The cross-linking of mfp-1 was studied by investigating the oxidation and aggregation rate under different conditions, and a kinetic model was proposed thereof.<sup>11</sup> The Dopa oxidation rate ( $K_{\text{ox}}$ ) and cross-linking rate are strongly dependent on the redox potential (with/without oxidant, iodate) and Dopaquinone dismutation rate ( $K_{\text{dis}}$ ), respectively (Fig. 11).<sup>11</sup> When  $K_{\text{ox}}$  is lower than  $K_{\text{dis}}$ , the cross-linking is more powerful and controlled by  $K_{\text{ox}}$ . When  $K_{\text{ox}}$  exceeds  $K_{\text{dis}}$ , the cross-linking is insufficient owing to rapid consumption of reducing Dopa.<sup>11</sup> These two regimes provide insights into how to control the cross-linking levels by adapting  $K_{\text{ox}}$  as well as  $K_{\text{dis}}$ . Compared to diDopa, cysteinylDopa was detected in two forms in byssal threads of *Perna canaliculus* (*P. canaliculus*): 5-S-cysteinylDopa ( $\geq 1$  mol %) and 2-S-cysteinylDopa (10 times less), which are generated by a thiolate addition to Dopaquinone.<sup>129</sup> Metal ions are deficient in byssal threads of *P. canaliculus*, whereas abundant Cys residues yield cross-linking by means of cysteinylDopa, which is not common in mussels.<sup>129</sup> In addition, 5-S-cysteinylDopa was also discovered at nearly 1 mol % in plaques of *Mytilus californianus*, which is suggested to be associated with plaque curing.<sup>49</sup> A Dopa-functionalized atomic force microscopy (AFM) tip was used to investigate the interaction of Dopa with an organic amine-modified Si surface.<sup>82</sup> The approach and retraction curves revealed an extremely large force with subsequent adhesion abolition, which is in accordance with covalent bond rupture, suggesting formation of Dopa-nitrogen adducts.<sup>82</sup> Dopa-incorporated polymers are considered as good candidates, e.g. for tissue adhesives.

#### 1.4.3 Cation- $\pi$ interactions

Cation- $\pi$  interactions, are present between electron-rich orbitals (e.g. Dopa, Tyr, Trp, Phe) and adjacent cations (e.g. Lys, Arg, His,  $\text{K}^+$ ) and are important non-covalent interactions in living organisms (Fig. 13A).<sup>130-132</sup> Cation- $\pi$  interactions play indispensable roles in physiological activities, such as T cell antigen receptor binding,<sup>133</sup> protein folding,<sup>134</sup> potassium channel blocking,<sup>135, 136</sup> and nicotinic acetylcholine (ACh) signal transmission.<sup>137</sup> The strength of cation- $\pi$  interactions is comparable to that of H-bonds and charge-charge interactions in aqueous solutions.<sup>130, 138, 139</sup>

There are large amounts of aromatic groups (e.g. Dopa, Tyr, Trp) as well as positively charged residues (e.g. Arg, Lys) in mussel foot proteins, reminiscent of the potential existence of cation- $\pi$  interactions, especially for some Dopa-deficient proteins, such as mussel foot protein-1 (pvfp-1) from green mussel *Perna viridis* (*P. viridis*).<sup>68</sup> It is proposed that the cation- $\pi$  interactions between C<sub>2</sub>-mannosyl-7-hydroxytryptophan (Man7OHTrp) and Lys as well as conformational changes contribute most likely to the strong bridging cohesion between pvfp-1 films.<sup>68</sup> Two mfp-1 films without Dopa modification showed strong cohesion as well, which was mainly due to cation- $\pi$  interactions together with other interactions such as  $\pi$ - $\pi$  interactions, H-bonds and van der Waals interactions.<sup>68</sup> There are no detectable cohesion between two poly-L-tyrosine (pTyr) films, suggestive of scanty contributions of  $\pi$ - $\pi$  interaction to the cohesion.<sup>68</sup>

A series of short model peptides, possessing conserved Lys residues as well as substituent aromatic residues X, including Dopa, Tyr, Phe, and Leu (non-aromatic control), were engineered, and corresponding films were generated on mica surfaces by means of self-assembly (Fig. 14A).<sup>70</sup> Since the slope of approaching force-distance profiles is related to the compressibility of films, the three aromatic films showed similar mechanical properties during compression (Fig. 14B). During separation, three aromatic peptides exhibited prominent high adhesion compared to the Leu control (Fig. 14C).<sup>70</sup> The Phe-incorporated peptide showed unexpected adhesion strength based on cation- $\pi$  interactions nearly three times higher than that of Dopa-incorporated peptide, which is consistent with the order of binding strength in previous studies of indole > benzene > phenol (Fig. 14C).<sup>69, 70</sup>

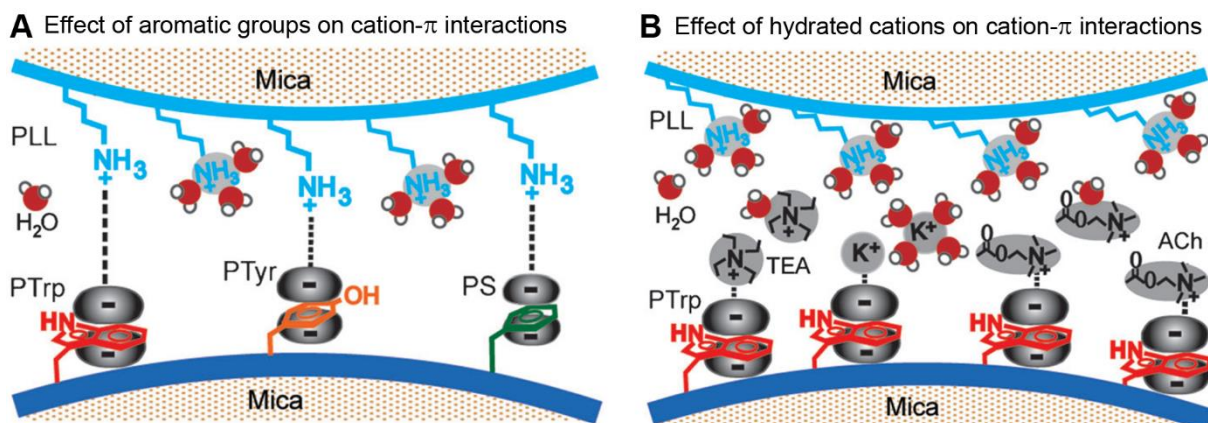


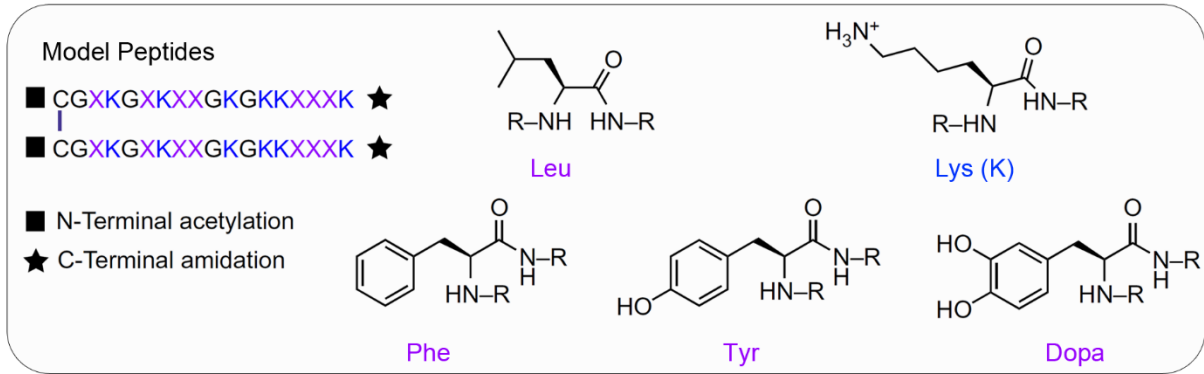
**Figure 13.** Illustration of cation- $\pi$  interactions in aqueous solution. (A) Cation- $\pi$  interactions between positively charged poly-L-lysine (PLL) and aromatic groups of poly-L-tryptophan (PTrp), poly-L-tyrosine (PTyr) and polystyrene (PS). Efficient cation- $\pi$  interactions occur when cations are perpendicular to the plane of benzene rings. Different electron densities of benzene rings in PTrp, PTyr and PS could give rise to a different strength of cation- $\pi$  interactions. (B) Effect of hydrated cations on cation- $\pi$  interactions. The introduced hydrated cations (e.g. K<sup>+</sup>, tetraethylammonium (TEA), nicotinic acetylcholine (ACh)) could compete with positively charged groups of polymers. Reprinted and adapted with permission from Ref. <sup>69</sup>, Copyright 2013, John Wiley and Sons.

The cation- $\pi$  interactions can be affected by other types of cations (e.g. K<sup>+</sup>, Na<sup>+</sup>, NH<sub>4</sub><sup>+</sup>), competing with the positively charged groups by interacting with aromatic groups (Fig. 13B).<sup>68-71</sup> With increasing concentrations of cations, the competition effect increases, thereby screening the bridging adhesion.<sup>68-71</sup> Since the binding energy of mono-valent cations to aromatic groups is mainly subject to the hydration radius of the cations with increasing hydrated radius decreasing the binding strength, the binding strength follows the order of NR<sub>4</sub><sup>+</sup> > NH<sub>3</sub>R<sup>+</sup> > NH<sub>4</sub><sup>+</sup>  $\approx$  K<sup>+</sup> > Na<sup>+</sup> > Li<sup>+</sup> in aqueous solution.<sup>69, 136, 140</sup> The cation- $\pi$  interaction is, therefore, unlikely to

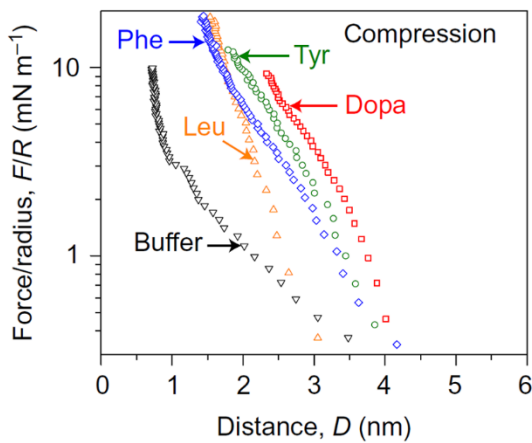
change from acidic pH to ocean pH.<sup>1, 69</sup>

A strong Dopa-mediated adhesion consists of proportional interfacial adhesion and bridging cohesion, whereas unavoidable auto-oxidation gives rise to uncontrollable adhesion loss.<sup>70</sup> The cation- $\pi$  interactions between cations and aromatic residues, especially Phe, provide an additional strategy to complement the bridging cohesion without sacrifice of Dopa.

**A**



**B**



**C**

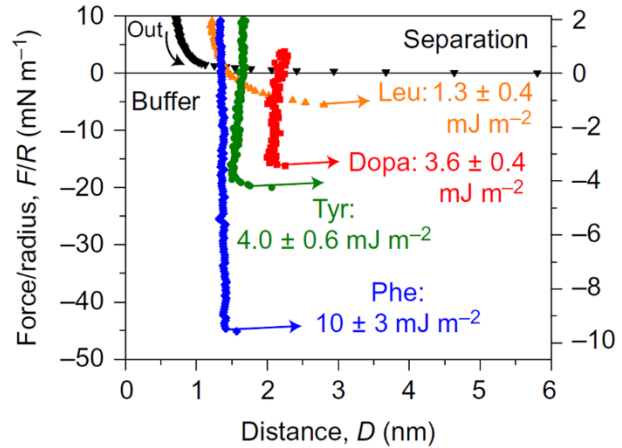


**Figure 14.** (A) Model peptides with both Lys (K) and aromatic residues (X). Besides aromatic residues X (Phe, Tyr, Dopa, Leu (nonaromatic control)), other residues are conserved in all model peptides. Each model peptide possesses one conserved aromatic residue X. The abbreviations of aromatic residues in (B) and (C) represent the corresponding model peptide. Force-distance profiles during approach (B) and separation (C) between two mica surfaces coated with model peptides. Surface forces apparatus (SFA) measurements were performed in pH 2.5 buffer with 100 mM acetic acid and 250 mM  $\text{KNO}_3$ . Reprinted and adapted with permission from Ref.<sup>70</sup>, Copyright 2017, Springer Nature.

## 2. Aims

Mussel byssus, a proteinaceous holdfast, can achieve strong and rapid adhesion on various wet substrates. Numbers of mussel-mimicking tissue adhesives have been inspired recently, whereas none of them exhibit as high wet adhesion as the natural counterpart. To mimic mussel adhesion, getting fundamental understanding of the natural system is an essential prerequisite.

The mussel foot proteins in plaques, e.g. mfp-3, -5, are directly in contact with wet substrates and act as primers in adhesion. The extraordinary high Dopa content in byssus indicates the existence of at least one polyphenol oxidase for post-translational modification of Tyr residues. Both mussel foot proteins in plaques and predicted polyphenol oxidase are vital for understanding the adhesion system. In this work, mussel foot protein 3b (mfp-3b), one predominant protein at the plaque-substrate interface, as well as polyphenol oxidase like protein (PPOL) from *M. galloprovincialis* were investigated. In order to get insight into their contributions to mussel adhesion, this work has been divided into three objectives:

It is not practical to produce mussel-derived proteins by natural extractions due to the low production level and high production cost. Recently, recombinant protein production provides an alternative production method for mussel-derived proteins. Therefore, the first aim was to establish the recombinant production of mfp-3b (rmfp-3b), PPOL (rPPOL) and variants (rP319) thereof by varying cloning constructs, host organisms, fermentation conditions and purification methods.

The next aim was to characterize rmfp-3b at various temperatures, pH, salt ion, and ionic strength conditions. Comparison of rmfp-3b properties at different secretion and seawater conditions should provide insights into the molecular reactivity of rmfp-3b during adhesion, especially how the soluble proteinaceous rmfp-3b can be placed onto wet substrates without dispersion into ambient seawater.

The PPOL shows a high homology to other polyphenol oxidases (PPOs), especially the essential copper-binding sites (CuA and CuB). The catalytic activity of rPPOL at both secretion pH (pH 3.0) and seawater pH (pH 8.0) as well as its contributions to mussel underwater adhesion were investigated.

### 3. Synopsis

This dissertation consists of one first author review ([publication I](#)) and two first author research publications ([publication II](#) and [publication III](#)); the publication list is presented in [section 5](#); my contributions to each publication are listed in [section 6](#).

The current state of recombinant production and application of mussel inspired proteins is comprehensively reviewed and discussed in [publication I](#). [Table 1](#) thereof shows a summary of recombinant mussel-derived proteins produced in different heterogeneous hosts, gene engineering strategies, purification strategies, and post-translational modification strategies. It is promising to produce recombinant mussel inspired proteins and variants thereof in *Escherichia coli* (*E. coli*) with relatively low cost and high efficiency.

Based thereon, production of recombinant mfp-3b ([publication II](#)) and PPOL ([publication III](#)) were carried out in *E. coli* with corresponding optimizations. The particular coacervation process of mfp-3b was investigated under the influence of pH, temperature, and ionic strength relevant to the conditions of protein secretion within glands as well as seawater ([publication II](#)). In the case of PPOL, antioxidant activity of rPPOL was characterized by investigating the influence of pH, amount of free thiols and protein concentrations ([publication III](#)).

#### 3.1 Recombinant production of mussel inspired proteins

The first objective was to produce recombinant mfp-3 and PPOL. Direct extraction from mussels is possible but unpractical for applications due to the low yield ( $\mu\text{g}$  protein/g tissue). Recombinant production, as reviewed in [publication I](#), has therefore been established to overcome this impediment. Recombinant production and application of thread collagenous proteins, thread matrix proteins and mussel foot proteins were reviewed and discussed. Recombinant protein production includes DNA identification from mussels, molecular cloning, fermentation, and protein purification, which needed optimization to get a high production yield ([Figure 15](#)). Bacterial expression hosts are attractive due to high productivity, low costs and easy culture, whereas *in vivo* post-translational modifications, e.g. Tyr to Dopa, are not possible.

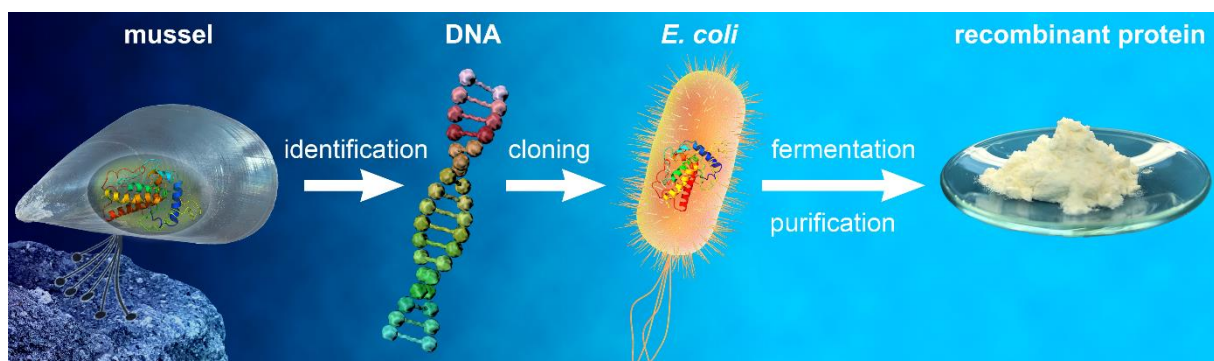


**Figure 15.** Recombinant production of mussel inspired proteins by means of DNA identification from mussel cDNA library, molecular cloning, choice of a suitable expression host (e.g. *E. coli*), fermentation and protein purification. Optimizations are necessary to produce recombinant proteins with high yield.

The gene sequence of mfp-3b of *M. galloprovincialis* was obtained from GenBank (AB049580) ([publication II](#)). rmfp-3b was expressed in insoluble inclusion bodies (IBs) in *E. coli*, and the purification included IB washing, acidic extraction and phase separation. rmfp-3b possesses 18 positively charged residues (shown in green), 2 negatively charged residues (shown in red) and 11 Tyr residues (MGSSHHHHHSQDPNSSDYYGPNYGPSRRWGGYGNRYNGRRYGGYGGYKGNRGRGRRGSWGRRKYNKY, shown in purple). For the initial analysis on Dopa-deficient proteins, it is beneficial to have no further post-translational modification ([section 3.2, publication II](#)).

The gene sequence of PPOL was identified after screening of a foot cDNA library of *M. galloprovincialis* using degenerated PCR primers ([publication III](#)). PPOL shows high homology with other PPOs from different species, especially with 59 % identity to the tyrosinase 2 (GenBank KF318705.1) of green mussel *P. viridis*. rPPOL was expressed in insoluble IBs, which further underwent IB washing and affinity chromatography purifications. rPPOL is composed of 15 Cys residues, ~13 of which are free thiols and ~2 of which are disulfide bonded. A short variant (rP319) was engineered with the C-terminal domain (10 free thiols) removed. Comparative investigations between the full-length and short variants were carried out ([section 3.3, publication III](#)).

### **3.2 Mussel foot protein-3b (mfp-3b) shows coacervation behavior**

Once natural mfp-3b is secreted from mussel foot to seawater, it undergoes a pH jump from pH 2.5 to 8.0, as well as an ionic strength switch from 0.15 M to 0.7 M. Therefore, it was necessary to investigate the influence of pH and salinity to rmfp-3b. The experimental isoelectric point (pI) of rmfp-3b was revealed to be around pH 6.0. At low pH (pH 3.0-4.0), rmfp-3b was positively charged, giving rise to a soluble state.

In the presence of citrate, rmfp-3b showed UCST mediated complex coacervation at pH 3.0. With respect to UCST behavior, there is a cloud point temperature ( $T_{cp}$ ). Upon decreasing temperature, the rmfp-3b solution changed from being transparent ( $T > T_{cp}$ ) to turbid ( $T < T_{cp}$ ), which was reversible upon increasing temperature. The size distribution was also temperature-dependent in virtue of dynamic light scattering (DLS) measurements. Upon cooling/heating, the hydrodynamic diameter  $D_h$  of rmfp-3b increased/decreased, confirming the UCST-mediated coacervation. rmfp-3b is hydrophilic, and decreasing temperature probably reduces the surrounding water shell, but increases hydrogen bonding as well as deprotonation of citrate, which results in increased molecular interactions. The consequence is UCST-mediated coacervation. Imaging of the coacervate phase by optical microscopy and scanning electron microscopy (SEM) revealed spherical droplets between 0.2 and 5  $\mu\text{m}$ . The  $T_{cp}$  of rmfp-3b is highly dependent on protein and citrate concentrations. The entanglement of protein chains is favored at high protein concentrations. Increasing concentrations of protein and citrate give rise to an increased  $T_{cp}$ . With increasing citrate concentration (above 100 mM), coacervation of rmfp-3b (5 mg mL<sup>-1</sup>) was identified without UCST behavior.

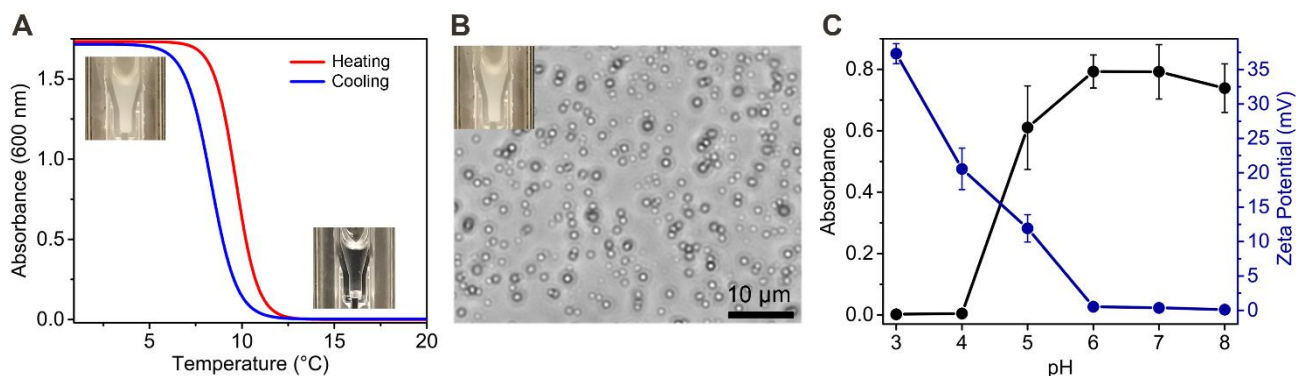


**Figure 16.** (A) Turbidity measurements of *rmfp-3b* ( $5 \text{ mg ml}^{-1}$ ,  $20 \text{ mM}$  citrate buffer,  $\text{pH } 3.0$ ) with increasing/decreasing temperature. The inset photographs show transparency/turbidity at a temperature above/beneath  $T_{cp}$  ( $\sim 7 \text{ }^\circ\text{C}$  under this condition). (B) Optical microscopy image of the turbid sample from (A) showing granular coacervates. (C) Turbidity and zeta potential of *rmfp-3b* as a function of pH at  $20 \text{ }^\circ\text{C}$ . The turbidity was measured at  $600 \text{ nm}$ . Error bars indicate the standard deviation ( $n=3$ ). Reprinted and adapted with permission from [publication II](#),<sup>141</sup> Copyright 2018, American Chemical Society.

pH elevation by pipetting soluble *mfp-3b* ( $\text{pH } 3.0$ ) into  $\text{pH } 8.0$  buffer can trigger the coacervation as well, resulting in an immediate liquid-liquid phase separation, but without showing UCST behavior. Upon elevation of pH, the acidic residues of *mfp-3b* get deprotonated, which results in formation of zwitterions with increased electrostatic attractions, thereby increasing the intermolecular interactions and yielding a coacervate. Compared to UCST-mediated coacervate at  $\text{pH } 3.0$ , pH elevation mediated coacervate was more accumulated. Low molarity of multivalent anions (e.g. sulfate and citrate salts) are proposed to form complex coacervation with *rmfp-3b*, whereas high molarity of monovalent anions (e.g. chloride salts) can screen the long-range electrostatic repulsions, both advancing intermolecular interactions. The optimal coacervation conditions at  $\text{pH } 8.0$  were close to the seawater composition, suggesting seawater could be a natural coacervation regulator.

Multivalent anions at low concentrations can give rise to prominent coacervation, reminiscing that *mfp-3b* is probably secreted from the acidic secretory granules as condensed coacervate with multivalent anions, such as sulfate. By means of coacervate, secretion and spreading on wet substrates are beneficial due to its specific properties, such as shear-thinning behavior and low interfacial energy. Upon an exposure to seawater at elevated pH and ionic strength, a condensed coacervate of *mfp-3b* is formed due to increased intermolecular interactions. By this way, *mfp-3b* can settle on wet substrates without dispersion into the surrounding seawater.

### 3.3 Mussel polyphenol oxidase-like protein (PPOL) shows antioxidant activity

The catalytic activities of rPPOL and rP319, including tyrosinase and catecholase activity, could not be identified during this study. Considering the acidic secretion pH, the post translational modification of Tyr residues to Dopa mostly occurs at acidic secretion pH. Copper has a poor coordination with His at  $\text{pH } 3.0$ , which might cause inactivation of rPPOL. Presumably, a particular metallochaperone is required to accommodate copper ions within the His catalytic center. On the other hand, PPOL might not possess polyphenol oxidase activity.

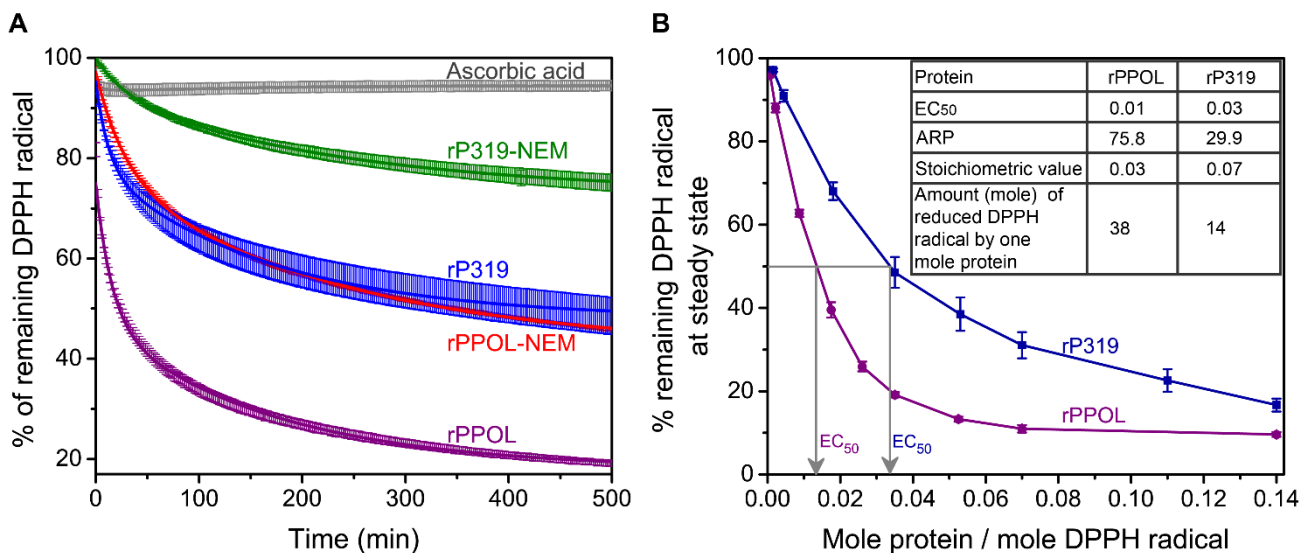


**Figure 16.** Radical scavenging of rPPOL and variants thereof using the 2,2-diphenyl-1-picrylhydrazyl (DPPH) assay. (A) Kinetics of DPPH radical (100  $\mu$ M) quenching by rPPOL and variants thereof at identical molar concentrations (3.5  $\mu$ M) at pH 3.0 and 20 °C. Ascorbic acid was used as a positive control. (B) Extrapolated percentage (%) of remaining DPPH radical at 500 min (steady state) at different protein (rPPOL and rP319) concentrations. Half-maximal effective concentration (EC<sub>50</sub>), were calculated from the curves. The inset table exhibits the EC<sub>50</sub>, APR (1/EC<sub>50</sub>, antiradical power), stoichiometric value (2\*EC<sub>50</sub>) and the amount (mole) of reduced DPPH by one mole protein (1/stoichiometric value). Error bars indicate the standard deviation (n=3). Reprinted and adapted with permission from [publication III](#),<sup>142</sup> Copyright 2019, Elsevier.

rPPOL or rP319 was capable of inhibiting Dopa oxidation to some extent. rPPOL with ~13 free thiols exhibited stronger inhibition than rP319 with ~3 free thiols, reminiscent of free thiols as probably contributors. To confirm this, free thiols of rPPOL and rP319 were alkylated using N-Ethylmaleimide (NEM), yielding thiol-blocked variants rPPOL-NEM and rP319-NEM. In comparison, both rPPOL-NEM and rP319-NEM showed weak inhibition of Dopa oxidation, suggesting that rPPOL probably works as a thiol-based antioxidant.

An optimized 2,2-diphenyl-1-picrylhydrazyl (DPPH) assay was taken to determine the antioxidant activity in this study. DPPH with free radicals exhibited maximal absorption at 515 nm, which gradually reduced upon addition of rPPOL variants. The rPPOL with the most thiols showed the fastest initial decay and maximum reductive capacity, whereas rP319-NEM with the least thiols exhibited the slowest initial decay and the minimum reductive capacity. Alkylated rPPOL variants still exhibited non-negligible reductive capacity, which might be due to the incomplete alkylation of thiols and/or unidentified reductive groups. With respect to antiradical power (APR, 1/EC<sub>50</sub>), that of rPPOL was ~2.5 times higher than that of rP319 and ~6 times higher than that of gallic acid. One molecule rPPOL is capable of reducing 38 DPPH radicals, indicating that there should be other reactive groups besides 13 free thiols devoting to the antioxidant activity. Considering the antioxidant property, PPOL probably locates at the plaque-substrate interface to protect Dopa from oxidation, like mfp-6; however, verification of the location of PPOL needs further investigations.

To sum up, the mussel foot protein mfp-3b in plaques reveals coacervation property at conditions of protein secretion within glands as well as seawater. The polyphenol oxidase like protein PPOL exhibits antioxidant activity, protecting Dopa from oxidation. This work provides insights into understanding byssus assembly, which advances the development of novel adhesives by means of mimicking the natural system.

## 4. References

1. J. H. Waite, Mussel adhesion - essential footwork. *Journal of Experimental Biology* **2017**, 220(4), 517-530.
2. B. P. Lee, P. B. Messersmith, J. N. Israelachvili, J. H. Waite, Mussel-inspired adhesives and coatings. *Annual review of materials research* **2011**, 41 99-132.
3. R. J. Stewart, J. C. Weaver, D. E. Morse, J. H. Waite, The tube cement of *Phragmatopoma californica*: a solid foam. *Journal of Experimental Biology* **2004**, 207(26), 4727-4734.
4. Y. Tan, S. Hoon, P. A. Guerette, W. Wei, A. Ghadban, C. Hao, A. Miserez, J. H. Waite, Infiltration of chitin by protein coacervates defines the squid beak mechanical gradient. *Nature chemical biology* **2015**, 11(7), 488.
5. H. Shao, K. N. Bachus, R. J. Stewart, A water-borne adhesive modeled after the sandcastle glue of *P. californica*. *Macromolecular bioscience* **2009**, 9(5), 464-471.
6. J. H. Waite, M. L. Tanzer, Polyphenolic substance of *Mytilus edulis*: Novel adhesive containing L-Dopa and hydroxyproline. *Science* **1981**, 212(4498), 1038-1040.
7. M. Yu, J. Hwang, T. J. Deming, Role of L-3, 4-dihydroxyphenylalanine in mussel adhesive proteins. *Journal of the American Chemical Society* **1999**, 121(24), 5825-5826.
8. V. V. Papov, T. V. Diamond, K. Biemann, J. H. Waite, Hydroxyarginine-containing polyphenolic proteins in the adhesive plaques of the marine mussel *Mytilus edulis*. *Journal of Biological Chemistry* **1995**, 270(34), 20183-20192.
9. J. H. Waite, Adhesion a la moule. *Integrative and comparative biology* **2002**, 42(6), 1172-1180.
10. P. Kord Forooshani, B. P. Lee, Recent approaches in designing bioadhesive materials inspired by mussel adhesive protein. *Journal of Polymer Science Part A: Polymer Chemistry* **2017**, 55(1), 9-33.
11. S. Haemers, G. J. M. Koper, G. Frens, Effect of oxidation rate on cross-linking of mussel adhesive proteins. *Biomacromolecules* **2003**, 4(3), 632-640.
12. J. Yu, W. Wei, E. Danner, J. N. Israelachvili, J. H. Waite, Effects of interfacial redox in mussel adhesive protein films on mica. *Advanced materials* **2011**, 23(20), 2362-2366.
13. E. W. Danner, Y. Kan, M. U. Hammer, J. N. Israelachvili, J. H. Waite, Adhesion of mussel foot protein Mefp-5 to mica: an underwater superglue. *Biochemistry* **2012**, 51(33), 6511-6518.
14. W. Wei, J. Yu, C. Broomell, J. N. Israelachvili, J. H. Waite, Hydrophobic enhancement of dopa-mediated adhesion in a mussel foot protein. *Journal of the American Chemical Society* **2012**, 135(1), 377-383.
15. K. W. Desmond, N. A. Zacchia, J. H. Waite, M. T. Valentine, Dynamics of mussel plaque detachment. *Soft Matter* **2015**, 11(34), 6832-6839.
16. J. Yu, W. Wei, E. Danner, R. K. Ashley, J. N. Israelachvili, J. H. Waite, Mussel protein adhesion depends on interprotein thiol-mediated redox modulation. *Nature chemical biology* **2011**, 7(9), 588.
17. T. J. Deming, Mussel byssus and biomolecular materials. *Current opinion in chemical biology* **1999**, 3(1), 100-105.
18. J. H. Waite, X.-X. Qin, K. J. Coyne, The peculiar collagens of mussel byssus. *Matrix Biology* **1998**, 17(2), 93-106.
19. K. J. Coyne, X.-X. Qin, J. H. Waite, Extensible collagen in mussel byssus: a natural block copolymer. *Science* **1997**, 277(5333), 1830-1832.

20. A. Tamarin, P. Lewis, J. Askey, The structure and formation of the byssus attachment plaque in *Mytilus*. *Journal of morphology* **1976**, 149(2), 199-221.
21. N. Holten-Andersen, G. E. Fantner, S. Hohlbauch, J. H. Waite, F. W. Zok, Protective coatings on extensible biofibres. *Nature materials* **2007**, 6(9), 669.
22. N. Holten-Andersen, T. E. Mates, M. S. Toprak, G. D. Stucky, F. W. Zok, J. H. Waite, Metals and the integrity of a biological coating: the cuticle of mussel byssus. *Langmuir* **2008**, 25(6), 3323-3326.
23. M. J. Harrington, A. Masic, N. Holten-Andersen, J. H. Waite, P. Fratzl, Iron-clad fibers: a metal-based biological strategy for hard flexible coatings. *Science* **2010**, 328(5975), 216-220.
24. L. M. Rzepecki, K. M. Hansen, J. H. Waite, Characterization of a cystine-rich polyphenolic protein family from the blue mussel *Mytilus edulis* L. *The Biological Bulletin* **1992**, 183(1), 123-137.
25. J. H. Waite, Evidence for a repeating 3, 4-dihydroxyphenylalanine-and hydroxyproline-containing decapeptide in the adhesive protein of the mussel, *Mytilus edulis* L. *Journal of Biological Chemistry* **1983**, 258(5), 2911-2915.
26. T. Priemel, E. Degtyar, M. N. Dean, M. J. Harrington, Rapid self-assembly of complex biomolecular architectures during mussel byssus biofabrication. *Nature communications* **2017**, 8 14539.
27. E. Filippidi, D. G. DeMartini, P. Malo de Molina, E. W. Danner, J. Kim, M. E. Helgeson, J. H. Waite, M. T. Valentine, The microscopic network structure of mussel (*Mytilus*) adhesive plaques. *Journal of The Royal Society Interface* **2015**, 12(113), 20150827.
28. C. V. Benedict, J. H. Waite, Composition and ultrastructure of the byssus of *Mytilus edulis*. *Journal of morphology* **1986**, 189(3), 261-270.
29. E. Hennebert, P. Viville, R. Lazzaroni, P. Flammang, Micro- and nanostructure of the adhesive material secreted by the tube feet of the sea star *Asterias rubens*. *Journal of structural biology* **2008**, 164(1), 108-118.
30. R. Santos, S. Gorb, V. Jamar, P. Flammang, Adhesion of echinoderm tube feet to rough surfaces. *Journal of Experimental Biology* **2005**, 208(13), 2555-2567.
31. C. J. Ong, M. Wong, J. Smit, Attachment of the adhesive holdfast organelle to the cellular stalk of *Caulobacter crescentus*. *Journal of bacteriology* **1990**, 172(3), 1448-1456.
32. D. Bodenmiller, E. Toh, Y. V. Brun, Development of surface adhesion in *Caulobacter crescentus*. *Journal of bacteriology* **2004**, 186(5), 1438-1447.
33. R. L. Fletcher, M. E. Callow, The settlement, attachment and establishment of marine algal spores. *British phycological journal* **1992**, 27(3), 303-329.
34. S. N. Gorb, M. Varenberg, Mushroom-shaped geometry of contact elements in biological adhesive systems. *Journal of Adhesion Science and Technology* **2007**, 21(12-13), 1175-1183.
35. S. Gorb, M. Varenberg, A. Peressadko, J. Tuma, Biomimetic mushroom-shaped fibrillar adhesive microstructure. *Journal of The Royal Society Interface* **2006**, 4(13), 271-275.
36. G. Carbone, E. Pierro, S. N. Gorb, Origin of the superior adhesive performance of mushroom-shaped microstructured surfaces. *Soft Matter* **2011**, 7(12), 5545-5552.
37. L. Heepe, S. N. Gorb, Biologically inspired mushroom-shaped adhesive microstructures. *Annual review of materials research* **2014**, 44 173-203.
38. A. Spuskanyuk, R. McMeeking, V. Deshpande, E. Arzt, The effect of shape on the adhesion of fibrillar surfaces. *Acta biomaterialia* **2008**, 4(6), 1669-1676.
39. M. Varenberg, S. Gorb, A beetle-inspired solution for underwater adhesion. *Journal of The Royal*

- Society Interface* **2007**, 5(20), 383-385.
40. E. Kizilkan, L. Heepe, S. Gorb, Underwater adhesion of mushroom-shaped adhesive microstructure: An air-entrapment effect. The Royal Society of Chemistry: Cambridge, UK**2013**.
  41. N. Hosoda, S. N. Gorb, Underwater locomotion in a terrestrial beetle: combination of surface de-wetting and capillary forces. *Proceedings of the Royal Society B: Biological Sciences* **2012**, 279(1745), 4236-4242.
  42. A. Hagenau, M. H. Suhre, T. R. Scheibel, Nature as a blueprint for polymer material concepts: Protein fiber-reinforced composites as holdfasts of mussels. *Progress in Polymer Science* **2014**, 39(8), 1564-1583.
  43. J. H. Waite, N. H. Andersen, S. Jewhurst, C. Sun, Mussel adhesion: finding the tricks worth mimicking. *The journal of adhesion* **2005**, 81(3-4), 297-317.
  44. N. Bandara, H. Zeng, J. Wu, Marine mussel adhesion: biochemistry, mechanisms, and biomimetics. *Journal of Adhesion Science and Technology* **2013**, 27(18-19), 2139-2162.
  45. K. Inoue, Y. Takeuchi, D. Miki, S. Odo, Mussel adhesive plaque protein gene is a novel member of epidermal growth factor-like gene family. *Journal of Biological Chemistry* **1995**, 270(12), 6698-6701.
  46. S. Warner, J. Waite, Expression of multiple forms of an adhesive plaque protein in an individual mussel, *Mytilus edulis*. *Marine Biology* **1999**, 134(4), 729-734.
  47. H. Zhao, J. H. Waite, Proteins in load-bearing junctions: the histidine-rich metal-binding protein of mussel byssus. *Biochemistry* **2006**, 45(47), 14223-14231.
  48. H. Zhao, N. B. Robertson, S. A. Jewhurst, J. H. Waite, Probing the adhesive footprints of *Mytilus californianus* byssus. *Journal of Biological Chemistry* **2006**, 281(16), 11090-11096.
  49. H. Zhao, J. H. Waite, Linking adhesive and structural proteins in the attachment plaque of *Mytilus californianus*. *Journal of Biological Chemistry* **2006**, 281(36), 26150-26158.
  50. J. H. Waite, X. Qin, Polyphosphoprotein from the adhesive pads of *Mytilus edulis*. *Biochemistry* **2001**, 40(9), 2887-2893.
  51. S. C. Nicklisch, J. E. Spahn, H. Zhou, C. M. Gruian, J. H. Waite, Redox capacity of an extracellular matrix protein associated with adhesion in *Mytilus californianus*. *Biochemistry* **2016**, 55(13), 2022-2030.
  52. C. Brown, Some structural proteins of *Mytilus edulis*. *Journal of Cell Science* **1952**, 3(24), 487-502.
  53. A. Tamarin, P. Keller, An ultrastructural study of the byssal thread forming system in *Mytilus*. *Journal of ultrastructure research* **1972**, 40(3-4), 401-416.
  54. N. R. Martinez Rodriguez, S. Das, Y. Kaufman, J. N. Israelachvili, J. H. Waite, Interfacial pH during mussel adhesive plaque formation. *Biofouling* **2015**, 31(2), 221-227.
  55. C. G. De Kruif, F. Weinbreck, R. de Vries, Complex coacervation of proteins and anionic polysaccharides. *Current opinion in colloid & interface science* **2004**, 9(5), 340-349.
  56. H. Bungenberg de Jong, H. Kruyt, Colloid science. *Kruyt, H, Ed* **1949**, 335-432.
  57. S. Boeynaems, S. Alberti, N. L. Fawzi, T. Mittag, M. Polymenidou, F. Rousseau, J. Schymkowitz, J. Shorter, B. Wolozin, L. Van Den Bosch, Protein phase separation: a new phase in cell biology. *Trends in cell biology* **2018**, 28(6), 420-435.
  58. Y. Shin, C. P. Brangwynne, Liquid phase condensation in cell physiology and disease. *Science* **2017**, 357(6357), 4382.
  59. K.-Y. Huang, H. Y. Yoo, Y. Jho, S. Han, D. S. Hwang, Bicontinuous fluid structure with low cohesive

- energy: molecular basis for exceptionally low interfacial tension of complex coacervate fluids. *ACS nano* **2016**, 10(5), 5051-5062.
60. S. Kim, H. Y. Yoo, J. Huang, Y. Lee, S. Park, Y. Park, S. Jin, Y. M. Jung, H. Zeng, D. S. Hwang, Salt triggers the simple coacervation of an underwater adhesive when cations meet aromatic  $\pi$  electrons in seawater. *ACS nano* **2017**, 11(7), 6764-6772.
61. W. Wei, Y. Tan, N. R. M. Rodriguez, J. Yu, J. N. Israelachvili, J. H. Waite, A mussel-derived one component adhesive coacervate. *Acta biomaterialia* **2014**, 10(4), 1663-1670.
62. R. J. Stewart, C. S. Wang, I. T. Song, J. P. Jones, The role of coacervation and phase transitions in the sandcastle worm adhesive system. *Advances in colloid and interface science* **2017**, 239 88-96.
63. N. Lebesgue, G. Da Costa, R. M. Ribeiro, C. Ribeiro-Silva, G. G. Martins, V. Matranga, A. Scholten, C. Cordeiro, A. J. Heck, R. Santos, Deciphering the molecular mechanisms underlying sea urchin reversible adhesion: a quantitative proteomics approach. *Journal of proteomics* **2016**, 138 61-71.
64. D. R. Miller, S. Das, K.-Y. Huang, S. Han, J. N. Israelachvili, J. H. Waite, Mussel coating protein-derived complex coacervates mitigate frictional surface damage. *ACS biomaterials science & engineering* **2015**, 1(11), 1121-1128.
65. S. Lim, Y. S. Choi, D. G. Kang, Y. H. Song, H. J. Cha, The adhesive properties of coacervated recombinant hybrid mussel adhesive proteins. *Biomaterials* **2010**, 31(13), 3715-3722.
66. D. S. Hwang, H. Zeng, A. Srivastava, D. V. Krogstad, M. Tirrell, J. N. Israelachvili, J. H. Waite, Viscosity and interfacial properties in a mussel-inspired adhesive coacervate. *Soft Matter* **2010**, 6(14), 3232-3236.
67. W. Wei, L. Petrone, Y. Tan, H. Cai, J. N. Israelachvili, A. Miserez, J. H. Waite, An Underwater Surface-Drying Peptide Inspired by a Mussel Adhesive Protein. *Advanced Functional Materials* **2016**, 26(20), 3496-3507.
68. D. S. Hwang, H. Zeng, Q. Lu, J. Israelachvili, J. H. Waite, Adhesion mechanism in a DOPA-deficient foot protein from green mussels. *Soft Matter* **2012**, 8(20), 5640-5648.
69. Q. Lu, D. X. Oh, Y. Lee, Y. Jho, D. S. Hwang, H. Zeng, Nanomechanics of cation- $\pi$  interactions in aqueous solution. *Angewandte Chemie* **2013**, 125(14), 4036-4040.
70. M. A. Gebbie, W. Wei, A. M. Schrader, T. R. Cristiani, H. A. Dobbs, M. Idso, B. F. Chmelka, J. H. Waite, J. N. Israelachvili, Tuning underwater adhesion with cation- $\pi$  interactions. *Nature chemistry* **2017**, 9(5), 473.
71. S. Kim, A. Faghihnejad, Y. Lee, Y. Jho, H. Zeng, D. S. Hwang, Cation- $\pi$  interaction in DOPA-deficient mussel adhesive protein mfp-1. *Journal of Materials Chemistry B* **2015**, 3(5), 738-743.
72. S. Kim, J. Huang, Y. Lee, S. Dutta, H. Y. Yoo, Y. M. Jung, Y. Jho, H. Zeng, D. S. Hwang, Complexation and coacervation of like-charged polyelectrolytes inspired by mussels. *Proceedings of the National Academy of Sciences* **2016**, 113(7), E847-E853.
73. B. Halliwell, J. M. Gutteridge, Free radicals in biology and medicine. Oxford University Press, USA **2015**.
74. I. Fridovich, Superoxide radical and superoxide dismutases. *Annual review of biochemistry* **1995**, 64(1), 97-112.
75. D. Livingstone, Oxidative stress in aquatic organisms in relation to pollution and aquaculture. *Revue de Medecine Veterinaire* **2003**, 154(6), 427-430.
76. L. E. S. Netto, M. A. de Oliveira, G. Monteiro, A. P. D. Demasi, J. R. R. Cussiol, K. F. Discola, M. Demasi, G. M. Silva, S. V. Alves, V. G. Faria, Reactive cysteine in proteins: protein folding, antioxidant

- defense, redox signaling and more. *Comparative Biochemistry and Physiology Part C: Toxicology & Pharmacology* **2007**, 146(1-2), 180-193.
77. D. R. Miller, J. E. Spahn, J. H. Waite, The staying power of adhesion-associated antioxidant activity in *Mytilus californianus*. *Journal of The Royal Society Interface* **2015**, 12(111), 20150614.
78. Y. Akdogan, W. Wei, K.-Y. Huang, Y. Kageyama, E. W. Danner, D. R. Miller, N. R. Martinez Rodriguez, J. H. Waite, S. Han, Intrinsic Surface-Drying Properties of Bioadhesive Proteins. *Angewandte Chemie International Edition* **2014**, 53(42), 11253-11256.
79. G. P. Maier, M. V. Rapp, J. H. Waite, J. N. Israelachvili, A. Butler, Adaptive synergy between catechol and lysine promotes wet adhesion by surface salt displacement. *Science* **2015**, 349(6248), 628-632.
80. J. Yu, W. Wei, M. S. Menyo, A. Masic, J. H. Waite, J. N. Israelachvili, Adhesion of mussel foot protein-3 to TiO<sub>2</sub> surfaces: the effect of pH. *Biomacromolecules* **2013**, 14(4), 1072-1077.
81. J. N. Israelachvili, Intermolecular and surface forces. Academic press **2011**.
82. H. Lee, N. F. Scherer, P. B. Messersmith, Single-molecule mechanics of mussel adhesion. *Proceedings of the National Academy of Sciences* **2006**, 103(35), 12999-13003.
83. L. M. McDowell, L. A. Burzio, J. H. Waite, J. Schaefer, Rotational echo double resonance detection of cross-links formed in mussel byssus under high-flow stress. *Journal of Biological Chemistry* **1999**, 274(29), 20293-20295.
84. J. Yu, Y. Kan, M. Rapp, E. Danner, W. Wei, S. Das, D. R. Miller, Y. Chen, J. H. Waite, J. N. Israelachvili, Adaptive hydrophobic and hydrophilic interactions of mussel foot proteins with organic thin films. *Proceedings of the National Academy of Sciences* **2013**, 110(39), 15680-15685.
85. W. Wei, J. Yu, M. A. Gebbie, Y. Tan, N. R. Martinez Rodriguez, J. N. Israelachvili, J. H. Waite, Bridging Adhesion of mussel-inspired peptides: role of charge, chain length, and surface type. *Langmuir* **2015**, 31(3), 1105-1112.
86. Q. Lu, E. Danner, J. H. Waite, J. N. Israelachvili, H. Zeng, D. S. Hwang, Adhesion of mussel foot proteins to different substrate surfaces. *Journal of The Royal Society Interface* **2013**, 10(79), 20120759.
87. D. S. Hwang, H. Zeng, A. Masic, M. J. Harrington, J. N. Israelachvili, J. H. Waite, Protein-and metal-dependent interactions of a prominent protein in mussel adhesive plaques. *Journal of Biological Chemistry* **2010**, 285(33), 25850-25858.
88. S. George, B. Pirie, T. Coombs, The kinetics of accumulation and excretion of ferric hydroxide in *Mytilus edulis* and its distribution in the tissues. *Journal of Experimental Marine Biology and Ecology* **1976**, 23(1), 71-84.
89. R.-. Pentreath, The accumulation from water of 65 Zn, 54 Mn, 58 Co and 59 Fe by the mussel, *Mytilus edulis*. *Journal of the Marine Biological Association of the United Kingdom* **1973**, 53(1), 127-143.
90. R. J. Pentreath, The accumulation from sea water of 65 Zn, 54 Mn, 58 Co and 59 Fe by the thornback ray, *Raja clavata* L. *Journal of Experimental Marine Biology and Ecology* **1973**, 12(3), 327-334.
91. R. J. Pentreath, The accumulation and retention of 59 Fe and 58 Co by the plaice, *Pleuronectes platessa* L. *Journal of Experimental Marine Biology and Ecology* **1973**, 12(3), 315-326.
92. J. Monahan, J. J. Wilker, Specificity of metal ion cross-linking in marine mussel adhesives. *Chemical Communications* **2003**, (14), 1672-1673.
93. J. Monahan, J. J. Wilker, Cross-linking the protein precursor of marine mussel adhesives: bulk measurements and reagents for curing. *Langmuir* **2004**, 20(9), 3724-3729.
94. M. J. Sever, J. T. Weisser, J. Monahan, S. Srinivasan, J. J. Wilker, Metal - mediated cross - linking in

- the generation of a marine - mussel adhesive. *Angewandte Chemie International Edition* **2004**, 43(4), 448-450.
95. H. Zeng, D. S. Hwang, J. N. Israelachvili, J. H. Waite, Strong reversible Fe<sup>3+</sup>-mediated bridging between dopa-containing protein films in water. *Proceedings of the National Academy of Sciences* **2010**, 107(29), 12850-12853.
96. S. W. Taylor, G. W. Luther III, J. H. Waite, Polarographic and spectrophotometric investigation of iron (III) complexation to 3, 4-dihydroxyphenylalanine-containing peptides and proteins from *Mytilus edulis*. *Inorganic Chemistry* **1994**, 33(25), 5819-5824.
97. S. W. Taylor, D. B. Chase, M. H. Emptage, M. J. Nelson, J. H. Waite, Ferric ion complexes of a DOPA-containing adhesive protein from *Mytilus edulis*. *Inorganic Chemistry* **1996**, 35(26), 7572-7577.
98. B. J. Kim, D. X. Oh, S. Kim, J. H. Seo, D. S. Hwang, A. Masic, D. K. Han, H. J. Cha, Mussel-mimetic protein-based adhesive hydrogel. *Biomacromolecules* **2014**, 15(5), 1579-1585.
99. R. H. Holm, P. Kennepohl, E. I. Solomon, Structural and functional aspects of metal sites in biology. *Chemical reviews* **1996**, 96(7), 2239-2314.
100. N. Holten-Andersen, M. J. Harrington, H. Birkedal, B. P. Lee, P. B. Messersmith, K. Y. C. Lee, J. H. Waite, pH-induced metal-ligand cross-links inspired by mussel yield self-healing polymer networks with near-covalent elastic moduli. *Proceedings of the National Academy of Sciences* **2011**, 108(7), 2651-2655.
101. V. M. Nurchi, T. Pivetta, J. I. Lachowicz, G. Crisponi, Effect of substituents on complex stability aimed at designing new iron (III) and aluminum (III) chelators. *Journal of inorganic biochemistry* **2009**, 103(2), 227-236.
102. J. Yang, M. A. C. Stuart, M. Kamperman, Jack of all trades: versatile catechol crosslinking mechanisms. *Chemical Society Reviews* **2014**, 43(24), 8271-8298.
103. V. Tomišić, S. Blanc, M. Elhabiri, D. Expert, A.-M. Albrecht-Gary, Iron (III) uptake and release by chrysoactin, a siderophore of the phytopathogenic bacterium *Erwinia chrysanthemi*. *Inorganic Chemistry* **2008**, 47(20), 9419-9430.
104. A. Butler, Acquisition and utilization of transition metal ions by marine organisms. *Science* **1998**, 281(5374), 207-209.
105. M. Mochizuki, S.-i. Yamazaki, K. Kano, T. Ikeda, Kinetic analysis and mechanistic aspects of autoxidation of catechins. *Biochimica et Biophysica Acta (BBA)-General Subjects* **2002**, 1569(1-3), 35-44.
106. V. Roginsky, A. E. Alegria, Oxidation of tea extracts and tea catechins by molecular oxygen. *Journal of agricultural and food chemistry* **2005**, 53(11), 4529-4535.
107. E. Mentasti, E. Pelizzetti, Reactions between iron (III) and catechol (o-dihydroxybenzene). Part I. Equilibria and kinetics of complex formation in aqueous acid solution. *Journal of the Chemical Society, Dalton Transactions* **1973**, (23), 2605-2608.
108. E. Mentasti, E. Pelizzetti, G. Saini, Reactions between iron (III) and catechol (o-dihydroxybenzene). Part II. Equilibria and kinetics of the redox reaction in aqueous acid solution. *Journal of the Chemical Society, Dalton Transactions* **1973**, (23), 2609-2614.
109. L. Burdine, T. G. Gillette, H.-J. Lin, T. Kodadek, Periodate-triggered cross-linking of dopa-containing peptide-protein complexes. *Journal of the American Chemical Society* **2004**, 126(37), 11442-11443.
110. J. H. Waite, Catechol oxidase in the byssus of the common mussel, *Mytilus edulis* L. *Journal of the*

- Marine Biological Association of the United Kingdom* **1985**, 65(2), 359-371.
111. J. Smyth, A technique for the histochemical demonstration of polyphenol oxidase and its application to egg-shell formation in helminths and byssus formation in *Mytilus*. *Journal of Cell Science* **1954**, 3(30), 139-152.
112. B. P. Lee, J. L. Dalsin, P. B. Messersmith, Synthesis and gelation of DOPA-modified poly (ethylene glycol) hydrogels. *Biomacromolecules* **2002**, 3(5), 1038-1047.
113. J. C. Danilewicz, Review of reaction mechanisms of oxygen and proposed intermediate reduction products in wine: Central role of iron and copper. *American Journal of Enology and Viticulture* **2003**, 54(2), 73-85.
114. C. A. Ramsden, P. A. Riley, Studies of the competing rates of catechol oxidation and suicide inactivation of tyrosinase. *Arkivoc* **2010**, 10 248-254.
115. C. J. Cooksey, P. J. Garratt, E. J. Land, S. Pavel, C. A. Ramsden, P. A. Riley, N. P. Smit, Evidence of the indirect formation of the catecholic intermediate substrate responsible for the autoactivation kinetics of tyrosinase. *Journal of Biological Chemistry* **1997**, 272(42), 26226-26235.
116. M. C. van der Leeden, Are conformational changes, induced by osmotic pressure variations, the underlying mechanism of controlling the adhesive activity of mussel adhesive proteins? *Langmuir* **2005**, 21(24), 11373-11379.
117. E. Mentasti, E. Pelizzetti, C. Baiocchi, Interactions of Fe (III) with adrenaline, L-dopa and other catechol derivatives: Electron-exchange kinetics and mechanism in acidic perchlorate media. *Journal of Inorganic and Nuclear Chemistry* **1976**, 38(11), 2017-2021.
118. D. E. Fullenkamp, D. G. Barrett, D. R. Miller, J. W. Kurutz, P. B. Messersmith, pH-dependent cross-linking of catechols through oxidation via Fe<sup>3+</sup> and potential implications for mussel adhesion. *RSC advances* **2014**, 4(48), 25127-25134.
119. D. G. Barrett, D. E. Fullenkamp, L. He, N. Holten - Andersen, K. Y. C. Lee, P. B. Messersmith, pH - Based regulation of hydrogel mechanical properties through mussel - inspired chemistry and processing. *Advanced Functional Materials* **2013**, 23(9), 1111-1119.
120. D. P. Nair, M. Podgorski, S. Chatani, T. Gong, W. Xi, C. R. Fenoli, C. N. Bowman, The thiol-Michael addition click reaction: a powerful and widely used tool in materials chemistry. *Chemistry of Materials* **2013**, 26(1), 724-744.
121. M. G. Peter, Chemical modifications of biopolymers by quinones and quinone methides. *Angewandte Chemie International Edition in English* **1989**, 28(5), 555-570.
122. G. Dryhurst, Biological electrochemistry. Elsevier **2012**.
123. D. P. Nair, M. Podgórski, S. Chatani, T. Gong, W. Xi, C. R. Fenoli, C. N. Bowman, The thiol-michael addition click reaction: a powerful and widely used tool in materials chemistry. *Chemistry of Materials* **2014**, 26(1), 724-744.
124. G. P. Maier, A. Butler, Siderophores and mussel foot proteins: the role of catechol, cations, and metal coordination in surface adhesion. *JBIC Journal of Biological Inorganic Chemistry* **2017**, 22(5), 739-749.
125. J. Sagert, C. Sun, Chemical subtleties of mussel and polychaete holdfasts. Biological adhesives, Springer **2006**, pp. 125-143.
126. B. Feringa, H. Wynberg, Biomimetic asymmetric oxidative coupling of phenols. *Bioorganic Chemistry* **1978**, 7(4), 397-408.

127. L. M. Rzepecki, T. Nagafuchi, J. H. Waite,  $\alpha$ ,  $\beta$ -Dehydro-3, 4-dihydroxyphenylalanine derivatives: potential sclerotization intermediates in natural composite materials. *Archives of biochemistry and biophysics* **1991**, 285(1), 17-26.
128. R. Mirshafian, W. Wei, J. N. Israelachvili, J. H. Waite,  $\alpha$ ,  $\beta$ -Dehydro-Dopa: a hidden participant in mussel adhesion. *Biochemistry* **2016**, 55(5), 743-750.
129. H. Zhao, J. H. Waite, Coating proteins: structure and cross-linking in fp-1 from the green shell mussel *Perna canaliculus*. *Biochemistry* **2005**, 44(48), 15915-15923.
130. J. C. Ma, D. A. Dougherty, The cation- $\pi$  interaction. *Chemical reviews* **1997**, 97(5), 1303-1324.
131. J. Sunner, K. Nishizawa, P. Kebarle, Ion-solvent molecule interactions in the gas phase. The potassium ion and benzene. *The Journal of physical chemistry* **1981**, 85(13), 1814-1820.
132. S. Burley, G. Petsko, Amino - aromatic interactions in proteins. *FEBS letters* **1986**, 203(2), 139-143.
133. C. Mazza, N. Auphan - Anezin, C. Gregoire, A. Guimezanes, C. Kellenberger, A. Roussel, A. Kearney, P. A. Van Der Merwe, A. M. Schmitt - Verhulst, B. Malissen, How much can a T - cell antigen receptor adapt to structurally distinct antigenic peptides? *The EMBO journal* **2007**, 26(7), 1972-1983.
134. E. V. Pletneva, A. T. Laederach, D. B. Fulton, N. M. Kostić, The Role of cation- $\pi$  interactions in biomolecular association. Design of peptides favoring interactions between cationic and aromatic amino acid side chains. *Journal of the American Chemical Society* **2001**, 123(26), 6232-6245.
135. R. MacKinnon, G. Yellen, Mutations affecting TEA blockade and ion permeation in voltage-activated K<sup>+</sup> channels. *Science* **1990**, 250(4978), 276-279.
136. C. A. Ahern, A. L. Eastwood, H. A. Lester, D. A. Dougherty, R. Horn, A cation- $\pi$  interaction between extracellular TEA and an aromatic residue in potassium channels. *The Journal of general physiology* **2006**, 128(6), 649-657.
137. N. Unwin, Acetylcholine receptor channel imaged in the open state. *Nature* **1995**, 373(6509), 37.
138. D. A. Dougherty, Cation- $\pi$  interactions in chemistry and biology: a new view of benzene, Phe, Tyr, and Trp. *Science* **1996**, 271(5246), 163-168.
139. N. Zacharias, D. A. Dougherty, Cation- $\pi$  interactions in ligand recognition and catalysis. *Trends in Pharmacological Sciences* **2002**, 23(6), 281-287.
140. R. Kumpf, D. Dougherty, A mechanism for ion selectivity in potassium channels: computational studies of cation- $\pi$  interactions. *Science* **1993**, 261(5129), 1708-1710.
141. J. Wang, T. Scheibel, Coacervation of the recombinant *Mytilus galloprovincialis* foot protein-3b. *Biomacromolecules* **2018**, 19(9), 3612-3619.
142. J. Wang, M. H. Suhre, T. Scheibel, A mussel polyphenol oxidase-like protein shows thiol-mediated antioxidant activity. *European Polymer Journal* **2019**, 113 305-312.

## 5. Publication list

1. **Wang, J.**, Scheibel, T. Recombinant production of mussel byssus inspired proteins. *Biotechnol. J.* 2018, 13.  
<https://doi.org/10.1002/biot.201800146>
2. **Wang, J.**, Scheibel, T. Coacervation of the recombinant *Mytilus galloprovincialis* foot protein-3b. *Biomacromolecules*, 2018, 28, 14.  
<https://pubs.acs.org/doi/10.1021/acs.biomac.8b00583>
3. **Wang, J.**, Suhre, M.; Scheibel, T. A mussel polyphenol oxidase-like protein shows thiol-mediated antioxidant activity. *Eur. Polym. J.* 2019, 113, 305-312.  
<https://doi.org/10.1016/j.eurpolymj.2019.01.069>

## 6. Individual contribution to joined publications

1. **Wang, J.**, Scheibel, T. Recombinant production of mussel byssus inspired proteins. *Biotechnol. J.* 2018, 13.

<https://doi.org/10.1002/biot.201800146>

The concept of this review article was prepared by Scheibel, T and myself. I wrote the manuscript (text and figures) and Scheibel, T contributed to the completion of the manuscript.

2. **Wang, J.**, Scheibel, T. Coacervation of the recombinant *Mytilus galloprovincialis* foot protein-3b. *Biomacromolecules*, 2018, 28, 14.

<https://pubs.acs.org/doi/10.1021/acs.biomac.8b00583>

The concept of the research publication was developed by Scheibel, T and myself. Almost all experiments were performed by myself except specific mentioned below. SEM imaging was completed with Bargel, H, MALDI-TOF with Schmidt, A. I wrote the manuscript including text and figures. Scheibel, T supervised the project and contributed to the completion of the manuscript.

3. **Wang, J.**, Suhre, M., Scheibel, T. A mussel polyphenol oxidase-like protein shows thiol-mediated antioxidant activity. *Eur. Polym. J.* 2019,113, 305-312.

<https://doi.org/10.1016/j.eurpolymj.2019.01.069>

The concept of the research publication was developed by Scheibel, T, Suhre, M and myself. The cDNA sequence screening and cloning of pET-sumo-PPOL and pET28a-His-PPOL were performed by Suhre, M. Cloning of pET-sumo-P319 and pET28a-His-P319, the following recombinant productions and purifications, activity and antioxidant assay were carried out by myself. I wrote the manuscript and the figures in cDNA sequence screening part were modified from the PhD thesis of Suhre, M. Scheibel, T supervised the project and contributed to the completion of the manuscript.

## Publications

### *Publication I*

#### *Recombinant production of mussel byssus inspired proteins*

**Jia Wang**, Thomas Scheibel

Published in *Biotechnology Journal*, 2018, 13

Reprinted with kind permission from John Wiley and Sons

# Recombinant Production of Mussel Byssus Inspired Proteins

Jia Wang and Thomas Scheibel\*

Mussel byssus, the holdfast of mussels, has attracted much attention due to the mechanical gradient properties of its threads and the robust and flexible adhesion to various substrates, features that originate mainly from mussel byssus proteins and could be used in potential applications in biomedicine. However, the applications have been impeded owing to the difficulties concerning the extraction of the natural materials, that is, proteins. Recent advances in recombinant production provide a novel approach to generate mussel byssus inspired proteins, even with the opportunities for scale-up production. Here, we review the recently investigated mussel byssus inspired proteins produced by biotechnological approaches and applications thereof with particular emphasis on adhesion and coatings.

distal section, and a soft adhesive plaque at the end of the distal section.<sup>[2]</sup> Each byssal thread shows gradual mechanical properties from stiff to elastic with a good load bearing property,<sup>[3]</sup> which allows the byssus to dissipate the mechanical forces from the external tidal currents without damaging the soft organ inside the mussel.<sup>[4]</sup> The byssus also displays a cuticle acting as an outer coating of the byssal thread and plaque.<sup>[5–7]</sup> Mussel adhesive plaques exhibit excellent water-resistant adhesion on various substrates.<sup>[8,9]</sup>

The mussel byssus comprises ≈96% of proteins by dry mass.<sup>[10]</sup> However, there are impediments in extracting sufficient amounts of fully functional byssus proteins from mussels, owing to the harsh conditions needed therefore. For example, extraction

## 1. Introduction

Sessile marine mussels, such as members of the family Mytilidae, inhabiting the intertidal zones with intense waves and currents, have evolved a specific holdfast system, the byssus, to attach to various hard substrates.<sup>[1]</sup> The intriguing byssus consists of several dozens of threads, each showing three mechanically different parts: an elastic proximal section, a stiff

from ≈10 000 *Mytilus edulis* (*M. edulis*) mussels produces 1 g mussel foot protein-1 (Mfp-1).<sup>[11,12]</sup> Recent advances in genetic engineering have provided an alternative route to produce mussel byssus proteins. Various heterologous hosts, including prokaryotes and eukaryotes, have been used to develop suitable production systems for mussel byssus proteins. As mussel byssus proteins are typically highly post-translationally modified, the recombinant production approaches have to be optimized using in vitro modification as well as metabolic and cellular engineering to gain proteins with desired properties. Here, recombinant production of various mussel byssus proteins is reviewed using different host systems with an emphasis on microbial production. Based on the successful recombinant production of mussel foot proteins, their adhesion, and coating applications are also discussed.

## 2. The Mussel Byssus

The byssus with dozens of threads, secreted from the mussel foot, is a holdfast of mussels for getting stable attachment on different hard substrates in the intertidal zone (Figure 1A).<sup>[1,13]</sup> There are three distinct mussel foot glands, including core (collagen) gland, cuticle (accessory) gland, and plaque (phenol) gland, which are involved in producing the mussel byssus proteins (Figure 1B, D, and E).<sup>[2,13–16]</sup> The secreted thread proteins from the core gland are released into the ventral groove, followed by secretion of the plaque proteins from the plaque gland into the distal depression at the foot-tip (Figure 1B).<sup>[13,17–19]</sup> Then a protective cuticle from the accessory gland is coating the nascent assembled structure before disengagement from the groove (Figure 1C).<sup>[13,17,20]</sup>

J. Wang, Prof. Dr. T. Scheibel  
Lehrstuhl Biomaterialien  
Universität Bayreuth  
Universitätsstraße 30, 95440 Bayreuth, Germany  
E-mail: thomas.scheibel@bm.uni-bayreuth.de

Prof. Dr. T. Scheibel  
Forschungszentrum für Bio-Makromoleküle (BIOmac)  
Universität Bayreuth  
Bayreuth, Germany

Prof. Dr. T. Scheibel  
Bayreuther Zentrum für Kolloide und Grenzflächen (BZKG)  
Universität Bayreuth  
Bayreuth, Germany

Prof. Dr. T. Scheibel  
Bayreuther Materialzentrum (BayMat)  
Universität Bayreuth  
Bayreuth, Germany

Prof. Dr. T. Scheibel  
Bayreuther Zentrum für Molekulare Biowissenschaften (BZMB)  
Universität Bayreuth  
Bayreuth, Germany

Prof. Dr. T. Scheibel  
Bayrisches Polymerinstitut (BPI)  
Universität Bayreuth  
Bayreuth, Germany

DOI: 10.1002/biot.201800146

Each byssal thread can be divided into proximal and distal sections (Figure 2).<sup>[2,21,22]</sup> The proximal section is connected to the stem gland of the mussel foot, whereas the distal section is broadened into an adhesive plaque with oval plate-like structure (Figure 1B and 2).<sup>[2,13,21,23]</sup> The proteins involved in the individual sections of the byssus (Figure 2) are discussed in detail in the following paragraphs, including the collagenous thread proteins (preCol-D, -P, -NG), the thread matrix proteins (PTMP1 and TMPs), the mussel foot proteins (Mfp-1, -2, -3, -4, -5, -6), and the enzymes needed for post-translational modification.

### 2.1. Collagenous Thread Proteins

The collagenous proteins make up  $\approx 96\%$  and  $\approx 66\%$  of the total protein amount by dry weight in the distal and proximal region of total proteins,<sup>[10]</sup> respectively, and are denoted as preCols,<sup>[3]</sup> derived from “pre-pepsinized collagens” (Figure 2). preCols, originate from a core gland (Figure 1D,E)<sup>[24]</sup> and can be considered as block copolymers with a dominant and central collagenous domain  $(\text{Gly-X-Y})_n$  ( $(\text{Gly-Pro-Hyp})_n$  as the common sequence) being the basis for the formation of collagen triple helices.<sup>[23,25]</sup> In addition, there are two distinct flanking domains terminated by His/DOPA (3,4-dihydroxyphenylalanine)-enriched domains, which have been shown to cooperatively bind metal ions.<sup>[23]</sup>

There are three known variants of preCol (-D,<sup>[26]</sup> -P,<sup>[27]</sup> and -NG<sup>[28]</sup>), in which the flanking domains are the most divergent parts and have been considered as a major contributor to mechanical variation.<sup>[9,23,29–31]</sup> preCol-D ( $\approx 97$  kDa) with silk-like flanking domains prevails in the stiff distal section, whereas preCol-P ( $\approx 95$  kDa) with elastin-like flanking domains predominates in the crimped and elastic proximal part of the byssal thread.<sup>[23,26,27]</sup> Each thread has axial and complementary gradual distributions of preCol-D and -P, providing stiffness and elasticity to the byssal thread, and consequently represents gradient properties from distally stiff to proximally elastic.<sup>[10]</sup> preCol-NG ( $\approx 76$  kDa) with Gly-enriched plant cell wall-like domains is evenly distributed along the entire thread.<sup>[23,28]</sup> preCol-NG is proposed to be a mediator between preCol-D and -P molecules.<sup>[28]</sup>

### 2.2. Thread Matrix Proteins

The byssal collagens are arranged in fibrils surrounded by non-collagenous thread matrix proteins, also originating from the core gland (Figure 1D,E).<sup>[32]</sup> One of these proteins is the proximal thread matrix protein 1 (PTMP1,  $\approx 30\%$  by dry weight) identified in the proximal section and other thread matrix proteins (TMPs,  $\approx 4\%$  by dry weight) detected in the whole byssal thread (Figure 2).<sup>[10,33]</sup> PTMP1 ( $\approx 50$  kDa), a glycoprotein, consists of two tandem-repeated domains enriched with Gly, Gln, and Asn residues, showing high homology ( $\approx 50\%$ ) to the group of von Willebrand factor type A (vWF) domains of integrin receptors with collagen binding capability.<sup>[33]</sup> It has been demonstrated that PTMP1 binds collagens with high affinity, consequently influencing the assembly of collagens.<sup>[34,35]</sup>

The family of TMPs ( $\approx 56$  kDa) is composed of repeated sequence motifs enriched with Gly, Tyr, and Asn residues showing significant



**Jia Wang** received her Bachelor's degree in bioengineering (2011) from Qilu University of Technology (China, Jinan) and Master's degree in biochemical engineering (2014) from Donghua University (China, Shanghai) in. She is currently a Ph.D. candidate at University of Bayreuth (Germany) under the supervision of Thomas Scheibel and

her current research focuses on recombinant production of mussel foot proteins as well as its usage as a surgical adhesive.



**Thomas Scheibel** has been full professor at the department of biomaterials at the Universität Bayreuth (Germany) since 2007. He received both his Diploma of Biochemistry (1994) and a Dr. rer. nat. (1998) from the Universität Regensburg (Germany). After his postdoc at the University of Chicago (1998–2001), he received his

habilitation (2007) from the Technische Universität München (Germany). His research focuses on biotechnological production and processing of structural proteins, as well as their biomedical and technical applications.

deamidation.<sup>[32]</sup> Since deamidation is pH dependent, the pH switch from the acidic secretory gland to more or less neutral seawater could be a trigger for deamidation, which contributes to the rapid maturation of solid byssal threads out of solution.<sup>[32,36]</sup> Considering the biological function, the thread matrix proteins are proposed as connector,<sup>[10,32]</sup> lubricant,<sup>[11]</sup> spacer and mediator<sup>[34]</sup> between collagenous proteins in byssal threads.

### 2.3. Mussel Foot Proteins

The mussel adhesive plaque contains at least six distinct types of Mfps, including type 1 (Mfp-1) to type 6 (Mfp-6), distributed mostly with specific locations and functions (Figure 2). Mfp-2, -3, -4, and -5 originate from the plaque gland, while Mfp-1 and -6 originate from the cuticle gland of the mussel.<sup>[13,15,37]</sup>

Mfp-1 ( $\approx 115$  kDa, 10–15 mol% DOPA) is so far the only discovered coating protein in the cuticle layer of the byssus, including the plaque and byssal thread (Figure 1C and 2).<sup>[13,38,39]</sup> Mfp-1 consists of a repeated consensus decapeptide motif  $\text{AKP}^* \text{SY}^* \text{P}'' \text{P}' \text{TY}' \text{K}$  (\* indicates weak hydroxylation [modification efficiency  $\leq 30\%$ ], ' and '' indicate strong single and double hydroxylation of precedent amino acid residue, respectively).<sup>[20,38,40]</sup>

Mfp-2 (42–47 kDa) is the most abundant protein (25–40 wt%) within the plaque, resembling a foam-like structure (Figure 2).<sup>[39]</sup> Compared to other Mfps, Mfp-2 has a relatively low DOPA

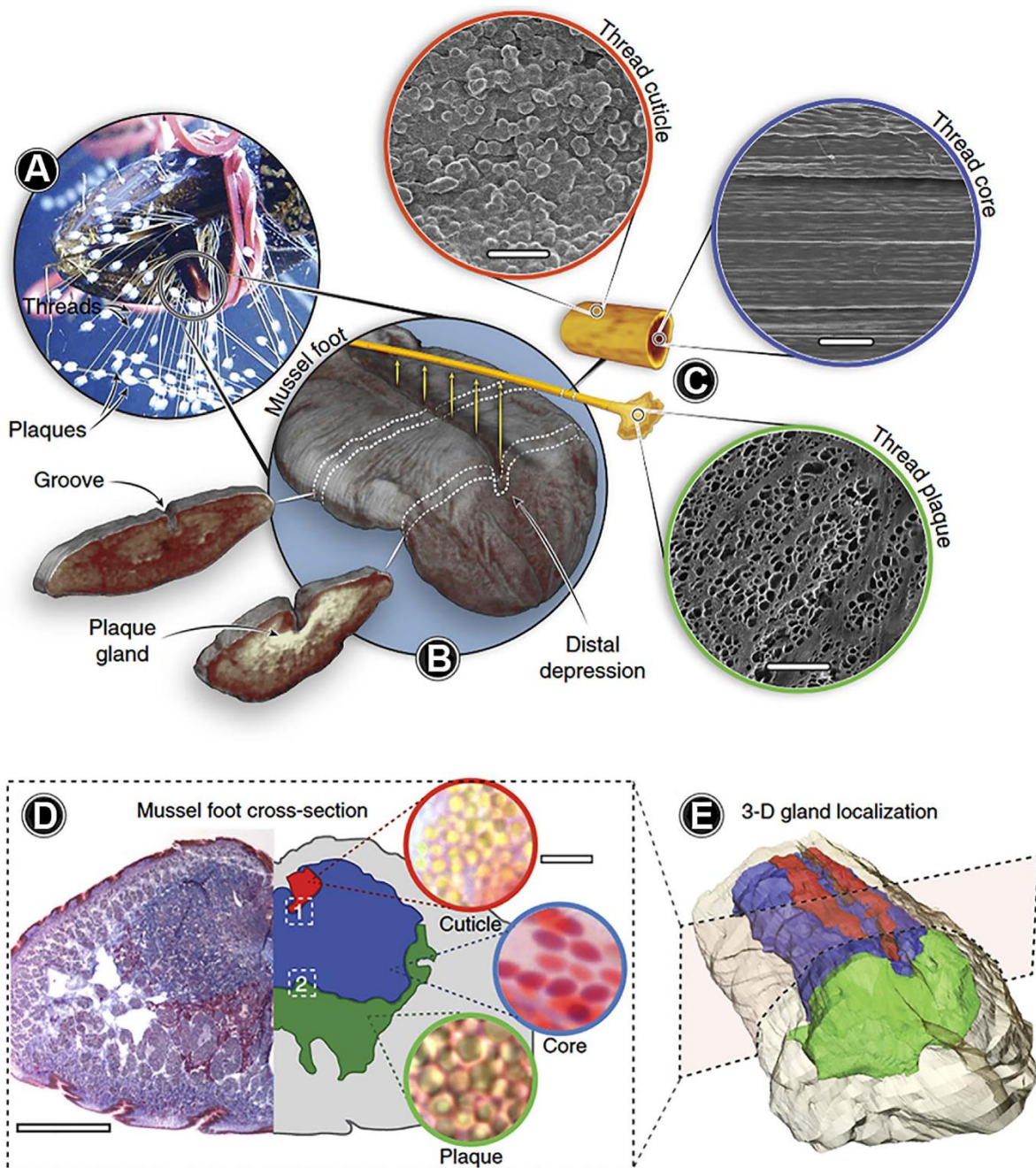


**Figure 1.** Morphology of the mussel byssus (A–C) and its localization of secretory glands in the mussel foot (D, E). A) Photo of a mussel in the process of extruding threads onto plexiglass surface with its foot. B)  $\mu$ -CT image of the ventral surface of an iodine-stained mussel foot with two sections cut out to show the inner gland and groove structure in the middle of the foot and near the distal depression. Byssal threads are synthesized one at a time, by secreting protein building blocks into the groove on the ventral side of the mussel foot. C) Schematic of a single byssal thread, with SEM images highlighting the complex micron-scale morphologies of the protective cuticle (scale bar, 3  $\mu$ m), fibrous core (scale bar, 5  $\mu$ m), and the adhesive plaque (scale bar, 50  $\mu$ m). D) Trichrome stained transverse cross-section of the mussel foot tissue (left; scale bar, 1 mm) and accompanying color-coded illustration showing localization of the three secretory glands (right). Collagens can be stained by trichrome in bright blue and most other proteins in red. High magnification light microscopy images of the vesicles in each gland are shown on the far right (scale bar, 3  $\mu$ m for all three images). E) 3D reconstruction of a mussel foot in the resting state made from serial trichrome stained transverse foot sections showing gland distribution using the same color scheme shown in (D). Reprinted and adapted from Ref. [13] under a Creative Commons license.

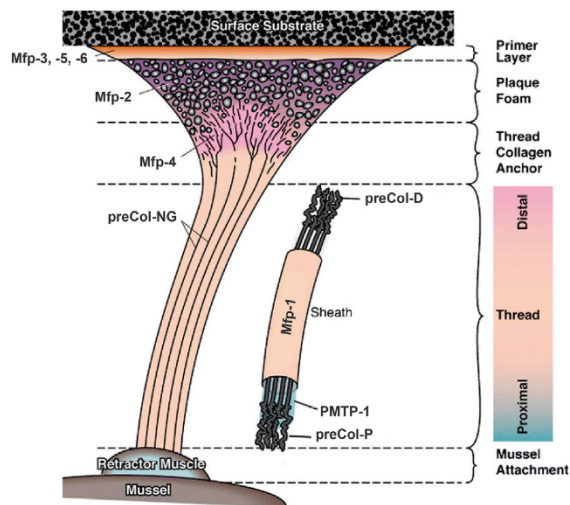


**Figure 2.** Location of structural (collagens) and adhesive (mfp) proteins identified in the byssus of *M. edulis*. Adapted with permission.<sup>[22]</sup> Copyright 2007, Springer Science + Business Media, LLC.

content (2–3 mol%), whereas it has a high content of cysteine residues (6–7 mol%).<sup>[39]</sup> Mfp-2 contains 11 tandem epidermal growth factor (EGF)-like motifs, which are coupled by intramolecular disulfide bonds.<sup>[41]</sup> Accordingly, Mfp-2 is proposed as a stabilizer in the byssus.<sup>[41]</sup> Mfp-4 (≈79 kDa, ≈4 mol% DOPA) is located at the junction between the distal section of the thread and the adhesive plaque, mediating the morphological and mechanical transition from thread to plaque.<sup>[42,43]</sup> Mfp-4 has a His-enriched amino-terminus, which is speculated to contribute to the interconnection with collagens.<sup>[43]</sup>

Mfp-3, -5, and -6 are located at the plaque-substrate interface (Figure 2). Mfp-3 (5–7.5 kDa) is the smallest and the most polymorphic (30–35 variants) Mfp.<sup>[42,44]</sup> There are in principle two types of Mfp-3: Mfp-3 fast (Mfp-3f) and slow (Mfp-3s) electrophoretic variants.<sup>[45]</sup> Both variants of Mfp-3 have abundant amount of Gly (25–29 mol%) and Asp (10–18 mol%) residues.<sup>[45]</sup> The hydrophilic Mfp-3f contains high contents of DOPA (≈26 mol%) and positively charged residues (26 mol%), whereas the hydrophobic Mfp-3s, in contrast, shows less DOPA (5–10 mol%) and positively charged residues (9 mol%).<sup>[45]</sup> Mfp-5 (8.9–9.5 kDa), containing the highest DOPA content (≈27 mol%) among the Mfps, is also highly positively charged (≈20 mol%) and contains extra charges from phosphoserine residues (≈10 mol%).<sup>[46,47]</sup> Mfp-3 and -5 function as primer for the adhesion on different substrates. Mfp-6 (≈11.6 kDa) exhibits low post-translational modifications of Tyr residues (≈20 vs. ≈5 mol% DOPA content), whereas it contains high amounts of Cys residues (≈11 mol%).<sup>[46,48]</sup> It was confirmed that the thiols in Mfp-6 function as antioxidant to “rescue” oxidized DOPA residues in Mfp-3 and -5, enabling a sufficient adhesion of Mfp-3 and -5 to substrates.<sup>[48,49]</sup>

## 2.4. Enzymes

All the aforementioned mussel byssus proteins contain post-translational modifications such as hydroxylation of Tyr, Pro,

Arg, Lys and Trp residues, phosphorylation of Ser as well as glycosylation. To date, two associated enzymes, prolyl 4-hydroxylase (P4H, EC 1.14.11.2)<sup>[50]</sup> and catechol oxidase (EC 1.10.3.1),<sup>[51]</sup> have been discovered. The hydroxyprolines (Hyp), produced by P4H, play a crucial role in formation of a stable collagen triple helix of preCols and can be detected in the cuticle as well.<sup>[50]</sup> The catechol oxidase, oxidizing DOPA into Dopakinones, could be surprisingly extracted from the cuticle glands as well as the byssal threads.<sup>[51,52]</sup> The DOPA oxidation leads to formation of covalent cross-links and consequently tanning of the byssus.<sup>[53]</sup> Nevertheless, there are still some unexploited enzymes, for example, the existence of DOPA indicates the presence of a tyrosinase and the available phosphorylated Ser in Mfp-5 and -6 indicates the presence of a kinase in the byssus or the gland.<sup>[46,47,54]</sup>

## 3. Production of Mussel Byssus Inspired Proteins

### 3.1. Extraction Approaches Out of Mussels

According to the localization of the proteins, the freshly collected and rinsed tissues have been dissected into several parts. The byssus proteins are highly cross-linked due to the high content of DOPA and His residues, which makes the extraction of soluble proteins from byssal threads or plaques difficult. Until now, the extraction was performed using acidic extraction,<sup>[32,33,55]</sup> while an extensive pepsin treatment is necessary for solubilizing the effectively cross-linked preCols.<sup>[25,56]</sup> Effort has been made to produce biocompatible films or matrices using extracted byssus protein hydrolysates, which preserves some natural byssus properties but not the mechanical ones.<sup>[57–59]</sup> Acidic extraction directly from mussel feet is more suitable,<sup>[38,60–62]</sup> however, the yield is low in the μg proteins/g tissue regime.<sup>[63]</sup> So far, two commercial mussel-based glues are derived from mussel extracts. One is Cell-Tak™ (BD Bioscience Clontech, Palo Alto, CA, USA), which is an extracted mixture with mainly Mfp-1 and -2 from *M. edulis*, and the other one is MAP™ (Swedish Bioscience, Floda, Sweden) with extracted Mfp-1 from *M. edulis*. Until now, they are only employed as adhesion agents for cell and tissue culture owing to the low extraction yield and high production cost.

### 3.2. Recombinant Production Approaches

The limited availability of mussel byssus proteins from natural sources has impeded their investigations as well as practical applications. Therefore, recombinant production has been established in various heterologous hosts, including bacteria, yeast, insect cells, and mussel primary cells (Table 1). In the following paragraphs, the attempts are summarized to produce the individual mussel byssus inspired protein.

#### 3.2.1. Collagenous Thread Proteins

The commonly used host *Escherichia coli* (*E. coli*) is not suitable for full-length collagenous protein production due to the lack of

Table 1. Summary of recombinantly produced mussel byssus proteins.

	Host <sup>a)</sup>	Origin <sup>b)</sup>	Protein type	Protein description <sup>c)</sup>	MW <sup>d)</sup> [kDa]	Expression level and solubility <sup>e)</sup>	Purification strategy <sup>f)</sup>	DOPA <sup>g)</sup>	Refs.
preCols	<i>E. coli</i>	<i>M. californianus</i>	preCol-D	preCol-D with central collagen domain deleted; fused with baculoviral polyhedrin at N-terminus; with codon usage adapted	37	N/A; IB	N/A	W/O	[64]
			preCol-NG	C-terminal flank region; fused with SUMO at N-terminus and CBD at C-terminus; with codon usage adapted	7.2	N/A	Chitin affinity column	W/O	[31]
		<i>P. pastoris</i>	<i>M. galloprovincialis</i>	preCol-D	Full-length; fused with an $\alpha$ -secretion factor at N-terminus	89.7	N/A	Extraction in a PBS buffer with 4 M GdmCl, followed by IMAC under denaturing conditions	W/O
TMPs	<i>E. coli</i>	<i>M. galloprovincialis</i>	TMP	C-terminus of TMP	21.3	N/A; IB	Extraction in a PBS buffer with 6 M GdmCl, followed by IMAC under denaturing conditions	W/O	[32]
			PTMP1	Full-length; fused with SUMO fusion tag	48.9	N/A; IB	Extraction in a buffer with 8 M urea and 5 mM DTT, followed by IMAC under denaturing conditions	W/O	[34,67,68]
					Full-length; with codon usage adapted	48.9	$\approx$ 25% of total cell proteins; IB	Extraction with 10% acetic acid, followed by HPLC to remove endotoxins	W/O
Mfps	<i>E. coli</i>	<i>M. edulis</i>	Mfp-1	20 decapeptide repeats	25	$\approx$ 60% of total cell proteins; $\approx$ 67% in IB, $\approx$ 33% soluble	Extraction with 2.5 M urea, 0.8 M acetic acid and 0.5% CTAB, followed by IEC and SEC	W/O	[69]
				6 decapeptide repeats	7	N/A; IB	Extraction with 10% acetic acid, followed by IEC	W/O	[70]
				7 decapeptide repeats; fused with OmpA signal peptide at N-terminus	8	N/A; the soluble expression was twice higher than without OmpA	N/A	W/O	[72]
			<i>D. polymorpha</i>	Dfp1	Full-length	110	N/A; soluble	Amylose affinity column, followed by HPLC	W/O
		<i>M. galloprovincialis</i>	Mfp-3A	Full-length	7	$\approx$ 56% ( $\approx$ 3%) of total cell proteins with (without) codon usage adapted; half soluble and half in IB	Extraction with 8 M urea, followed by IMAC	W/O	[77,80]
				+ In vivo DOPA incorporation by TyrRS	7	N/A	Extraction with 8 M urea, followed by IMAC	W	[91]
			Mfp-5	Full-length	13.5	$\approx$ 40% ( $\approx$ 10%) of total cell proteins with (without) codon usage adapted; mainly soluble	Extraction with 8 M urea, followed by IMAC	W/O	[78,79,81]
			fp-151	6 Mfp-1 decapeptide repeats at each Mfp-5 terminus	24.5	$\approx$ 40% of total cell proteins; IB	Extraction with 25% acetic acid, followed by IMAC under denaturing conditions	W/O	[83,84]
	+ Co-expression with tyrosinase	24.5	N/A; mainly soluble	N/A	W	[92]			
	+ Co-expression with hemoglobin	24.5	$\approx$ 1.9-fold higher expression; N/A;	N/A	W/O	[90]			

(Continued)

Table 1. (Continued)

Host <sup>a)</sup>	Origin <sup>b)</sup>	Protein type	Protein description <sup>c)</sup>	MW <sup>d)</sup> [kDa]	Expression level and solubility <sup>e)</sup>	Purification strategy <sup>f)</sup>	DOPA <sup>g)</sup>	Refs.
	<i>M. galloprovincialis</i>	fp-353	Mfp-3A at each Mfp-5 terminus	22	≈21% of total cell proteins; IB	Extraction with 6 M GdmCl, followed by IMAC	W/O	[85]
<i>S. cerevisiae</i>	<i>M. edulis</i>	Mfp-1	20–80 decapeptide repeats	24–96	3–5% of total cell proteins; IB	Extraction with 10% formic acid, followed by IEC	W/O	[73]
	<i>M. edulis</i>	Mfp-1	Full-length	130	N/A	N/A	W/O	[74]
	<i>M. edulis</i>	Mfp-2	Full-length	42–47	N/A	N/A	W/O	[75]
<i>K. lactis</i>	<i>M. californianus</i>	Mfp-3	Full-length; fused with first 9 amino acids of HA' at N-terminus; with codon usage adapted	7	N/A; soluble	HA' affinity chromatography	W/O	[82]
Insect Sf9 cells	<i>M. galloprovincialis</i>	fp-151	6 Mfp-1 decapeptide repeats at each Mfp-5 terminus	24.5	≈50% of total cell proteins; soluble	IMAC	W	[93]
Mussel foot cells	<i>M. galloprovincialis</i>	Mfp-1, -2, -3	Full-length	130; 47; 6	Transcription of three genes were detected	N/A	W	[94]

<sup>a)</sup> *E. coli*, *Escherichia coli*; *P. pastoris*, *Pichia pastoris*; *S. cerevisiae*, *Saccharomyces cerevisiae*; *K. lactis*, *Kluyveromyces lactis*; <sup>b)</sup> *M. californianus*, *Mytilus californianus*; *M. galloprovincialis*, *Mytilus galloprovincialis*; *M. edulis*, *Mytilus edulis*; *D. polymorpha*, *Dreissena polymorpha*; <sup>c)</sup> SUMO, small ubiquitin-like modifier; CBD, chitin binding domain; TyrRS, tyrosyl-tRNA synthetase; HA', human-influenza-virus hemagglutinin; Codon usage adapted, with corresponding host codon usage adapted; <sup>d)</sup> MW, the final molecular weight after removal of fusion tag; <sup>e)</sup> IB, inclusion body; N/A, not applicable; <sup>f)</sup> DTT, 1,4-dithiothreitol; PBS, phosphate buffered saline; CTAB, cetrimonium bromide; GdmCl, guanidine hydrochloride; IMAC, immobilized metal affinity chromatography; IEC, ion exchange chromatography; SEC, size exclusion chromatography; HPLC, high performance liquid chromatography; <sup>g)</sup> W (W/O), with (without) modification of Tyr residues into DOPA.

modifying enzymes and cellular compartments necessary for collagen folding and assembly. Nevertheless, expression of the flank region of preCol has been accomplished in *E. coli*.<sup>[31,64]</sup> In order to increase the production level, they were fused with special tags, such as small ubiquitin-like modifier (SUMO) for stabilization<sup>[31]</sup> and baculoviral polyhedrin protein as an insoluble inclusion body formation-inducing fusion partner.<sup>[64]</sup> Full-length non-hydroxylated preCol-D in contrast has been recombinantly produced in yeast *Pichia pastoris* (*P. pastoris*).<sup>[65]</sup> The recombinant preCol-D exhibited the ability to form fibrils with correctly folded collagen triple helix, even in the absence of post-translational modifications.<sup>[65]</sup>

### 3.2.2. Thread Matrix Proteins

Compared to collagenous proteins, the recombinant production of TMPs has less obstacles. The carboxy-terminal domain of TMP<sup>[4]</sup> and full-length PTMP1<sup>[34,35,66–68]</sup> have been produced in *E. coli* in inclusion bodies. Based on the vWF motif, the recombinant PTMP1 promoted cell adhesion and cell viability,<sup>[66]</sup> which indicates that PTMP1 has a potential for tissue engineering.

### 3.2.3. Mussel Foot Proteins

First, the attempts to produce recombinant foot proteins were focused on Mfp-1 of *M. edulis*, which was the first identified Mfp. Partial consensus decapeptide repeats (6–20) of Mfp-1 have been produced in *E. coli* at high yields.<sup>[69,70]</sup> The 20 decapeptide repeats of Mfp-1 yielded up to 60% of total cell proteins in *E. coli*

with both a soluble and insoluble fraction.<sup>[69]</sup> The six decapeptide repeats of Mfp-1 were produced in inclusion bodies.<sup>[70]</sup> The in vitro Tyr modification into DOPA lead to insolubilization, and the quantity was too low to check the adhesion properties.<sup>[70]</sup>

The OmpA signal peptide, an outer membrane protein of *E. coli*, has been employed to transfer recombinant proteins into the periplasm of *E. coli*.<sup>[71]</sup> To increase soluble Mfp-1 expression in *E. coli*, a fusion protein of seven decapeptide repeats of Mfp-1 with OmpA variants at the N-terminus was produced.<sup>[72]</sup> It showed an increased soluble expression at a minimum-length of the OmpA sequence.<sup>[72]</sup>

The yeast *Saccharomyces cerevisiae* (*S. cerevisiae*) was also used to express partial Mfp-1 decapeptide repeats.<sup>[73]</sup> The construct was designated 14-1 carrying 20 tandem repetitive sequence (19 decapeptide repeats and one hexapeptide) of Mfp-1.<sup>[73]</sup> Since the natural Mfp-1 carries up to 80 repetitive motifs and the molecular weight likely influences its adhesion performance, constructs carrying between one and four copies of construct 14-1 were engineered and expressed yielding proteins between 24 and 96 kDa.<sup>[73]</sup> A method of cloning and expression of recombinant Mfp-1 and -2 in *S. cerevisiae* has been patented.<sup>[74,75]</sup>

Full-length *Dreissena polymorpha* (*D. polymorpha*, freshwater zebra mussel) foot protein 1 (Dfpf1) has been expressed in *E. coli*, which was the first recombinant non-*Mytilus* protein.<sup>[76]</sup> The recombinant Dfpf1 was utilized for polyclonal antibody production.<sup>[76]</sup> Immunohistochemistry revealed that the Dfpf1 existed in foot tissue and byssal threads.<sup>[76]</sup>

With the cDNA sequence of Mfp-3A (one variant of Mfp-3f) and Mfp-5 from *Mytilus galloprovincialis* (*M. galloprovincialis*) being identified, recombinant Mfp-3A and Mfp-5, both fused with a hexahistidine affinity TAG, were produced in *E. coli*.<sup>[77–79]</sup>

In order to increase the recombinant production, sequence optimization of Mfp-3A and Mfp-5 was performed based on the codon usage preference of *E. coli*.<sup>[80,81]</sup> As a result, the expression level of Mfp-3A was greatly improved from  $\approx 3$  to  $\approx 56\%$  of the total cell proteins and Mfp-5 from  $\approx 10$  to  $\approx 40\%$ , correspondingly.<sup>[80,81]</sup> The yield of recombinant Mfp-3A increased from  $\approx 0.8$  to  $\approx 47 \text{ mg mL}^{-1}$  and of Mfp-5 from  $\approx 2.6$  to  $\approx 50 \text{ mg mL}^{-1}$ .<sup>[80,81]</sup> Additionally, Mfp-3 from *Mytilus californianus* (*M. californianus*) with a codon usage adapted to yeast *Kluyveromyces lactis* (*K. lactis*) was fused with nine amino acids from human-influenza-virus hemagglutinin (HA') as a fusion-tag.<sup>[82]</sup> HA'-Mfp-3 was successfully expressed in *K. lactis* and showed self-assembly capability after the removal of the HA' TAG by using enterokinase.<sup>[82]</sup>

Besides above-mentioned partial expression, codon usage adaptation, and fusion with HA' to improve the low expression level, low purification yield, and insolubility of recombinant Mfps, the hybrid mussel adhesives fp-151,<sup>[83,84]</sup> and fp-353<sup>[85]</sup> were constructed. The hybrid fp-151 comprised six Mfp-1 decapeptide repeats at each Mfp-5 terminus and the hybrid fp-353 contained one Mfp-3A at each Mfp-5 terminus.<sup>[83–85]</sup> Both fp-151 and fp-353 were produced in *E. coli* in inclusion bodies and did not inhibit cell growth.<sup>[83–85]</sup> While the yield of fp-353 could not be improved in comparison to that of Mfp-3A,<sup>[77,80,85]</sup> fp-151 showed a much higher yield with  $\approx 1 \text{ g L}^{-1}$  bacterial culture.<sup>[83,84]</sup> Interestingly, the fp-151 showed good post-purification solubility ( $\approx 330 \text{ g L}^{-1}$ ) and, therefore, could be concentrated for adhesion applications.<sup>[83,84]</sup>

Since the oxygen supply is a crucial factor for growth of aerobic microorganism, the vitreoscilla hemoglobin (VHb) has been introduced into several expression systems with efficient oxygen utilization to improve the expression level.<sup>[86–89]</sup> Recombinant production of fp-151 with VHb in *E. coli* showed a  $\approx 1.9$ -fold higher yield compared to that without VHb co-expression.<sup>[90]</sup>

### 3.3. Post-Translational Modification of Tyr Residues

#### 3.3.1. In Vitro Modification

The recombinant Mfps produced in *E. coli* and yeast required further in vitro modifications to become functional,<sup>[95]</sup> since the microbes cannot be post-translationally modify, for example, Tyr residues into DOPA. Owing to the existence of high amounts of DOPA residues in most byssus proteins, the modification of Tyr residues into DOPA is mainly discussed here. Tyrosinase from mushrooms can be used for in vitro Tyr modification at a pH between 6.0 and 7.0. However, Mfps tend to aggregate easily in solution especially upon increasing the pH from acidic to neutral owing to their high amount of basic amino acids. Therefore, the in vitro modification efficiency of recombinant Mfps is relatively low with  $\approx 1$  to  $\approx 2 \text{ mol\%}$  DOPA, compared to that of natural Mfps with  $\approx 10$  to  $\approx 30 \text{ mol\%}$  DOPA.<sup>[80,81,83,96]</sup>

#### 3.3.2. In Vivo Modification

Even though some Mfps have been successfully produced in *E. coli* at high yield, the low in vitro modification efficiency made it

difficult to gain a similar adhesion ability as found in natural mussel glue. To improve the modification efficiency, in vivo modification has therefore been attempted. A co-expression of fp-151 and mushroom tyrosinase was performed with a dual vector system of pET and pACYC-Duet.<sup>[92]</sup> The co-expression level of fp-151 was similar to that of the individual expression levels, indicating that the co-expression system did not inhibit host growth.<sup>[92]</sup> The modification of Tyr residues was confirmed by nitroblue tetrazolium stain and liquid-chromatography-mass/mass spectrometry analyses.<sup>[92]</sup> The adhesive strength of in vivo modified fp-151 was  $\approx 4$ -fold higher than that of in vitro modified fp-151.<sup>[92]</sup>

Baculovirus-based expression of recombinant fp-151 in insect *Sf9* cells showed that the insect-derived fp-151 underwent in vivo post-translational modification of Tyr residues as well as other modifications, including hydroxylation of Pro and phosphorylation of Ser.<sup>[93]</sup> Compared to the *E. coli*-derived fp-151, the insect-derived fp-151 exhibited  $\approx 2$ -fold higher coating ability, which was mainly based on the modification of Tyr residues into DOPA.<sup>[93,95]</sup> With co-expression or baculovirus-based recombinant production, the Tyr residue at position five in the Mfp-1 decapeptide unit (sequence AKPSYPPTYK) of fp-151 was modified into DOPA or Dopaquinone.<sup>[92,93]</sup> However, the Tyr modification was more frequently detected at position nine in natural Mfp-1 decapeptides, which might be due to different hydroxylation position preferences of different enzymes.<sup>[92,93]</sup>

Since neither co-expression with tyrosinase nor eukaryotic expression did significantly increase the DOPA concentration toward the natural level found in mussel byssus proteins,<sup>[92,93]</sup> non-natural amino acids were incorporated into the recombinant proteins as an alternative approach of modification.<sup>[97,98]</sup> Previously, direct incorporation of DOPA into proteins in an *E. coli* cell-free transcription/translation system was studied by replacing Tyr with DOPA in the reaction mixture.<sup>[99]</sup> The  $K_M$  of tyrosyl-tRNA synthetase (TyrRS) for DOPA was reported to be  $\approx 200$ -fold higher than for Tyr.<sup>[100,101]</sup> Therefore, a high DOPA incorporation level ( $>90\%$ ) at each Tyr site was obtained.<sup>[99]</sup> However, the production yield of recombinant proteins in cell-free systems is low.<sup>[97]</sup> Correspondingly, efforts on DOPA incorporation in *E. coli* cells have been made,<sup>[91,102–104]</sup> for example, in a protein-polysaccharide conjugate<sup>[102]</sup> and a protein-based biosensor with copper-binding sites,<sup>[103]</sup> and a DOPA-incorporated Mfp-3.<sup>[91]</sup> With regard to Mfp-3, the DOPA incorporation efficiency reached  $\approx 94\%$ , with  $\approx 16.5 \text{ mol\%}$  DOPA content, which is close to natural Mfps. This recombinant Mfp-3 exhibited a great surface adhesion and strong water resistance.<sup>[91]</sup> However, only flask cultivation was tested until now and it has to be tested whether scale-up production is possible.

Efforts have also been made to directly culture isolated foot cells of the mussel *M. galloprovincialis* on a dish coated with collagen type I. The transcription of the genes encoding Mfp-1, -2, and -3 was detected in the primary and secondary cultures using gene-specific probes.<sup>[94]</sup> This finding suggested that the mussel foot cell culture could be an alternative expression system for mussel byssus proteins, which allows directly integrating post-translational modifications.<sup>[94]</sup>

#### 4. Applications of Recombinant Mussel Byssus Proteins

Concerning the so far low yield of recombinant production of preCols, the applications are discussed with particular emphasis on recombinant Mfps. Recombinant Mfps have been mainly developed as bioadhesives due to their adhesion and biocompatibility<sup>[83]</sup> properties, for example, they have been shown to function as effective microbial cell-immobilizing linker in cell biosensors,<sup>[105]</sup> and glue for urinary fistula sealing.<sup>[106]</sup> Additionally, due to their specific distribution in byssal cuticle (Mfp-1) and at the plaque-substrate interface (Mfp-3, -5), they have also been tested as coating materials for cell culture applications. It was shown that they are capable of adhering to various substrates, such as mica, silicon dioxide (SiO<sub>2</sub>), polystyrene, and polymethylmethacrylate (PMMA).<sup>[9,78,83,85]</sup> Especially, Mfps showed low or no immunogenicity.<sup>[107,108]</sup> In the following sections, we discuss the used morphologies of Mfp-based materials employed as bioadhesives and coating materials.

##### 4.1. Mfp Solutions

DOPA modified fp-151 showed a higher bulk adhesive strength than recombinant Mfp-3A, Mfp-5, and the commercial product Cell-Tak<sup>TM</sup>.<sup>[80,83]</sup> The high post-purification solubility ( $\approx 300 \text{ g L}^{-1}$ ) of fp-151<sup>[83]</sup> makes it possible to obtain highly concentrated adhesive solutions, which could be directly employed as bioadhesives and coating materials. Coating could be obtained by various methods such as simple dipping, adsorption,<sup>[109,110]</sup> and spin coating.<sup>[111]</sup> Mfp-5 and fp-151 showed efficient cell adhesion and biocompatibility,<sup>[79,83]</sup> enabling their application as cell adhesion biomaterials. The RGD sequence found in fibronectin of the extracellular matrix (ECM) is a cell-adhesion recognition motif for integrin-mediated cell adhesion,<sup>[112,113]</sup> and fusion of fp-151 with the RGD sequence (GRGDSP) at its carboxy-terminus gained fp-151-RGD, which showed superior cell-adhesion and spreading abilities under serum-free conditions compared to the commercial cell adhesion materials poly-L-lysine (PLL) and Cell Tak<sup>TM</sup>.<sup>[109,110]</sup> Similarly, other ECM-derived peptides, such as YIGSR from laminin, GEFYFDLRLKGDK from type IV collagen and CRPKPQQFFGLM from substance P, were fused with fp-151, exhibiting similar cell-binding properties as fp-151-RGD.<sup>[109]</sup>

Additionally, other properties could be introduced into fp-151 by fusion with functional peptides, such as silver binding of AgNO<sub>3</sub> in solution.<sup>[114]</sup> The fp-151-silver binding peptide fusion proteins were capable of generating silver nanoparticles with good immobilization on the well-coated surface, which provided excellent antibacterial efficacy and good cytocompatibility.<sup>[111]</sup>

##### 4.2. Mfp Nanofibrils

To achieve strong underwater adhesion, mussels use hierarchically foam-like structured plaques with  $\approx 40\%$  porosity,<sup>[115]</sup> and therefore mimicking bioadhesives with a hierarchical structure were investigated. Self-assembled adhesive nanofibrils were obtained upon fusing Mfp-3/Mfp-5 with amyloidogenic

CsgA, the major subunit of curly fibrils in *E. coli* (Figure 3A).<sup>[116]</sup> The fibrils exhibited an underwater adhesion energy approaching  $20.9 \text{ mJ m}^{-2}$ , the highest value for bio-derived and protein-based underwater adhesives reported so far.<sup>[116]</sup> Moreover, since the nanofibrils are morphologically similar to collagen fibrils of the natural ECM, they have also been developed as tissue engineering scaffolds.<sup>[116]</sup> The high surface-to-volume ratio of nanofibrils provides more surface area for cell attachment, and the highly porous structure is capable of facilitating cellular migration and transporting of nutrients and metabolic waste.<sup>[117]</sup>

Production of Mfp nanofibrils failed due to the fast dissolution of formed fibrils.<sup>[118]</sup> Using a blending strategy, fp-151 nanofibrils could be formed in blends with a partner, such as polycaprolactone (PCL) (Figure 3B).<sup>[118]</sup> The PCL/fp-151 nanofibrils (ratio 90:10) showed a  $\approx 4$ -fold higher tensile strength and strengthened rigidity in comparison to plain PCL nanofibrils.<sup>[118]</sup> Cell attachment and proliferation were significantly enhanced, especially on PCL/fp-151-RGD nanofibrils.<sup>[118]</sup>

##### 4.3. Mfp Coacervates

Complex coacervation is a liquid–liquid phase separation, owing to the neutralization of two oppositely charged polyelectrolytes at a given pH.<sup>[119,120]</sup> Nevertheless, coacervation also can occur with single polyelectrolytes, such as in the natural adhesion process of mussels.<sup>[17]</sup> The self-coacervation of DOPA-deficient recombinant mfp-1 (rmfp-1, 12 tandem repeats of Mfp-1 decapeptide) was induced via cation- $\pi$  interaction at natural seawater conditions,<sup>[121–123]</sup> whereas coacervation of the nonpolar Mfp-3s was triggered by inter/intramolecular electrostatic interactions and hydrophobic interactions.<sup>[124]</sup> The cationic Mfp-5<sup>[81]</sup> and fp-151 (-RGD)<sup>[96,106,125,126]</sup> together with anionic hyaluronic acid (HA) were capable of forming a highly condensed complex coacervate (Figure 3C). This complex coacervate, exhibiting the superior property of water immiscibility and strong underwater adhesion, successfully sealed ex vivo-punctured bladders with good durability and high compliance.<sup>[96,106]</sup>

Titanium (Ti)-based materials are widely employed in biomedical and dental applications due to their desirable properties, such as light weight, high strength, biocompatibility, and high corrosion resistance in vitro.<sup>[127]</sup> Nevertheless, bacterial infection remains a major impediment to the utility of Ti-based implants, whereas coating strategies offer the possibility to overcome the problem.<sup>[128]</sup> Mfp coacervates showed great potential as coating materials due to their extremely low innate interfacial energy.<sup>[125]</sup> The freshly prepared fp-151-RGD/HA coacervate droplets coalesced, settled on the Ti surface and consequently coated the Ti.<sup>[126]</sup> The coating showed an increased cell proliferation of preosteoblast.<sup>[126]</sup> The coacervate of fp-151/HA was further used for microencapsulation and showed great potential as drug carrier.<sup>[96]</sup>

##### 4.4. Mfp Hydrogels

Inspired by cross-linking of DOPA, gelation of rmfp-1 was induced using Fe<sup>3+</sup>-mediated coordination (DOPA:FeCl<sub>3</sub> = 3:1, pH > 8) as well as Dopquinone-mediated covalent (DOPA:

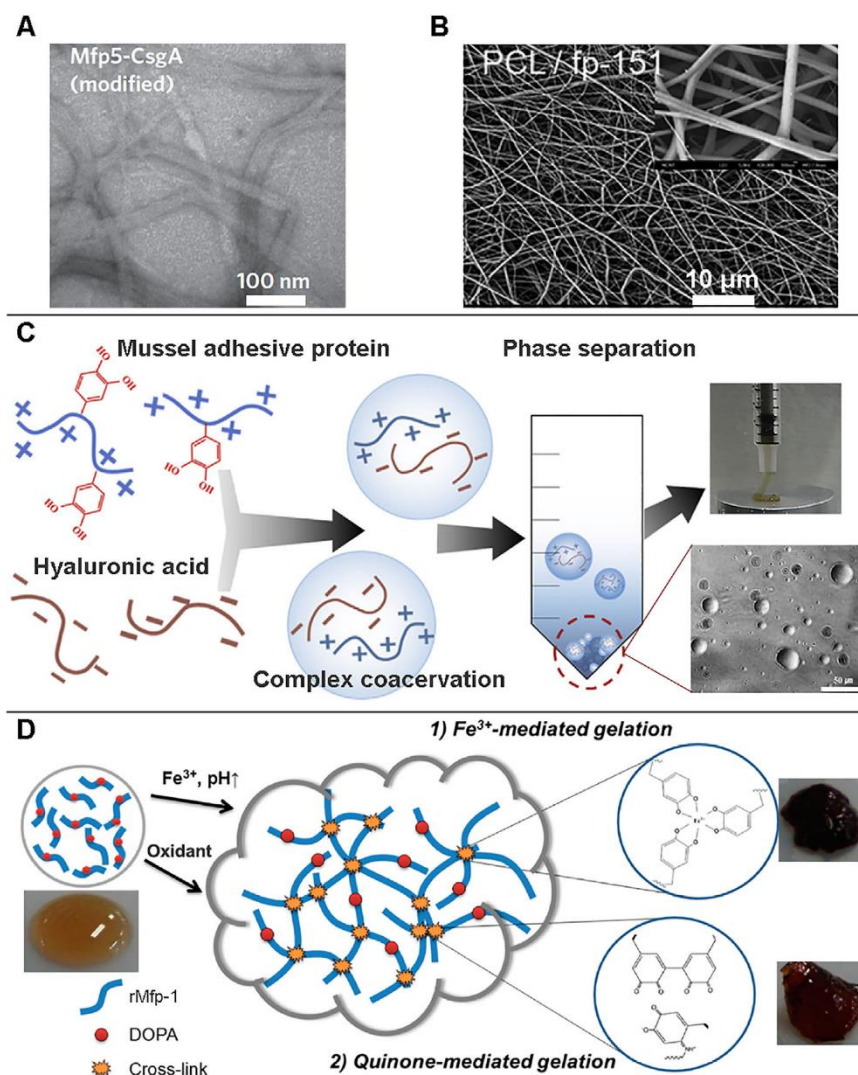


**Figure 3.** Different morphologies of mussel adhesive proteins. A) TEM image of purified Mfp5-CsgA (DOPA modified) solutions after 3-day incubation at 4 °C demonstrates the formation of self-assembled fibers. Adapted with permission.<sup>[116]</sup> Copyright 2014, Springer Nature. B) SEM image of electrospun nanofibers made of a mixture of fp-151/PCL with a ratio of 30:70 (wt/wt). Reproduced with permission.<sup>[118]</sup> Copyright 2011, John Wiley and Sons. C) Schematic representation of Mfp-based water-immiscible complex coacervation with Hyaluronic acid (HA). Light microscopic morphology of complex coacervates is shown in the right bottom image. Adapted with permission.<sup>[106]</sup> Copyright 2015, Elsevier Ltd. D) Schematic representation of the Mfp-based gelation process via  $\text{Fe}^{3+}$ -DOPA coordination-mediated noncovalent cross-linking or Dopaquinone-mediated covalent cross-linking. The results of the two cross-linking gelation processes are shown in the photographs. rmfp-1 refers to 12 tandem repeats of Mfp-1 decapeptide. Adapted with permission.<sup>[129]</sup> Copyright 2014, American Chemical Society.

$\text{NaIO}_4 = 2:1$ ) cross-linking, yielding DOPA-based Mfp hydrogels (Figure 3D).<sup>[6,129,130]</sup> The  $\text{Fe}^{3+}$ -mediated hydrogels exhibited a flexible viscoelastic and self-healing behavior, presumably owing to the reversible  $\text{Fe}^{3+}$ -DOPA bonding.<sup>[6,129,130]</sup> The Dopaquinone-mediated hydrogels showed a higher wet bulk adhesive strength and were easy to handle due to the convenient gelation time ( $\approx 5$  min).<sup>[129]</sup> In addition, DOPA-deficient fp-151 was capable of being fabricated as a rapidly light-activated hydrogel (LAMBA) via dityrosine cross-link formation.<sup>[131]</sup> LAMBA exhibited high bulk wet adhesion strength and good biocompatibility allowed the rapid ( $<60$  s) closure of an open wound on the back of a rat upon easy handling light irradiation.<sup>[131]</sup>

## 5. Conclusion and Outlook

Mussel byssus, possessing intriguing mechanical and excellent adhesion properties, is an appealing natural material inspiring various applications in biotechnology. Owing to the low efficiency of extraction of the underlying natural proteins, recombinant production provides an alternative approach to enable materials based thereon. Various heterologous hosts as well as gene and host engineering strategies have been investigated to develop appropriate production systems.

The recombinant production of preCols is currently at its infancy.<sup>[65]</sup> Inspired by recombinant production of spider silk,

the native-sized preCols might also be recombinantly produced via intein-mediated *trans*-splicing.<sup>[132,133]</sup> Furthermore, a suitable host system or co-expression with required enzymes might provide the necessary post-translational modifications.

The recombinant production of Mfeps has been more successful. Recombinant Mfeps exhibited higher bulk adhesive strength than the commercially available mussel-derived glue Cell-Tak™. In vivo modification strategies have been employed to enhance the modification efficiency. Recombinant Mfeps can be processed as solution, nanofibrils, coacervates, and hydrogels, and show great potential to be employed in medical and biotechnological applications especially as bioadhesives and coating materials.

## Abbreviations

DOPA, 3,4-dihydroxyphenylalanine; Dpfp, *Dreissena polymorpha* foot protein; *D. polymorpha*, *Dreissena polymorpha*; ECM, extracellular matrix; EGF, epidermal growth factor; *E. coli*, *Escherichia coli*; HA, hyaluronic acid; HA', human-influenza-virus hemagglutinin; Hyp, hydroxyprolines; *K. lactis*, *Kluyveromyces lactis*; LAMBA, light-activated hydrogel; *M. californianus*, *Mytilus californianus*; *M. edulis*, *Mytilus edulis*; Mfeps, mussel foot proteins; *M. galloprovincialis*, *Mytilus galloprovincialis*; P4H, prolyl 4-hydroxylase; PCL, polycaprolactone; PLL, poly-L-lysine; PMMA, polymethylmethacrylate; TMPs, thread matrix proteins; *P. pastoris*, *Pichia pastoris*; preCols, pre-pepsinized collagens; PTMP1, proximal thread matrix protein 1; *S. cerevisiae*, *Saccharomyces cerevisiae*; SUMO, small ubiquitin-like modifier; TyrRS, tyrosyl-tRNA synthetase; Vhb, vitreoscilla hemoglobin; vWF, von Willebrand factor.

## Acknowledgement

J.W. thanks the China Scholarship Council (CSC, 201406630012) for awarding a fellowship for carrying out her PhD in Germany in the lab of Prof. Dr. Thomas Scheibel.

## Conflict of Interest

The authors declare no financial or commercial conflict of interest.

## Keywords

bioadhesives, collagens, mussel byssus, post-translational modification, recombinant production

Received: May 20, 2018

Revised: June 28, 2018

Published online:

- [1] T. J. Deming, *Curr. Opin. Chem. Biol.* **1999**, *3*, 100.
- [2] C. H. Brown, *Q. J. Microsc. Sci.* **1952**, *93*, 487.
- [3] E. Bell, J. Gosline, *J. Exp. Biol.* **1996**, *199*, 1005.
- [4] J. H. Waite, H. C. Lichtenegger, G. D. Stucky, P. Hansma, *Biochemistry* **2004**, *43*, 7653.
- [5] M. J. Harrington, A. Masic, N. Holten-Andersen, J. H. Waite, P. Fratzl, *Science* **2010**, *328*, 216.
- [6] N. Holten-Andersen, M. J. Harrington, H. Birkedal, B. P. Lee, P. B. Messersmith, K. Y. C. Lee, J. H. Waite, *Proc. Natl. Acad. Sci. USA* **2011**, *108*, 2651.
- [7] N. Holten-Andersen, G. E. Fantner, S. Hohlbauch, J. H. Waite, F. W. Zok, *Nat. Mater.* **2007**, *6*, 669.
- [8] J. H. Waite, *Int. J. Adhes. Adhes.* **1987**, *7*, 9.
- [9] Q. Lu, E. Danner, J. H. Waite, J. N. Israelachvili, H. Zeng, D. S. Hwang, *J. R. Soc. Interface* **2013**, *10*, 20120759.
- [10] J. H. Waite, E. Vaccaro, C. Sun, J. M. Lucas, *Philos. Trans. R. Soc. London Ser. B* **2002**, *357*, 143.
- [11] R. L. Strausberg, R. P. Link, *Trends Biotechnol.* **1990**, *8*, 53.
- [12] D. Morgan, *Scientist* **1990**, *4*, 1.
- [13] T. Priemel, E. Degtyar, M. N. Dean, M. J. Harrington, *Nat. Commun.* **2017**, *8*, 14539.
- [14] R. D. Lillie, *Stain Technol.* **1940**, *15*, 17.
- [15] D. Miki, Y. Takeuchi, K. Inoue, S. Odo, *Biol. Bull.* **1996**, *190*, 213.
- [16] A. Tamarin, P. J. Keller, *J. Ultrastruct. Res.* **1972**, *40*, 401.
- [17] J. H. Waite, *J. Exp. Biol.* **2017**, *220*, 517.
- [18] A. Tamarin, P. Lewis, J. Askey, *J. Morphol.* **1976**, *149*, 199.
- [19] A. Tamarin, P. Lewis, J. Askey, *J. Morphol.* **1974**, *142*, 321.
- [20] N. Holten-Andersen, J. H. Waite, *J. Dent. Res.* **2008**, *87*, 701.
- [21] C. V. Benedict, J. H. Waite, *J. Morphol.* **1986**, *189*, 261.
- [22] H. G. Silverman, F. F. Roberto, *Mar. Biotechnol.* **2007**, *9*, 661.
- [23] J. H. Waite, X.-X. Qin, K. J. Coyne, *Matrix Biol.* **1998**, *17*, 93.
- [24] L. V. Zuccarello, *J. Ultrastruct. Res.* **1980**, *73*, 135.
- [25] X. Qin, J. H. Waite, *J. Exp. Biol.* **1995**, *198*, 633.
- [26] X.-X. Qin, K. J. Coyne, J. H. Waite, *J. Biol. Chem.* **1997**, *272*, 32623.
- [27] K. J. Coyne, X.-X. Qin, J. H. Waite, *Science* **1997**, *277*, 1830.
- [28] X.-X. Qin, J. H. Waite, *Proc. Natl. Acad. Sci. USA* **1998**, *95*, 10517.
- [29] A. Hagenau, P. Papadopoulos, F. Kremer, T. Scheibel, *J. Struct. Biol.* **2011**, *175*, 339.
- [30] A. A. Arnold, F. Byette, M.-O. Séguin-Heine, A. LeBlanc, L. Sleno, R. Tremblay, C. Pellerin, I. Marcotte, *Biomacromolecules* **2013**, *14*, 132.
- [31] M. Heim, M. B. Elsner, T. Scheibel, *Biomacromolecules* **2013**, *14*, 3238.
- [32] J. Sagert, J. H. Waite, *J. Exp. Biol.* **2009**, *212*, 2224.
- [33] C. Sun, J. M. Lucas, J. H. Waite, *Biomacromolecules* **2002**, *3*, 1240.
- [34] M. H. Suhre, M. Gertz, C. Steegborn, T. Scheibel, *Nat. Commun.* **2014**, *5*, 3392.
- [35] H. Y. Yoo, J. Huang, L. Li, M. Foo, H. Zeng, D. S. Hwang, *Biomacromolecules* **2016**, *17*, 946.
- [36] J. Sagert, C. Sun, J. H. Waite, *Biological Adhesives*, Vol. 7, (Eds: A. M. Smith, J. A. Callow), Springer, Berlin, Heidelberg **2006**.
- [37] K. Inoue, Y. Takeuchi, D. Miki, S. Odo, S. Harayama, J. H. Waite, *Eur. J. Biochem.* **1996**, *239*, 172.
- [38] J. H. Waite, *J. Biol. Chem.* **1983**, *258*, 2911.
- [39] L. M. Rzepecki, K. M. Hansen, J. H. Waite, *Biol. Bull.* **1992**, *183*, 123.
- [40] S. W. Taylor, J. H. Waite, M. M. Ross, J. Shabanowitz, D. F. Hunt, *J. Am. Chem. Soc.* **1994**, *116*, 10803.
- [41] K. Inoue, Y. Takeuchi, D. Miki, S. Odo, *J. Biol. Chem.* **1995**, *270*, 6698.
- [42] S. C. Warner, J. H. Waite, *Mar. Biol.* **1999**, *134*, 729.
- [43] H. Zhao, J. H. Waite, *Biochemistry* **2006**, *45*, 14223.
- [44] V. V. Papov, T. V. Diamond, K. Biemann, J. H. Waite, *J. Biol. Chem.* **1995**, *270*, 20183.
- [45] H. Zhao, N. B. Robertson, S. A. Jewhurst, J. H. Waite, *J. Biol. Chem.* **2006**, *281*, 11090.
- [46] H. Zhao, J. H. Waite, *J. Biol. Chem.* **2006**, *281*, 26150.
- [47] J. H. Waite, X. Qin, *Biochemistry* **2001**, *40*, 2887.
- [48] J. Yu, W. Wei, E. Danner, R. K. Ashley, J. N. Israelachvili, J. H. Waite, *Nat. Chem. Biol.* **2011**, *7*, 588.
- [49] S. C. T. Nicklisch, S. Das, N. R. Martinez Rodriguez, J. H. Waite, J. N. Israelachvili, *Biotechnol. Prog.* **2013**, *29*, 1587.
- [50] K. Marumo, J. H. Waite, *J. Exp. Zool.* **1987**, *244*, 365.
- [51] J. H. Waite, *J. Mar. Biol. Assoc. U.K.* **1985**, *65*, 359.
- [52] J. D. Smyth, *Q. J. Microsc. Sci.* **1954**, *95*, 139.

- [53] J. H. Waite, *Comp. Biochem. Physiol. Part B: Biochem. Mol. Biol.* **1990**, *97*, 19.
- [54] P. A. Guerette, S. Hoon, Y. Seow, M. Raida, A. Masic, F. T. Wong, V. H. B. Ho, K. W. Kong, M. C. Demirel, A. Pena-Francesch, S. Amini, G. Z. Tay, D. Ding, A. Miserez, *Nat. Biotechnol.* **2013**, *31*, 908.
- [55] Q. Lu, D. S. Hwang, Y. Liu, H. Zeng, *Biomaterials* **2012**, *33*, 1903.
- [56] C. V. Benedict, J. H. Waite, *J. Morphol.* **1986**, *189*, 171.
- [57] D. Montroni, F. Valle, S. Rapino, S. Fermani, M. Calvaresi, M. J. Harrington, G. Falini, *ACS Biomater. Sci. Eng.* **2018**, *4*, 57.
- [58] F. Burette, C. Pellerin, I. Marcotte, *J. Mater. Chem. B* **2014**, *2*, 6378.
- [59] F. Burette, A. Laventure, I. Marcotte, C. Pellerin, *Biomacromolecules* **2016**, *17*, 3277.
- [60] M. J. Harrington, J. H. Waite, *Biomacromolecules* **2008**, *9*, 1480.
- [61] M. J. Harrington, J. H. Waite, *Adv. Mater.* **2009**, *21*, 440.
- [62] J. H. Waite, M. L. Tanzer, *Science* **1981**, *212*, 1038.
- [63] A. Hagenau, M. H. Suhre, T. R. Scheibel, *Prog. Polym. Sci.* **2014**, *39*, 1564.
- [64] Y. J. Yang, Y. S. Choi, D. Jung, H. J. Cha, *Korean J. Chem. Eng.* **2011**, *28*, 1744.
- [65] A. V. Golser, T. Scheibel, *RSC Adv.* **2017**, *7*, 38273.
- [66] H. Y. Yoo, Y. H. Song, M. Foo, E. Seo, D. S. Hwang, J. H. Seo, *BMC Biotechnol.* **2016**, *16*, 16.
- [67] M. H. Suhre, T. Scheibel, *J. Struct. Biol.* **2014**, *186*, 75.
- [68] M. H. Suhre, T. Scheibel, C. Steegborn, M. Gertz, *Acta Crystallogr. Sect. F: Struct. Biol. Commun.* **2014**, *70*, 769.
- [69] A. J. Salerno, I. Goldberg, *Appl. Microbiol. Biotechnol.* **1993**, *39*, 221.
- [70] M. Kitamura, K. Kawakami, N. Nakamura, K. Tsumoto, H. Uchiyama, Y. Ueda, I. Kumagai, T. Nakaya, *J. Polym. Sci. Part A: Polym. Chem.* **1999**, *37*, 729.
- [71] N. R. Movva, K. Nakamura, M. Inouye, *J. Biol. Chem.* **1980**, *255*, 27.
- [72] S. J. Lee, Y. H. Han, B. H. Nam, Y. O. Kim, P. R. Reeves, *Mol. Cells* **2008**, *26*, 34.
- [73] D. R. Filpula, S.-M. Lee, R. P. Link, S. L. Strausberg, R. L. Strausberg, *Biotechnol. Prog.* **1990**, *6*, 171.
- [74] H. G. Silverman, F. F. Roberto, US Patent 6987170B1, **2004**.
- [75] H. G. Silverman, F. F. Roberto, US Patent 6995012B1, **2004**.
- [76] K. E. Anderson, J. H. Waite, *J. Exp. Biol.* **2000**, *203*, 3065.
- [77] D. S. Hwang, Y. Gim, H. J. Cha, *Biotechnol. Prog.* **2005**, *21*, 965.
- [78] D. S. Hwang, H. J. Yoo, J. H. Jun, W. K. Moon, H. J. Cha, *Appl. Environ. Microbiol.* **2004**, *70*, 3352.
- [79] D. S. Hwang, Y. Gim, D. G. Kang, Y. K. Kim, H. J. Cha, *J. Biotechnol.* **2007**, *127*, 727.
- [80] B. Yang, D. G. Kang, J. H. Seo, Y. S. Choi, H. J. Cha, *Biofouling* **2013**, *29*, 483.
- [81] Y. S. Choi, D. G. Kang, S. Lim, Y. J. Yang, C. S. Kim, H. J. Cha, *Biofouling* **2011**, *27*, 729.
- [82] J. D. Platko, M. Deeg, V. Thompson, Z. Al-Hinai, H. Glick, K. Pontius, P. Colussi, C. Taron, D. L. Kaplan, *Protein Expr. Purif.* **2008**, *57*, 57.
- [83] D. S. Hwang, Y. Gim, H. J. Yoo, H. J. Cha, *Biomaterials* **2007**, *28*, 3560.
- [84] H. J. Cha, D. S. Hwang, S. Lim, J. D. White, C. R. Matos-Perez, J. J. Wilker, *Biofouling* **2009**, *25*, 99.
- [85] Y. Gim, D. S. Hwang, S. Lim, Y. H. Song, H. J. Cha, *Biotechnol. Prog.* **2008**, *24*, 1272.
- [86] K. L. Dikshit, D. A. Webster, *Gene* **1988**, *70*, 377.
- [87] C. Khosla, J. E. Bailey, *Nature* **1988**, *331*, 633.
- [88] L.-J. Chien, C.-K. Lee, *Biotechnol. Prog.* **2007**, *23*, 1017.
- [89] D. Kang, Y. Kim, H. Cha, *Appl. Microbiol. Biotechnol.* **2002**, *59*, 523.
- [90] D. Kim, D. S. Hwang, D. G. Kang, J. Y. H. Kim, H. J. Cha, *Biotechnol. Prog.* **2008**, *24*, 663.
- [91] B. Yang, N. Ayyadurai, H. Yun, Y. S. Choi, B. H. Hwang, J. Huang, Q. Lu, H. Zeng, H. J. Cha, *Angew. Chem.* **2014**, *53*, 13360.
- [92] Y. S. Choi, Y. J. Yang, B. Yang, H. J. Cha, *Microb. Cell Fact.* **2012**, *11*, 139.
- [93] S. Lim, K. R. Kim, Y. S. Choi, D.-K. Kim, D. Hwang, H. J. Cha, *Biotechnol. Prog.* **2011**, *27*, 1390.
- [94] Y. Takeuchi, K. Inoue, D. Miki, S. Odo, S. Harayama, *J. Exp. Zool.* **1999**, *283*, 131.
- [95] J. H. Waite, *Integr. Comp. Biol.* **2002**, *42*, 1172.
- [96] S. Lim, Y. S. Choi, D. G. Kang, Y. H. Song, H. J. Cha, *Biomaterials* **2010**, *31*, 3715.
- [97] L. Wang, J. Xie, P. G. Schultz, *Annu. Rev. Biophys. Biomol. Struct.* **2006**, *35*, 225.
- [98] J. A. Johnson, Y. Y. Lu, J. A. Van Deventer, D. A. Tirrell, *Curr. Opin. Chem. Biol.* **2010**, *14*, 774.
- [99] K. Ozawa, M. J. Headlam, D. Mouradov, S. J. Watt, J. L. Beck, K. J. Rodgers, R. T. Dean, T. Huber, G. Otting, N. E. Dixon, *FEBS J.* **2005**, *272*, 3162.
- [100] R. Calendar, P. Berg, *Biochemistry* **1966**, *5*, 1690.
- [101] G. Högenauer, G. Kreil, H. Bernheimer, *FEBS Lett.* **1978**, *88*, 101.
- [102] N. Ayyadurai, N. S. Prabhu, K. Deepankumar, Y. J. Jang, N. Chitrapriya, E. Song, N. Lee, S. K. Kim, B.-G. Kim, N. Soundarajan, S. Lee, H. J. Cha, N. Budisa, H. Yun, *Bioconjugate Chem.* **2011**, *22*, 551.
- [103] N. Ayyadurai, N. S. Prabhu, K. Deepankumar, S.-G. Lee, H. H. Jeong, C. S. Lee, H. Yun, *Angew. Chem.* **2011**, *50*, 6534.
- [104] L. Alfonta, Z. Zhang, S. Uryu, J. A. Loo, P. G. Schultz, *J. Am. Chem. Soc.* **2003**, *125*, 14662.
- [105] C. S. Kim, B.-H. Choi, J. H. Seo, G. Lim, H. J. Cha, *Biosens. Bioelectron.* **2013**, *41*, 199.
- [106] H. J. Kim, B. H. Hwang, S. Lim, B.-H. Choi, S. H. Kang, H. J. Cha, *Biomaterials* **2015**, *72*, 104.
- [107] M. I. Pitman, D. Menche, E. K. Song, A. Ben-Yishay, D. Gilbert, D. A. Grande, *Bull. Hosp. Jt. Dis. Orthop. Inst.* **1989**, *49*, 213.
- [108] C. Sáez, J. Pardo, E. Gutierrez, M. Brito, L. O. Burzio, *Comp. Biochem. Physiol. B* **1991**, *98*, 569.
- [109] B.-H. Choi, Y. S. Choi, D. G. Kang, B. J. Kim, Y. H. Song, H. J. Cha, *Biomaterials* **2010**, *31*, 8980.
- [110] D. S. Hwang, S. B. Sim, H. J. Cha, *Biomaterials* **2007**, *28*, 4039.
- [111] Y. K. Jo, J. H. Seo, B.-H. Choi, B. J. Kim, H. H. Shin, B. H. Hwang, H. J. Cha, *ACS Appl. Mater. Interfaces* **2014**, *6*, 20242.
- [112] S. P. Massia, J. A. Hubbell, *Anal. Biochem.* **1990**, *187*, 292.
- [113] S. Wohlrab, S. Müller, A. Schmidt, S. Neubauer, H. Kessler, A. Leal-Egaña, T. Scheibel, *Biomaterials* **2012**, *33*, 6650.
- [114] R. R. Naik, S. J. Stringer, G. Agarwal, S. E. Jones, M. O. Stone, *Nat. Mater.* **2002**, *1*, 169.
- [115] B. P. Lee, P. B. Messersmith, J. N. Israelachvili, J. H. Waite, *Annu. Rev. Mater. Res.* **2011**, *41*, 99.
- [116] C. Zhong, T. Gurry, A. A. Cheng, J. Downey, Z. Deng, C. M. Stultz, T. K. Lu, *Nat. Nanotechnol.* **2014**, *9*, 858.
- [117] S. G. Kumbar, R. James, S. P. Nukavarapu, C. T. Laurencin, *Biomed. Mater.* **2008**, *3*, 034002.
- [118] B. J. Kim, Y. S. Choi, H. J. Cha, *Angew. Chem.* **2012**, *124*, 699.
- [119] J. T. G. Overbeek, M. J. Voorn, *J. Cell. Comp. Physiol.* **1957**, *49*, 7.
- [120] H. G. Bungenberg de Jong, *Colloid Science*, Vol. 2, (Ed: H. R. Kruyt), Elsevier, Amsterdam **1949**.
- [121] S. Kim, H. Y. Yoo, J. Huang, Y. Lee, S. Park, Y. Park, S. Jin, Y. M. Jung, H. Zeng, D. S. Hwang, Y. Jho, *ACS Nano* **2017**, *11*, 6764.
- [122] S. Kim, A. Faghihnejad, Y. Lee, Y. Jho, H. Zeng, D. S. Hwang, *J. Mater. Chem. B* **2015**, *3*, 738.
- [123] M. A. Gebbie, W. Wei, A. M. Schrader, T. R. Cristiani, H. A. Dobbs, M. Idso, *Nat. Chem.* **2017**, *9*, 473.
- [124] W. Wei, Y. Tan, N. R. Martinez Rodriguez, J. Yu, J. N. Israelachvili, J. H. Waite, *Acta Biomater.* **2014**, *10*, 1663.
- [125] D. S. Hwang, H. Zeng, A. Srivastava, D. V. Krogstad, M. Tirrell, J. N. Israelachvili, J. H. Waite, *Soft Matter* **2010**, *6*, 3232.

- [126] D. S. Hwang, J. H. Waite, M. Tirrell, *Biomaterials* **2010**, *31*, 1080.
- [127] M. Long, H. J. Rack, *Biomaterials* **1998**, *19*, 1621.
- [128] E. M. Hetrick, M. H. Schoenfisch, *Chem. Soc. Rev.* **2006**, *35*, 780.
- [129] B. J. Kim, D. X. Oh, S. Kim, J. H. Seo, D. S. Hwang, A. Masic, D. K. Han, H. J. Cha, *Biomacromolecules* **2014**, *15*, 1579.
- [130] M. Krogsgaard, V. Nue, H. Birkedal, *Chem. Eur. J.* **2016**, *22*, 844.
- [131] E. Y. Jeon, B. H. Hwang, Y. J. Yang, B. J. Kim, B.-H. Choi, G. Y. Jung, H. J. Cha, *Biomaterials* **2015**, *67*, 11.
- [132] H. Wu, Z. Hu, X.-Q. Liu, *Proc. Natl. Acad. Sci. USA* **1998**, *95*, 9226.
- [133] H. Wu, M.-Q. Xu, X.-Q. Liu, *Biochim. Biophys. Acta Protein Struct. Mol. Enzymol.* **1998**, *1387*, 422.

***Publication II***

***Coacervation of the recombinant *Mytilus galloprovincialis* foot protein-3b.***

**Jia Wang, Thomas Scheibel**

Published in *Biomacromolecules*, 2018, 28, 14

Reprinted with kind permission from American Chemical Society

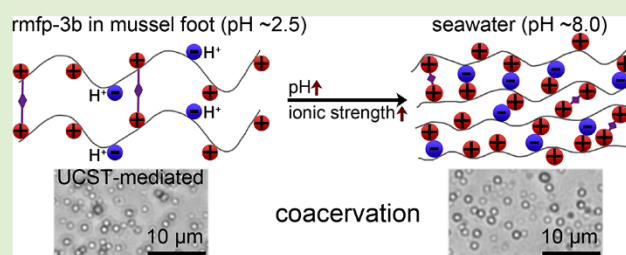
# Coacervation of the Recombinant *Mytilus galloprovincialis* Foot Protein-3b

Jia Wang<sup>†</sup> and Thomas Scheibel<sup>\*,†,‡,§,||,⊥,#</sup>

<sup>†</sup>Lehrstuhl Biomaterialien, <sup>‡</sup>Forschungszentrum für Bio-Makromoleküle (BIOMac), <sup>§</sup>Bayreuther Zentrum für Kolloide und Grenzflächen (BZKG), <sup>||</sup>Bayreuther Materialzentrum (BayMat), <sup>⊥</sup>Bayreuther Zentrum für Molekulare Biowissenschaften (BZMB), and <sup>#</sup>Bayrisches Polymerinstitut (BPI), Universität Bayreuth, 95440 Bayreuth, Germany

## Supporting Information

**ABSTRACT:** The underwater adhesion of marine mussels is a fascinating example of how proteinaceous adhesives, although water-soluble to begin with, can be used in seawater. Marine mussels adhere to the substrate via adhesive plaques, where the adhesive proteins are located especially at the substratum's interface. One major compound of the adhesives in Mytilidae is the mussel foot protein 3b (mfp-3b). Here, recombinant mfp-3b (rmfp-3b) was produced in *Escherichia coli*. rmfp-3b showed upper critical solution temperature (UCST) mediated complex coacervation at pH 3.0 in the presence of citrate yielding a liquid–liquid phase separation. Further, the rmfp-3b coacervation could also be induced in seawater conditions such as the respective pH and ionic strength, but without UCST behavior. In particular, sulfate and citrate anions could significantly induce complex coacervation. This study provides insights into the molecular behavior of one of the key proteins of mussels involved in underwater adhesion and may inspire new applications of bioadhesives using recombinant mussel foot proteins.



## INTRODUCTION

Some marine mussels, such as members of the family of Mytilidae, live in rocky intertidal habitats that are regularly exposed to strong waves and currents.<sup>1,2</sup> To survive in such environment, mussels attach themselves to a solid substrate (e.g., rocks) by proteinaceous adhesives.<sup>3,4</sup> For a material scientist, strong underwater adhesives have large potential for (biomedical) applications, for example, in wound closure devices.<sup>5</sup> Therefore, understanding the mechanism of mussel adhesion provides useful insights into the future design of bioinspired underwater adhesives. The mussel adhesives of Mytilidae comprise mussel foot proteins (mfps), which reflect water-soluble polycations, although some also carry a few acidic residues.<sup>4,6</sup> One important question of mussel underwater adhesion is how it is possible to secrete the soluble protein-based adhesives onto wet substrates without dispersion into the surrounding seawater.

In principle, at distinct conditions, oppositely charged polyelectrolytes can neutralize each other by electrostatic interaction, leading to liquid–liquid phase separation, which is called complex coacervation, and the polyelectrolytes enriched phase is referred to as coacervate.<sup>7,8</sup> Complex coacervation for dispensing adhesives is a feasible route for several marine organisms, such as sandcastle worms.<sup>9–11</sup> In the case of sandcastle worms, a glue is secreted in a dense coacervate with a set of oppositely charged polyelectrolytes and at high concentrations of calcium and magnesium ions.<sup>10</sup> Such condensed coacervate exhibits favorable physical properties

for underwater adhesion. One crucial mechanical property of coacervate is its extraordinarily low interfacial energy, which advances the spreading of the coacervate on substrates.<sup>12–14</sup> Additionally, the shear-thinning behavior of coacervate can improve its flow without clogging during secretion of the adhesive.<sup>14,15</sup> The mfps in Mytilidae adhesives have also been shown to exhibit liquid–liquid phase separation behavior. To induce complex coacervation of mfps, previously an artificial anionic polyelectrolyte, such as hyaluronic acid, was mixed with distinct mfps (fp151,<sup>16</sup> pf131,<sup>16</sup> and fp1<sup>12</sup>) at a mixing ratio neutralizing the net charges. Thereby, highly condensed coacervate of mfps was achieved with good adhesive strength in both dry and wet environments.<sup>16</sup>

In addition to complex coacervation, another type of coacervation is self-coacervation, in which only a single polyelectrolyte is necessary. Self-coacervation of zwitterionic polyelectrolytes with basic as well as acidic residues, however, can be compared with complex coacervation. Zwitterionic and hydrophobic mfp3S, for instance, undergoes phase separation driven by electrostatic attraction and hydrophobic interactions at solution conditions existing beneath the foot during plaque formation.<sup>17</sup> Without additional anionic polyelectrolyte, self-coacervation of cationic recombinant mfp-1 (rmfp-1) was induced by strong cation– $\pi$  interaction in the presence of 0.7 M

Received: April 8, 2018

Revised: July 29, 2018

Published: August 2, 2018

NaCl.<sup>14</sup> Similarly, cationic recombinant DgHBP-1 (recDgHBP-1), a highly modular histidine-rich protein from the beak of the jumbo squid *Dosidicus gigas*, also undergoes self-coacervation driven by hydrophobic interactions at seawater level conditions.<sup>15</sup>

Coacervation can also be triggered by temperature. Two types of temperature-related mechanisms have been detected, lower as well as upper critical solution temperature behavior. There is a vast number of polymers and proteins showing lower critical solution temperature (LCST) behavior. Exemplarily for hydrophobic tropoelastin<sup>18,19</sup> and elastin-mimic proteins (EMPs),<sup>20</sup> increasing temperature above their LCST induces their coacervation based on hydrophobic interactions. In contrast, only few examples of polymers have been reported showing upper critical solution temperature (UCST) behavior, and almost all UCST-based phase transitions are induced under relatively extreme conditions (below 0 °C or above 100 °C), which has restricted the development of UCST behavior based biomaterials so far.<sup>21–23</sup>

Here, it was detected that recombinant mfp-3b (rmfp-3b), a zwitterionic and hydrophilic protein based on an adhesive foot protein from *Mytilus galloprovincialis* (*M. galloprovincialis*) exhibits UCST-mediated complex coacervation at pH 3.0 in the presence of citrate and phase separates at temperatures below its UCST. To the best of our knowledge, this is the first example of mfps with UCST behavior. Additionally, the coacervation of rmfp-3b could also be induced at seawater level pH and ionic strength. Especially sulfate and citrate ions could significantly trigger complex coacervation. Insights into the coacervation of rmfp-3b were elucidated by investigating the effects of temperature, pH, and ionic strength on coacervate formation.

## MATERIALS AND METHODS

**Plasmid Construction.** *Escherichia coli* (*E. coli*) DH10B (Novagen, Madison, WI, U.S.A.) was used as a cloning strain. The gene sequence of mfp-3b<sup>24</sup> of *M. galloprovincialis* was obtained from GenBank AB049580 (<https://www.ncbi.nlm.nih.gov/nuccore/10641130>). A synthetic gene encoding mfp-3b adapted to *E. coli* codon usage (vector pEX-A2-mfp3b) was purchased from Eurofins Genomic (Ebersberg, Germany). The mfp-3b gene was amplified by polymerase chain reaction (PCR) with a mixture of pEX-A2-mfp3b as template, two mfp-3b primers (forward, 5'-atcgaattcaacgactactatgg-3'; reverse, 5'-atcgaagctttatcagtagttgtattg-3') and Phusion DNA polymerase (New England BioLabs (NEB)). The approximately 280-bp mfp-3b PCR product was digested using EcoR I and Hind III (NEB). The digested mfp-3b product was introduced into cloning site I encoding a hexahistidine (His<sub>6</sub>) at the protein's N-terminus within the pRSFDuet-1 plasmid (Novagen, Madison, WI, U.S.A.) digested with the same restriction enzymes. The constructed plasmid was denoted as pRSFDuet-mfp3b (3798 bp). To determine the influence of the His<sub>6</sub> tag, the mfp-3b gene was introduced in the pRSFDuet-1 plasmid without a His<sub>6</sub> tag yielding pRSFDuet-mfp3b-NT (3756 bp). This was obtained by using a different forward primer (5'-atccatggggcagcgactactatggcccg-3') and different restriction enzymes (Nco I and Hind III) (NEB).

**Recombinant Production.** The plasmids pRSFDuet-mfp3b and pRSFDuet-mfp3b-NT were transformed into *E. coli* BL21-CodonPlus (DE3)-RIPL (Novagen, Madison, WI, U.S.A.) as host strain for recombinant production of rmfp-3b and rmfp-3b without His<sub>6</sub> tag (rmfp-3b-NT). A single *E. coli* colony from a freshly streaked plate was cultured in 20 mL of LB medium with 50 µg mL<sup>-1</sup> kanamycin at 37 °C for 10 h. The preculture was then transferred into a bioreactor containing 4 L of modified ZYM-5052 autoinduction medium<sup>25</sup> (without 5000 × Trace element and 1000 × Mg<sup>2+</sup>) with 50 µg mL<sup>-1</sup> kanamycin and cultured at 37 °C until an OD<sub>600</sub> of 1.9–2.2 was

reached. Cells were harvested by centrifugation at 8000 rpm for 20 min at 4 °C, washed twice with lysis buffer (40 mM Tris-HCl, pH 8.0), and finally resuspended in 5 mL of lysis buffer per gram of wet weight. The cells were stored at –80 °C for further purification.

**Purification Using Phase Separation.** *E. coli* cells were thawed and incubated with 1 mg lysozyme per gram cells (wet weight), 1 vial Protease-Inhibitor Mix-HP (SERVA, Heidelberg, Germany) and 1 mM phenylmethylsulfonyl fluoride (PMSF) with gentle shaking for 30 min at 4 °C. The cells were further lysed on ice with a Sonopuls HD3200/KE76 ultrasonicator (Bandelin, Berlin, Germany) with a 2 s pulse and 1 s cooling period with sonication energy of 0.1 kJ per mL of cell solution. Lysates were centrifuged at 10000 rpm for 20 min at 4 °C to separate supernatant and pellet. The pellet was washed twice with wash buffer (40 mM Tris-HCl, 100 mM NaCl, 1% Triton X-100, pH 8.0), further washed four times with Millipore (MQ) water, and extracted using 25% (v/v) acetic acid at room temperature (RT) overnight. The protein extraction solution was centrifuged at 10000 rpm for 20 min, and the supernatant was dialyzed against 20 mM citrate buffer, pH 3.0 at 4 °C.

The dialyzed rmfp-3b and rmfp-3b-NT solutions were transferred into 15 mL Greiner tubes and incubated at 4 °C overnight for phase separation. The upper phase was removed carefully and the remaining lower phase underwent a second phase separation upon addition of dialysis buffer. The rmfp-3b and rmfp-3b-NT were obtained from the lower phase after the second phase separation with a purity above 95%.

**Sodium Dodecyl Sulfate-Polyacrylamide Gel Electrophoresis (SDS-PAGE) and Western Blot Analysis.** Samples were heated for 10 min to 95 °C in the presence of Laemmli buffer (60 mM Tris-HCl (pH 6.8), 10% glycerol, 2% SDS, 5% β-mercaptoethanol, 0.01% bromophenol blue). Proteins were separated using SDS-PAGE (20% Tris-Glycine gels) followed by coomassie blue staining. Western blot was performed by transferring proteins onto a polyvinylidene fluoride (PVDF) transfer membrane (GE Healthcare, Germany) for 50 min at 40 mA. rmfp-3b was detected using a horseradish peroxidase-conjugated antihexahistidine antibody (Novagen, Madison, WI, U.S.A.) followed by enhanced chemiluminescence (ECL) detection (GE Healthcare, Germany).

**MALDI-TOF Mass Spectrometry.** MALDI-TOF mass spectrometry was performed on a Bruker Reflex III (Bruker, Germany) equipped with a 337 nm N<sub>2</sub> laser in a linear mode and 20 kV acceleration voltage. rmfp-3b was mixed with a matrix solution (assisting in the ionization of the sample), 20 mg mL<sup>-1</sup> sinapinic acid in 90% acetonitrile and 0.2% trifluoroacetic acid at a ratio of 1:1 before spotting it onto a target plate.

**Nitro Blue Tetrazolium (NBT) Staining.** The 3,4-dihydroxyphenylalanine (DOPA) content of rmfp-3b was analyzed by redox cycling staining at an alkaline pH in the presence of NBT and glycinate.<sup>26</sup> As a positive control, rmfp-3b was incubated with mushroom tyrosinase (weight ratio of rmfp-3b/tyrosinase = 40:1; Sigma) at RT for 1 h. DOPA-deficient BSA was taken as a negative control. Electrophoresis was performed twice under identical conditions. One SDS-PAGE (20%) gel was immersed in NBT/glycinate solution and incubated in the dark until a blue-purple color developed at RT. The stained gel was further washed twice and stored in 0.1 M sodium borate solution. A second SDS-PAGE (20%) gel was stained with coomassie blue as a control.

**Turbidity Measurements.** Coacervation of rmfp-3b was analyzed as a function of pH, salt, and temperature by monitoring the turbidity of the solution in absorbance mode. The absorbance was recorded at a wavelength of 600 nm using a Varian Cary 50 UV–vis spectrophotometer (Agilent Technologies). The rmfp-3b was diluted to 0.1 mg mL<sup>-1</sup> upon addition of 20 mM citrate phosphate buffer at 20 °C, which has good pH buffering capacity within the pH range from 2.2 to 8.0. Similarly, turbidity measurements of rmfp-3b-NT (0.3 mg mL<sup>-1</sup>) were performed with 20 mM citrate phosphate buffer at different pH. To determine the influence of citrate, turbidity measurements were also performed in various buffers at 20 mM (Gly-HCl buffer (pH 3.0), acetate buffer (pH 4.0, pH 5.0, pH 5.6) and Tris-HCl buffer (pH 7.0, pH 8.0)). Each experiment was

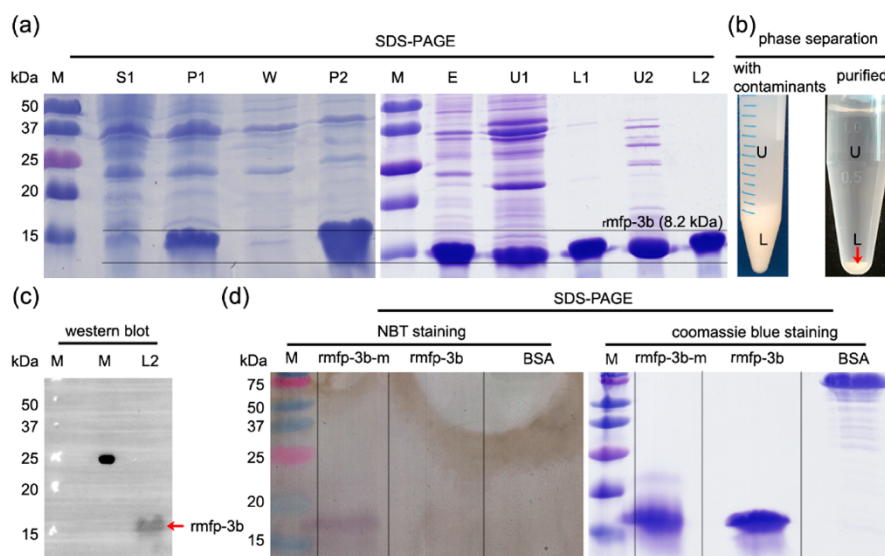


**Figure 1.** Purification of rmfp-3b. (a) Coomassie blue stained SDS-PAGE (20%). *E. coli* cells were lysed and centrifuged to separate supernatant (S1) and pellet (P1), which was further washed (W) to yield pellet P2. rmfp-3b extraction (E) from pellet P2 was performed using 25% acetic acid, and this solution was then dialyzed against 20 mM citrate buffer (pH 3.0). Therein, phase separation occurred (upper phase (U1) and lower phase (L1)) at 4 °C. rmfp-3b was almost pure in lower phase L1, which was again phase separated (upper phase (U2) and lower phase (L2)) to increase the purity. (b) Phase separation before (left panel) and after (right) purification at pH 3.0 and 4 °C. U and L indicate upper and lower phase, respectively. (c) Western blot using His<sub>6</sub> tag antibody HRP conjugate. (d) Qualitative analyses of DOPA content using SDS-PAGE (20%) followed by NBT staining (left panel) and corresponding coomassie blue staining (right panel). rmfp-3b was modified (rmfp-3b-m) using commercial mushroom tyrosinase and BSA was used as a negative control. M indicates prestained protein marker.

performed in triplicate and the shown graphs represent mean values  $\pm$  s.d.

To determine the effect of salt ions on turbidity, the absorbance at 600 nm was measured at 0.1 mg mL<sup>-1</sup> rmfp-3b in the presence of different ions such as chloride salts (NaCl, KCl, MgCl<sub>2</sub>, and CaCl<sub>2</sub>), sulfate salts (Na<sub>2</sub>SO<sub>4</sub>, K<sub>2</sub>SO<sub>4</sub>, and MgSO<sub>4</sub>), and sodium citrate in 80 mM Tris-HCl buffer (pH 8.0) at 20 °C. Artificial seawater<sup>27</sup> (480 mM NaCl, 28 mM MgSO<sub>4</sub>, 24 mM MgCl<sub>2</sub>, 16 mM CaCl<sub>2</sub>, 10 mM KCl, 2.4 mM NaHCO<sub>3</sub> and 20 mM Tris-HCl, pH 8.0) and 80 mM Tris-HCl buffer (pH 8.0) were used as positive and negative controls, respectively. Additionally, turbidity measurements of rmfp-3b and rmfp-3b-NT at different concentrations of Na<sub>2</sub>SO<sub>4</sub> in 20 mM Gly-HCl buffer (pH 3.0) were performed at 20 °C. The identical concentration of NaCl was used as a negative control. Each experiment was performed in triplicate and the shown graphs represent mean values  $\pm$  s.d.

UCST behavior was analyzed by using turbidity measurements. The solution turbidity of 5 mg mL<sup>-1</sup> rmfp-3b in 20 mM citrate buffer (pH 3.0) was measured as a function of temperature. The absorbance at 600 nm was measured continuously with cooling/heating rates of 1 °C per minute. The influence of citrate on the UCST behavior of rmfp-3b (5 mg mL<sup>-1</sup>) and rmfp-3b-NT (4 mg mL<sup>-1</sup>), revealing the identical molar concentration as rmfp-3b) was investigated using citrate concentrations from 0 to 200 mM at pH 3.0. Additionally, the UCST behavior of rmfp-3b (20 mM citrate buffer, pH 3.0) was investigated at protein concentrations from 1 to 13 mg mL<sup>-1</sup>.

**Optical Microscopy.** The UCST-mediated coacervate in the presence of 20 mM citrate buffer (pH 3.0) as well as the freshly prepared rmfp-3b coacervate at a protein concentration of 2 mg mL<sup>-1</sup> in 100 mM Tris-HCl buffer (pH 8.0) were immediately transferred onto a glass slide for bright-field microscopy (DM IL LED, Leica) at RT. The coacervate droplets triggered upon elevated pH grew and moved fast, and images were taken at 1, 2, 5, and 9 min to visualize this process.

**Scanning Electron Microscopy (SEM).** The condensed coacervate mediated by UCST behavior (pH 3.0) was dried by lyophilization overnight and mounted onto a silica wafer, which was then sputtered with 2.6 nm platinum. SEM was performed at an

accelerating voltage of 3 kV, using a Leo 1530 Gemini (Zeiss) equipped with Inlens SE and SE2 detectors.

**Dynamic Light Scattering (DLS) and Zeta Potential Measurements.** Coacervate droplets of rmfp-3b were analyzed using DLS (ZetaSizer NanoZS, Malvern Instruments, Worcestershire, U.K.). The size and zeta potential of coacervate droplets at a protein concentration of 0.05 mg mL<sup>-1</sup> were measured ( $n = 3$ ) in 20 mM citrate phosphate buffer at varying pH at 20 °C. The size of UCST-mediated coacervate of rmfp-3b at different temperatures (from 20 to 3 °C and back to 20 °C (1 °C/min)) was performed at a protein concentration of 1.7 mg mL<sup>-1</sup> in 20 mM citrate buffer (pH 3.0) employing DLS.

**Circular Dichroism (CD) Spectroscopy.** Far-UV CD spectra between 190 and 250 nm were measured at 0.1 mg mL<sup>-1</sup> in cuvettes with 1 mm path length using a Jasco J-715 spectropolarimeter (Jasco, Groß-Umstadt, Germany). The scan speed was 20 nm min<sup>-1</sup>, accumulations 3 times, data pitch 0.1 nm and bandwidth 1 nm. Measurements were performed at 5 °C (pH 3.0) and 25 °C (pH 3.0 and pH 8.0). The plotted spectra were smoothed using the Savitzky-Golay filter.

## RESULTS AND DISCUSSION

**Expression and Purification of rmfp-3b.** Engineered rmfp-3b based on the sequence of natural mfp-3b<sup>24</sup> of *M. galloprovincialis* was produced with as well as without a His<sub>6</sub> tag (MGSSHHHHHSQDPNSSDYYGPNYGPSRRWGGYGYNYNRYNGRRYGGYGGYKGWNRGWRGWSGRRKYN). rmfp-3b contains 2 negatively charged residues, 18 (12 in the absence of the His<sub>6</sub> tag) positively charged residues, and 11 Tyr residues.

rmfp-3b was produced in insoluble inclusion bodies in BL21-CodonPlus(DE3)-RIPL using the vector pRSFDuet-mfp3b (Figure 1a, lane P1, lane S1). Extraction of rmfp-3b (Figure 1a, lane E) from inclusion bodies (Figure 1a, lane P2) after washing (Figure 1a, lane W) was performed using 25% acetic acid, yielding ~80% purity. rmfp-3b appears in SDS-

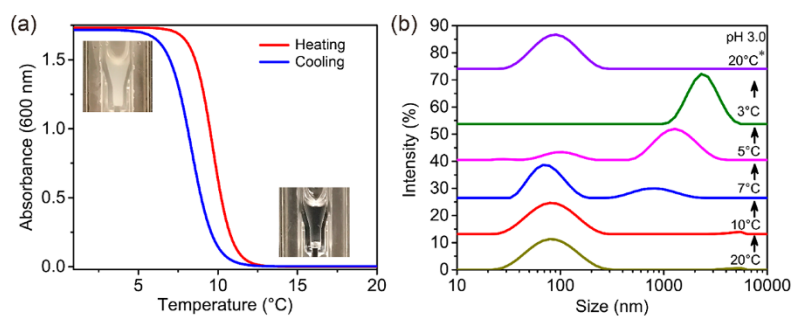


**Figure 2.** Characterization of UCST behavior of rmfp-3b at pH 3.0. (a) Turbidity measurements of rmfp-3b ( $5 \text{ mg mL}^{-1}$ , 20 mM citrate buffer, pH 3.0) at 600 nm as a function of temperature. The photographs show turbidity/transparency at temperatures beneath/above  $\sim 7^\circ\text{C}$ . (b) Size distribution of rmfp-3b ( $1.7 \text{ mg mL}^{-1}$ , 20 mM citrate buffer, pH 3.0) at different temperatures as measured by DLS. The measurements were carried out by ramping the temperature from 20 to  $3^\circ\text{C}$  and back to  $20^\circ\text{C}$  ( $1^\circ\text{C}/\text{min}$ ; indicated by  $20^\circ\text{C}^*$ ).

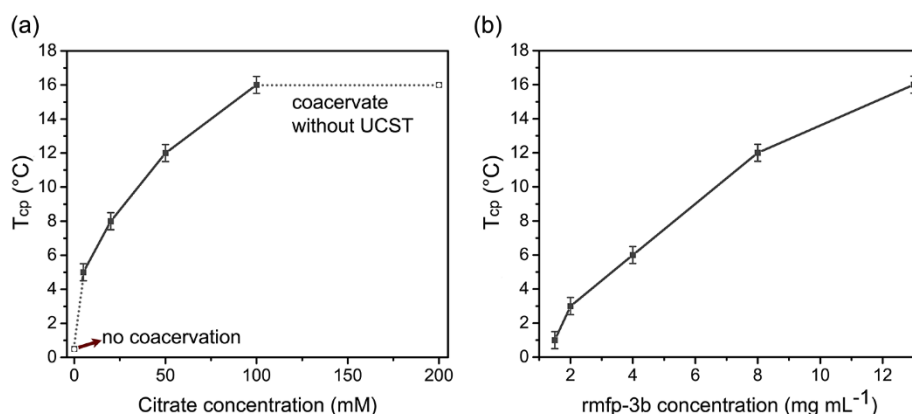


**Figure 3.** Characterization of  $T_{\text{cp}}$  of rmfp-3b at different citrate and protein concentrations at pH 3.0. (a) Influence of citrate concentration on the  $T_{\text{cp}}$  of rmfp-3b ( $5 \text{ mg mL}^{-1}$ ). (b) Influence of protein concentration on the  $T_{\text{cp}}$  of rmfp-3b (20 mM citrate buffer, pH 3.0).  $T_{\text{cp}}$  refers to the cloud point temperature of UCST behavior. Error bars indicate the standard deviation ( $n = 3$ ).

PAGE with an apparent higher molecular weight of  $\sim 14 \text{ kDa}$  (rmfp-3b-NT at  $\sim 12 \text{ kDa}$ ) than the calculated one of  $\sim 8.2 \text{ kDa}$  ( $\sim 6.6 \text{ kDa}$ ) (Figure 1a, S2), a phenomenon that was also observed in previous studies of other mfps.<sup>28,29</sup> This phenomenon is probably caused by nonproportional binding of SDS, due to the explicit amino acid composition.

rmfp-3b was dialyzed against 20 mM citrate buffer, pH 3.0 and purified using phase separation overnight at  $4^\circ\text{C}$ , resulting in two distinct phases (upper and lower phase) as shown in Figure 1b. rmfp-3b was found to be almost pure in the lower phase (Figure 1a, lane L1). Repeating the phase separation step for the lower phase, the purity of rmfp-3b was even increased yielding  $\sim 95\%$  (Figure 1a, lane L2), and the protein's identity could be confirmed by Western blot (Figure 1c, lane L2). rmfp-3b showed a molecular weight of  $8.1 \text{ kDa}$  by MALDI-TOF analysis, which is almost identical to the predicted one of  $8.2 \text{ kDa}$  (Figure S1). After an additional dialysis step, the purified protein was stored at  $-20^\circ\text{C}$ . The rmfp-3b-NT was produced and purified under the identical conditions as rmfp-3b (Figure S2).

Given that quinoproteins can be specifically stained with NBT/glycinate solution due to redox cycling,<sup>26</sup> the DOPA content of rmfp-3b was qualitatively investigated to see if it is possible to activate rmfp-3b (i.e., to post-translationally modify the Tyr residues into DOPA in vitro). rmfp-3b without tyrosinase treatment, like the DOPA-deficient negative control BSA, did not stain, but upon modification with mushroom tyrosinase, the resulting rmfp-3b-m was clearly stained (Figure

1d). This indicated that the Tyr residues of rmfp-3b could be modified after purification in vitro. In the following experiments, rmfp-3b (DOPA-deficient) without further modification was investigated concerning its assembly behavior without putatively interfering redox reactions of DOPA residues.

**UCST-Mediated Coacervation of rmfp-3b.** The temperature dependence of rmfp-3b coacervation was measured at pH 3.0. Upon cooling, the rmfp-3b solution ( $5 \text{ mg mL}^{-1}$ , 20 mM citrate buffer, pH 3.0) changed from being transparent to turbid at  $\sim 7^\circ\text{C}$  ( $T_{\text{cp}}$ , cloud point temperature for UCST behavior), which was reversible upon heating (Figure 2a). The result indicated a sharp phase transition of rmfp-3b showing UCST behavior. The temperature-dependent size distribution of rmfp-3b was determined using DLS measurements. For a globular protein of  $\sim 10 \text{ kDa}$ , its hydrodynamic diameter  $D_h$  should be  $\sim 3 \text{ nm}$ .<sup>30</sup> However, the  $D_h$  value of rmfp-3b was about  $80 \text{ nm}$  when in the soluble state at  $20^\circ\text{C}$  (Figure 2b). Upon cooling, an increase in the hydrodynamic diameter  $D_h$  was observed at approximately  $5^\circ\text{C}$ , which further confirmed the fully reversible UCST phase transition behavior (Figure 2b). Secondary structure analysis of rmfp-3b showed a polyglycine II helix-like structure almost independent of the temperature ( $5$  or  $25^\circ\text{C}$ , respectively) and pH, indicating no significant change in secondary structure upon coacervation (Figure S3).

The  $T_{\text{cp}}$  of rmfp-3b was significantly affected by both the citrate and protein concentration (Figure 3). There was no UCST-mediated coacervation detected without citrate (Figure

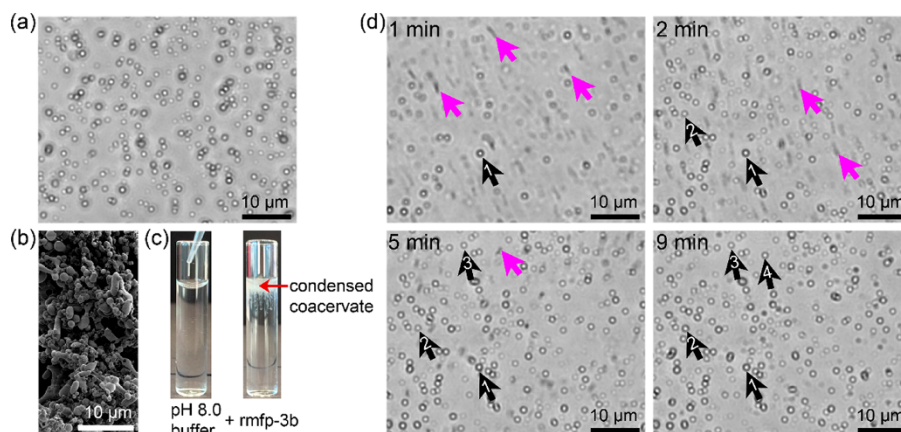


**Figure 4.** Morphology of rmfp-3b coacervate. (a) Optical microscopy image of UCST-mediated rmfp-3b coacervate obtained at pH 3.0. (b) SEM image of UCST-mediated rmfp-3b coacervate obtained at pH 3.0. (c) Visualization of rmfp-3b coacervate triggered upon elevated pH (pH 8.0) at RT. rmfp-3b coacervate was obtained by pipetting rmfp-3b (pH 3.0) into 100 mM Tris-HCl buffer (pH 8.0) at RT. (d) Optical microscopy images of rmfp-3b coacervate taken 1, 2, 5, and 9 min after initiation in 100 mM Tris-HCl buffer (pH 8.0) at RT. The freshly prepared coacervate (magenta arrows) moved fast and grew quickly into big size droplets (black arrows), which settled down to the glass surface gradually due to their high density. The black arrows with same Arabic numbers display the identical droplets at the identical position.

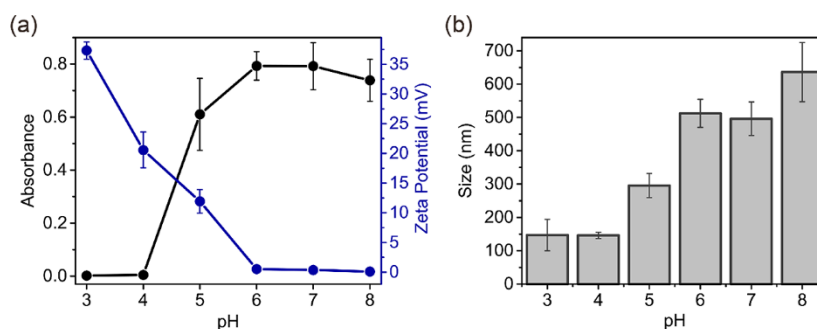


**Figure 5.** Characterization of rmfp-3b coacervation as a function of pH at 20 °C. (a) Turbidity (black) and zeta potential (blue) of rmfp-3b at different pH values. Turbidity was recorded at a wavelength of 600 nm. (b) Size distribution of rmfp-3b droplets at different pH values, as measured using DLS. Error bars indicate the standard deviation ( $n = 3$ ).

3a), indicating that citrate contributed to the complex coacervation with cationic rmfp-3b. The  $T_{cp}$  of rmfp-3b increased with increasing citrate (Figure 3a) and protein concentration (Figure 3b). The  $T_{cp}$  of rmfp-3b (5 mg mL<sup>-1</sup>) reached ~16 °C in the presence of 100 mM citrate (Figure 3a). Above 100 mM citrate, coacervation was detected without the appearance of UCST behavior (Figure 3a). Compared to rmfp-3b, rmfp-3b-NT exhibited a similar UCST behavior (Figure S4). Owing to the His<sub>6</sub> tag, rmfp-3b displayed a slightly higher  $T_{cp}$  at identical protein and citrate concentration (Figure 3a, S4). At high protein concentrations, entanglement between the protein chains is favored inducing the association of the protein chains.<sup>32–34</sup> When the concentration of rmfp-3b (20 mM citrate) was as high as 13 mg mL<sup>-1</sup>, the  $T_{cp}$  was ~16 °C and when below ~1.5 mg mL<sup>-1</sup>, the UCST behavior disappeared (Figure 3b).

rmfp-3b comprises 50.7% hydrophilic residues including 29% charged and 21.7% uncharged residues and is hydrophilic, as indicated by a Kyte-Doolittle<sup>31</sup> hydrophobicity plot (ExpAsy, Figure S7). At temperatures above UCST, the hydrophilic residues are surface exposed and form a shell with surrounding water molecules, which restrains the attractive forces between proteins and further enhances the stability. Below UCST, the extent of this shell reduces significantly and hydrogen bonding between hydrophilic residues as well as

deprotonated citrate (due to the slightly increase of buffer pH) increases, which results in increased molecular association.<sup>32</sup> Compared to LCST of hydrophobic tropoelastin<sup>18,19</sup> and EMPs,<sup>20</sup> the hydrophobic effect is less dominant in UCST-type polymers.<sup>32</sup>

**Morphology of the rmfp-3b Coacervate.** Precipitates can be distinguished from coacervate by optical microscopy.<sup>35</sup> As shown by Figure 4a, UCST-mediated rmfp-3b coacervates (20 mM citrate buffer, pH 3.0) are composed of well-dispersed spherical droplets with diameters between ~0.7 and ~1.5 μm and the corresponding SEM image displayed interconnected spheres with diameters between ~0.2 and ~5 μm (Figure 4b). Owing to the accumulation of coacervate droplets, the DLS experiments displayed bigger sizes (Figure 2b). Additionally, when such solution was pipetted into 100 mM Tris-HCl (pH 8.0) buffer at RT, a condensed coacervate was formed immediately as a result of liquid–liquid phase separation (Figure 4c), but without any detectable UCST behavior. The coacervate could be observed using optical microscopy (Figure 4d). After 1 min of incubation, a great number of spherical coacervate droplets could be determined to move fast and collide, making it difficult to capture a clear morphology (Figure 4d, 1 min, magenta arrows). As time elapsed, coacervate droplets (Figure 4d, magenta arrows) grew bigger and settled on the surface due to their high density (Figure 4d,

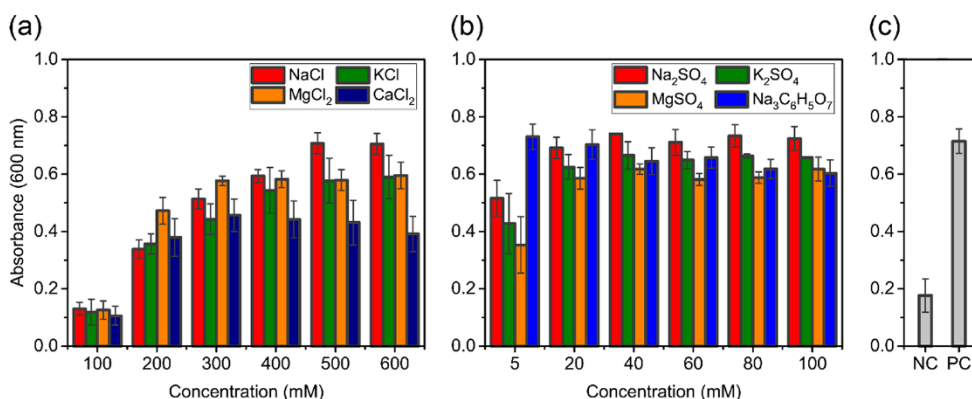


**Figure 6.** Turbidity of rmfp-3b at different ion composition and ionic strength at pH 8.0 and 20 °C. (a) Influence of different chloride salts on the turbidity of rmfp-3b in 80 mM Tris-HCl buffer, pH 8.0. (b) Influence of different sulfate salts as well as citrate on turbidity of rmfp-3b in 80 mM Tris-HCl buffer, pH 8.0. (c) Turbidity of rmfp-3b in 80 mM Tris-HCl buffer (pH 8.0) as a negative control (NC) and in artificial seawater<sup>27</sup> (480 mM NaCl, 28 mM MgSO<sub>4</sub>, 24 mM MgCl<sub>2</sub>, 16 mM CaCl<sub>2</sub>, 10 mM KCl, 2.4 mM NaHCO<sub>3</sub> and 20 mM Tris-HCl, pH 8.0) as a positive control (PC). Error bars indicate the standard deviation ( $n = 3$ ).

black arrows). At 9 min, most droplets settled on the glass surface and only a few small ones were still moving (Figure 4d, 9 min). During this process, the coacervate droplets retained a spherical shape, which is different to normal irregular aggregation and precipitation (Figure 4d).

**Effect of pH and Ionic Strength on Coacervation.** Due to the pH and ionic strength differences between the mussel foot and seawater, the influences of pH and ionic strength on rmfp-3b behavior were investigated more carefully. Coacervation was qualitatively measured using turbidity measurements at different buffer conditions, including different pH, ion composition and ionic strength. Comprising 10 Arg residues (+), 2 Lys residues (+), 6 His residues (+), and 2 Asp residues (−), the experimental isoelectric point (PI, zeta potential,  $\zeta = 0$ ) of rmfp-3b was observed at pH 6.0 (Figure 5a), compared to the theoretical value of pI  $\sim 10.3$  (ExPASy).

At low pH (pH 3.0–4.0), the acidic residues (Asp and carboxy-terminus) of rmfp-3b were protonated and the basic residues (Arg, Lys, His, and amino-terminus) displayed a positive net charge in the soluble state at 20 °C (Figure 5a). Notably, an increase in turbidity and hydrodynamic diameter  $D_h$  was observed between pH 4.0 and pH 6.0 with deprotonation of the acidic residues as well as citrate, and a corresponding decrease of the net charge to zero (Figure 5). To some degree, the His<sub>6</sub> tag in rmfp-3b slightly supported coacervation due to the additional positive charges, but did not significantly influence the coacervation behavior as seen in comparison to that of rmfp-3b-NT (Figures 5a and S5). To eliminate the influence of citrate, coacervation in various buffers without citrate was also investigated, displaying also a coacervation behavior, but with much lower turbidity intensity (Figure S5).

For the gastropod *Philine aperta*, it has been reported that its acidic secretion contains predominantly sulfate anions.<sup>36</sup> Therefore, we tested sulfate anions, which were also able to trigger the complex coacervation of rmfp-3b as well as rmfp-3b-NT at pH 3.0 (Figure S6). Similarly, phosphorylated Pc3 proteins, the cement proteins of sandcastle worms, were proposed to be packed as complex coacervate with magnesium ions in secretory granules.<sup>37,38</sup> This indicates that rmfp-3b probably already exists as coacervate in the acidic mussel phenol gland. Since ion composition as well as pH switches when secreted from the mussel phenol gland to seawater, the

influence of ion composition and ionic strength was also determined on coacervation at pH 8.0 using turbidity measurements with artificial seawater as a positive control as well as Tris-HCl buffer (pH 8.0) as a negative control (Figure 6). With regard to chloride salts, the turbidity reached its maximum at an ionic strength of around 500 mM at pH 8.0, since at that molarity salt screened the long-range electrostatic double layer repulsion (Figure 6a).<sup>14</sup> However, sulfate and citrate salts induced turbidity already at 20 mM at pH 8.0 (Figure 6b), due to complex coacervation. It should be noted that the optimal conditions for coacervation at pH 8.0 were close to the composition of seawater, including pH and salinity, which is an indicator that seawater could be a natural regulator to induce coacervation.

Recently, acidic secretion of marine mussels (*Mytilus californianus*) was identified at pH  $\sim 2.5$  by tethering a pH-sensitive fluorescent dye,<sup>39</sup> and the ionic strength was measured to be 0.15 M.<sup>40</sup> Upon acidic secretion, positively charged rmfp-3b could probably associate and induce complex coacervation with sulfate anions (Figures 6b, 7, and S6). Once the acidic rmfp-3b coacervate is in contact with the surrounding seawater, it undergoes a pH jump from  $\sim 2.5$  to  $\sim 8.0$ , resulting in a decrease of net charge, and the ionic strength switches from  $\sim 0.15$  to  $\sim 0.7$  M. Consequently, the long-range electrostatic repulsion of rmfp-3b is reduced by the decreasing net charge and the increasing ionic strength of surrounding seawater,<sup>14</sup> which leads to the formation of a condensed coacervate (Figure 7). The properties of the coacervate, such as low interfacial energy, shear-thinning behavior, and a high friction coefficient, make it ideal for secretion, spreading and location on various surfaces without dispersion in the ocean.<sup>12,13,15</sup>

## CONCLUSION

Using liquid–liquid phase separation at 4 °C in the presence of citrate, rmfp-3b was purified without requiring additional downstream purification steps. rmfp-3b showed a reversible UCST-mediated complex coacervation in the presence of citrate at pH 3.0 with solutions turning from soluble and transparent to turbid when the temperature was below UCST, due to the significant decrease of hydrogen bonding between hydrophilic residues with water and the slight increase of citrate deprotonation, as well as the consequent increase of

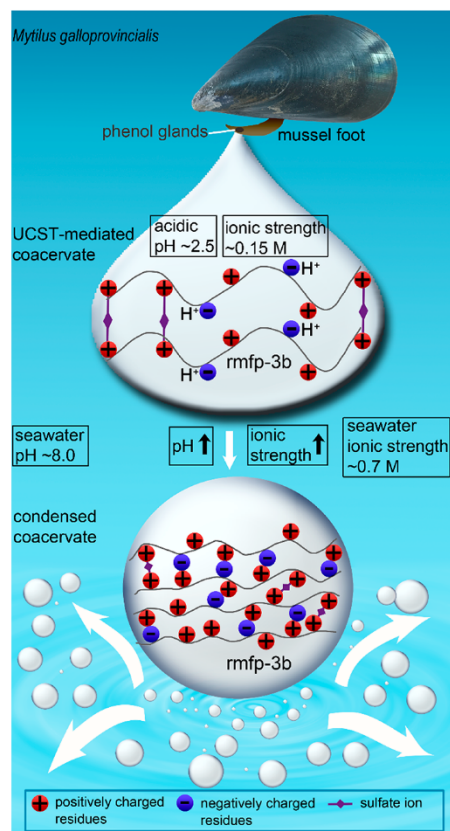


**Figure 7.** Schematic representation of rmfp-3b behavior upon contact with seawater. rmfp-3b is highly positively charged due to the protonation of basic residues in the acidic environment of the mussel foot (pH  $\sim$  2.5). Highly concentrated rmfp-3b is then secreted from the mussel phenol gland as coacervate probably with sulfate or other multivalent anions. Upon a pH jump in contact with seawater (pH  $\sim$  8.0), deprotonation of the acidic residues in rmfp-3b results in formation of zwitterions with electrostatic attraction between oppositely charged residues and a decrease of the net charge. Besides the pH jump, the ionic strength increases from  $\sim$ 0.15 M (mussel foot) to  $\sim$ 0.7 M (seawater), which largely screens the electrostatic repulsion.<sup>14</sup> Both, the increase of pH and ionic strength significantly reduces the electrostatic repulsion, yielding a condensed coacervate.

intermolecular association.<sup>32,33</sup> At sea-level pH (pH  $\sim$  8.0) and ionic strength ( $\sim$ 0.7 M), the electrostatic repulsion between rmfp-3b molecules was significantly reduced and their intermolecular interactions therefore increased, yielding maximum coacervation without detectable UCST behavior. Particularly, sulfate and citrate anions at relatively low concentration could induce the complex coacervation at both, pH 3.0 and pH 8.0. Our results reveal new insights into the mechanism of underwater adhesion of mussel foot proteins, opening up applications of rmfp-3b, such as being a purification tag or a thermally switchable drug delivery material.

## ■ ASSOCIATED CONTENT

### 📄 Supporting Information

The Supporting Information is available free of charge on the ACS Publications website at DOI: 10.1021/acs.biomac.8b00583.

Extended experimental section, MALDI-TOF mass spectra of rmfp-3b (Figure S1), Coomassie blue stained

SDS-PAGE (20%) (Figure S2), Far-UV CD spectra of rmfp-3b at pH 3.0 (Figure S3), Influence of citrate concentration on the  $T_{cp}$  of rmfp-3b-NT at pH 3.0. (Figure S4), Turbidity of rmfp-3b-NT as a function of pH at 20 °C (Figure S5), Turbidity of rmfp-3b and rmfp-3b-NT at different sodium sulfate concentrations at pH 3.0 and 20 °C (Figure S6), and Kyte-Doolittle hydrophobicity plot of rmfp-3b (Figure S7) (DOCX).

## ■ AUTHOR INFORMATION

### Corresponding Author

\*E-mail: thomas.scheibel@bm.uni-bayreuth.de.

### ORCID

Thomas Scheibel: 0000-0002-0457-2423

### Author Contributions

J.W. and T.S., conceptualization; J.W., investigation; J.W., writing (original draft); T.S., writing (review and editing); J.W., visualization; T.S., supervision.

### Notes

The authors declare no competing financial interest.

## ■ ACKNOWLEDGMENTS

We would like to thank Dr. Sushma Kumari and Heike Herold for help with the optical microscopy, Dr. Hendrik Bargel for help with SEM, Andreas Schmidt for MALDI-TOF measurements, and Elise Desimone for proof reading. J.W. thanks the China Scholarship Council (CSC, 201406630012) for awarding a fellowship for carrying out her Ph.D. in Germany in the lab of Prof. Dr. Thomas Scheibel.

## ■ REFERENCES

- (1) Gaylord, B. Detailing agents of physical disturbance: wave-induced velocities and accelerations on a rocky shore. *J. Exp. Mar. Biol. Ecol.* **1999**, *239* (1), 85–124.
- (2) Bell, E. C.; Denny, M. W. Quantifying “wave exposure”: a simple device for recording maximum velocity and results of its use at several field sites. *J. Exp. Mar. Biol. Ecol.* **1994**, *181* (1), 9–29.
- (3) Waite, J. H. Nature’s underwater adhesive specialist. *Int. J. Adhes. Adhes.* **1987**, *7* (1), 9–14.
- (4) Silverman, H. G.; Roberto, F. F. Understanding marine mussel adhesion. *Mar. Biotechnol.* **2007**, *9* (6), 661–681.
- (5) Jeon, E. Y.; Hwang, B. H.; Yang, Y. J.; Kim, B. J.; Choi, B.-H.; Jung, G. Y.; Cha, H. J. Rapidly light-activated surgical protein glue inspired by mussel adhesion and insect structural crosslinking. *Biomaterials* **2015**, *67*, 11–19.
- (6) Lee, B. P.; Messersmith, P. B.; Israelachvili, J. N.; Waite, J. H. Mussel-inspired adhesives and coatings. *Annu. Rev. Mater. Res.* **2011**, *41*, 99–132.
- (7) de Kruijf, C. G.; Weinbreck, F.; de Vries, R. Complex coacervation of proteins and anionic polysaccharides. *Curr. Opin. Colloid Interface Sci.* **2004**, *9* (5), 340–349.
- (8) Bungenberg de Jong, H. G. Complex colloid systems. In *Colloid Science*; Kruyt, H. R., Ed.; Elsevier: Amsterdam, 1949; Vol. 2, pp 335–432.
- (9) Stewart, R. J.; Wang, C. S.; Shao, H. Complex coacervates as a foundation for synthetic underwater adhesives. *Adv. Colloid Interface Sci.* **2011**, *167* (1–2), 85–93.
- (10) Stewart, R. J.; Weaver, J. C.; Morse, D. E.; Waite, J. H. The tube cement of *Phragmatopoma californica*: a solid foam. *J. Exp. Biol.* **2004**, *207* (26), 4727–4734.
- (11) Shao, H.; Stewart, R. J. Biomimetic underwater adhesives with environmentally triggered setting mechanisms. *Adv. Mater.* **2010**, *22* (6), 729–733.
- (12) Huang, K.-Y.; Yoo, H. Y.; Jho, Y.; Han, S.; Hwang, D. S. Bicontinuous fluid structure with low cohesive energy: molecular basis

for exceptionally low interfacial tension of complex coacervate fluids. *ACS Nano* **2016**, *10* (5), 5051–5062.

(13) Hwang, D. S.; Zeng, H.; Srivastava, A.; Krogstad, D. V.; Tirrell, M.; Israelachvili, J. N.; Waite, J. H. Viscosity and interfacial properties in a mussel-inspired adhesive coacervate. *Soft Matter* **2010**, *6* (14), 3232–3236.

(14) Kim, S.; Yoo, H. Y.; Huang, J.; Lee, Y.; Park, S.; Park, Y.; Jin, S.; Jung, Y. M.; Zeng, H.; Hwang, D. S.; Jho, Y. Salt triggers the simple coacervation of an underwater adhesive when cations meet aromatic  $\pi$  electrons in seawater. *ACS Nano* **2017**, *11* (7), 6764–6772.

(15) Tan, Y.; Hoon, S.; Guerette, P. A.; Wei, W.; Ghadban, A.; Hao, C.; Miserez, A.; Waite, J. H. Infiltration of chitin by protein coacervates defines the squid beak mechanical gradient. *Nat. Chem. Biol.* **2015**, *11* (7), 488–495.

(16) Lim, S.; Choi, Y. S.; Kang, D. G.; Song, Y. H.; Cha, H. J. The adhesive properties of coacervated recombinant hybrid mussel adhesive proteins. *Biomaterials* **2010**, *31* (13), 3715–3722.

(17) Wei, W.; Tan, Y.; Martinez-Rodriguez, N. R.; Yu, J.; Israelachvili, J. N.; Waite, J. H. A mussel-derived one component adhesive coacervate. *Acta Biomater.* **2014**, *10* (4), 1663–1670.

(18) Vrhovski, B.; Jensen, S.; Weiss, A. S. Coacervation characteristics of recombinant human tropoelastin. *Eur. J. Biochem.* **1997**, *250* (1), 92–98.

(19) Yeo, G. C.; Keeley, F. W.; Weiss, A. S. Coacervation of tropoelastin. *Adv. Colloid Interface Sci.* **2011**, *167* (1–2), 94–103.

(20) Nuhn, H.; Klok, H.-A. Secondary structure formation and LCST behavior of short elastin-like peptides. *Biomacromolecules* **2008**, *9* (10), 2755–2763.

(21) Aseyev, V.; Tenhu, H.; Winnik, F. M. Non-ionic thermoresponsive polymers in water. In *Self Organized Nanostructures of Amphiphilic Block Copolymers II*; Müller, A. H. E., Borisov, O., Eds.; Springer-Verlag: Berlin, 2011; Vol. 242, pp 29–89.

(22) Seuring, J.; Agarwal, S. Polymers with upper critical solution temperature in aqueous solution. *Macromol. Rapid Commun.* **2012**, *33* (22), 1898–1920.

(23) Seuring, J.; Agarwal, S. Polymers with upper critical solution temperature in aqueous solution: unexpected properties from known building blocks. *ACS Macro Lett.* **2013**, *2* (7), 597–600.

(24) Inoue, K.; Takeuchi, Y.; Miki, D.; Odo, S.; Harayama, S.; Waite, J. H. Cloning, sequencing and sites of expression of genes for the hydroxyarginine-containing adhesive-plaque protein of the mussel *Mytilus galloprovincialis*. *Eur. J. Biochem.* **1996**, *239* (1), 172–176.

(25) Studier, F. W. Protein production by auto-induction in high-density shaking cultures. *Protein Expression Purif.* **2005**, *41* (1), 207–234.

(26) Paz, M. A.; Flückiger, R.; Boak, A.; Kagan, H. M.; Gallop, P. M. Specific detection of quinoproteins by redox-cycling staining. *J. Biol. Chem.* **1991**, *266* (2), 689–692.

(27) Hagenau, A.; Papadopoulos, P.; Kremer, F.; Scheibel, T. Mussel collagen molecules with silk-like domains as load-bearing elements in distal byssal threads. *J. Struct. Biol.* **2011**, *175* (3), 339–347.

(28) Hwang, D. S.; Gim, Y.; Cha, H. J. Expression of functional recombinant mussel adhesive protein type 3A in *Escherichia coli*. *Biotechnol. Prog.* **2005**, *21* (3), 965–970.

(29) Hwang, D. S.; Gim, Y.; Yoo, H. J.; Cha, H. J. Practical recombinant hybrid mussel bioadhesive fp-151. *Biomaterials* **2007**, *28* (24), 3560–3568.

(30) Erickson, H. P. Size and shape of protein molecules at the nanometer level determined by sedimentation, gel filtration, and electron microscopy. *Biol. Proced. Online* **2009**, *11* (1), 32–51.

(31) Kyte, J.; Doolittle, R. F. A simple method for displaying the hydropathic character of a protein. *J. Mol. Biol.* **1982**, *157* (1), 105–132.

(32) Dutta, N. K.; Truong, M. Y.; Mayavan, S.; Choudhury, N. R.; Elvin, C. M.; Kim, M.; Knott, R.; Nairn, K. M.; Hill, A. J. A genetically engineered protein responsive to multiple stimuli. *Angew. Chem., Int. Ed.* **2011**, *50* (19), 4428–4431.

(33) Niskanen, J.; Tenhu, H. How to manipulate the upper critical solution temperature (UCST)? *Polym. Chem.* **2017**, *8* (1), 220–232.

(34) Asadujjaman, A.; Kent, B.; Bertin, A. Phase transition and aggregation behaviour of an UCST-type copolymer poly(acrylamide-co-acrylonitrile) in water: effect of acrylonitrile content, concentration in solution, copolymer chain length and presence of electrolyte. *Soft Matter* **2017**, *13* (3), 658–669.

(35) Comert, F.; Dubin, P. L. Liquid-liquid and liquid-solid phase separation in protein-polyelectrolyte systems. *Adv. Colloid Interface Sci.* **2017**, *239*, 213–217.

(36) Thompson, T. E. Detection of epithelial acid secretions in marine molluscs: review of techniques, and new analytical methods. *Comp. Biochem. Physiol. Part A: Physiol.* **1983**, *74* (3), 615–621.

(37) Stewart, R. J.; Wang, C. S.; Song, I. T.; Jones, J. P. The role of coacervation and phase transitions in the sandcastle worm adhesive system. *Adv. Colloid Interface Sci.* **2017**, *239*, 88–96.

(38) Song, I. T.; Stewart, R. J. Complex coacervation of Mg (II) phospho-polymethacrylate, a synthetic analog of sandcastle worm adhesive phosphoproteins. *Soft Matter* **2018**, *14* (3), 379–386.

(39) Martinez-Rodriguez, N. R.; Das, S.; Kaufman, Y.; Israelachvili, J. N.; Waite, J. H. Interfacial pH during mussel adhesive plaque formation. *Biofouling* **2015**, *31* (2), 221–227.

(40) Yu, J.; Wei, W.; Danner, E.; Ashley, R. K.; Israelachvili, J. N.; Waite, J. H. Mussel protein adhesion depends on interprotein thiol-mediated redox modulation. *Nat. Chem. Biol.* **2011**, *7* (9), 588–590.

Supporting Information for

***Coacervation of the recombinant *Mytilus galloprovincialis* foot protein-3b***

*Biomacromolecules* 2018, 19, 3612–3619

DOI: 10.1021/acs.biomac.8b00583

**Jia Wang**,<sup>†</sup> Thomas Scheibel<sup>\*†‡§||L#</sup>

<sup>†</sup>Lehrstuhl Biomaterialien, <sup>‡</sup>Forschungszentrum für Bio-Makromoleküle (BIOmac), <sup>§</sup>Bayreuther Zentrum für Kolloide und Grenzflächen (BZKG), <sup>||</sup>Bayreuther Materialzentrum (BayMat), <sup>⊥</sup>Bayreuther Zentrum für Molekulare Biowissenschaften (BZMB), and <sup>#</sup>Bayrisches Polymerinstitut (BPI), Universität Bayreuth, 95440 Bayreuth, Germany

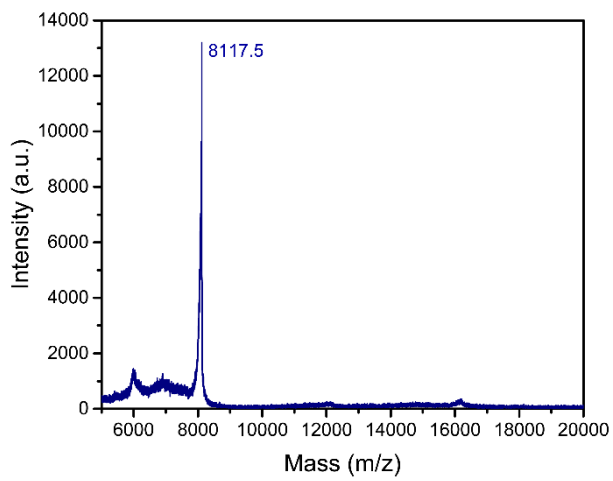


**Figure S1.** MALDI-TOF mass spectrum of rmfp-3b at pH 3.0.

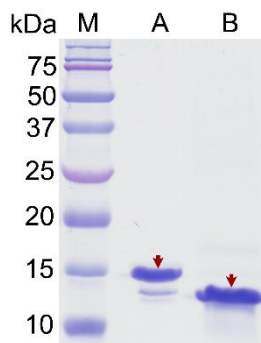


**Figure S2.** Coomassie blue stained SDS-PAGE (20%). M, pre-stained protein marker; lane A, purified rmfp-3b; lane B, purified rmfp-3b-NT.

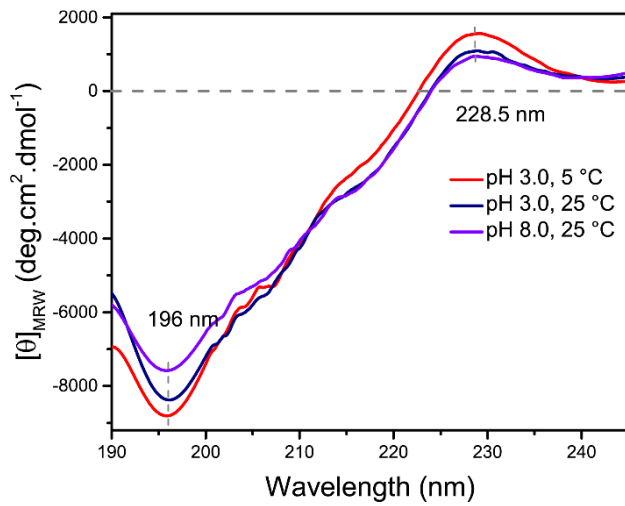


**Figure S3.** Far-UV CD spectra of rmfp-3b. The measurements were performed at 5 and 25 °C (pH 3.0 and pH 8.0), respectively.

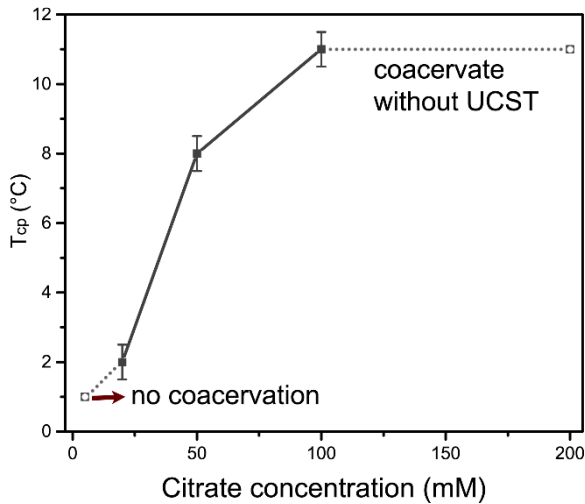


**Figure S4.** Influence of citrate concentration on the  $T_{cp}$  of rmfp-3b-NT at pH 3.0. The rmfp-3b-NT concentration was  $4 \text{ mg mL}^{-1}$ , providing the identical molar concentration as with  $5 \text{ mg mL}^{-1}$  rmfp-3b (see Figure 3a).  $T_{cp}$  refers to the cloud point temperature of UCST behavior. Error bars indicate the standard deviation ( $n = 3$ ).

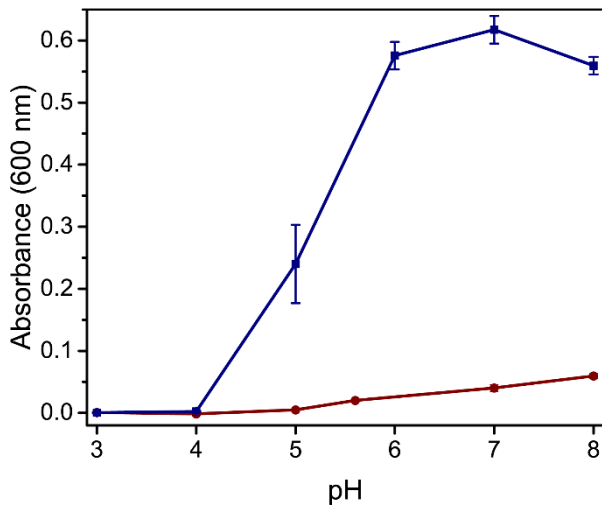


**Figure S5.** Turbidity of rmfp-3b-NT as a function of pH at 20°C. Citrate buffer (blue) and various other buffers (red) were used, such as Gly-HCl buffer (pH 3.0), acetate buffer (pH 4.0, pH 5.0, pH 5.6) and Tris-HCl (pH 7.0, pH 8.0). Turbidity was recorded at a wavelength of 600 nm. Error bars indicate the standard deviation ( $n = 3$ ).

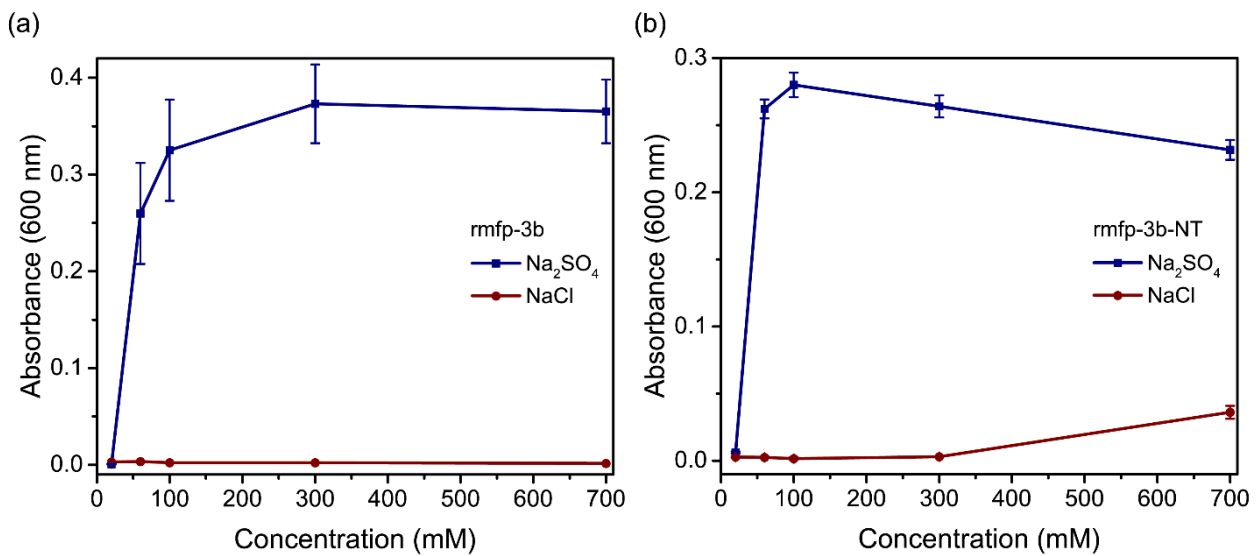


**Figure S6.** Turbidity of rmfp-3b and rmfp-3b-NT at different sodium sulfate concentrations at pH 3.0 and 20 °C. The identical concentration of sodium chloride was used as a control. Turbidity was recorded at a wavelength of 600 nm. Error bars indicate the standard deviation ( $n = 3$ ).

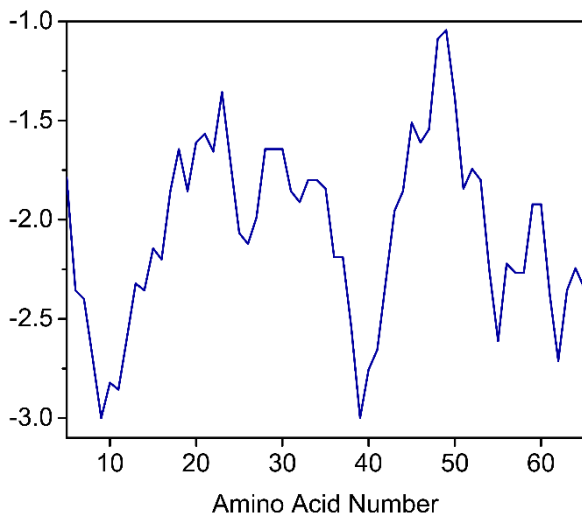


**Figure S7.** Kyte-Doolittle<sup>1</sup> hydrophobicity plot of rmfp-3b. All regions of rmfp-3b exhibit values below zero indicating its hydrophilicity.

#### REFERENCE

1. Kyte, J.; Doolittle, R. F. A simple method for displaying the hydropathic character of a protein. *J. Mol. Biol.* **1982**, 157 (1), 105-132.

***Publication III***

***A mussel polyphenol oxidase-like protein shows thiol-mediated antioxidant activity.***

**Jia Wang**, Michael H. Suhre, Thomas Scheibel

Published in *European Polymer Journal*, 2019, 113, 305-312

Reprinted with kind permission from Elsevier



Contents lists available at ScienceDirect

European Polymer Journal

journal homepage: [www.elsevier.com/locate/europolj](http://www.elsevier.com/locate/europolj)

## A mussel polyphenol oxidase-like protein shows thiol-mediated antioxidant activity

Jia Wang<sup>a</sup>, Michael H. Suhre<sup>a,1</sup>, Thomas Scheibel<sup>a,b,c,d,e,f,\*</sup>

<sup>a</sup> Lehrstuhl Biomaterialien, Universität Bayreuth, 95440 Bayreuth, Germany

<sup>b</sup> Forschungszentrum für Bio-Makromoleküle (BIOMac), Universität Bayreuth, 95440 Bayreuth, Germany

<sup>c</sup> Bayreuther Zentrum für Kolloide und Grenzflächen (BZKG), Universität Bayreuth, 95440 Bayreuth, Germany

<sup>d</sup> Bayreuther Materialzentrum (BayMat), Universität Bayreuth, 95440 Bayreuth, Germany

<sup>e</sup> Bayreuther Zentrum für Molekulare Biowissenschaften (BZMB), Universität Bayreuth, 95440 Bayreuth, Germany

<sup>f</sup> Bayrisches Polymerinstitut (BPI), Universität Bayreuth, 95440 Bayreuth, Germany

### ARTICLE INFO

#### Keywords:

Mussel foot  
Polyphenol oxidase-like protein  
Recombinant production  
Antioxidant  
Free thiols

### ABSTRACT

Marine mussels adhere underwater to a variety of substrates using adhesive proteins with post-translationally modified amino acids, such as 3,4-dihydroxyphenylalanine (DOPA) residues, as a key chemical signature. DOPA can auto-oxidize easily in seawater reducing the adhesion strength, but contributing to subsequent cohesion (cross-linking) of the underlying proteins. To maintain both reduced and oxidized forms of DOPA with corresponding adhesion and cohesion properties, strict redox regulation is necessary for mussel underwater adhesion. In this study, a full-length polyphenol oxidase-like protein (PPOL) from *Mytilus galloprovincialis* was identified after screening of a mussel foot cDNA library using different degenerated PCR primers. The recombinant PPOL (rPPOL) was successfully produced in *Escherichia coli*. The rPPOL exhibits thiol-dependent antioxidant activity suppressing DOPA oxidation. This finding provides insights into how DOPA chemistry could be regulated and presumably inspires future applications of DOPA-mediated adhesion materials.

### 1. Introduction

In nature, marine mussels use a holdfast system containing a bundle of so-called byssal threads with a disk-like adhesive plaque at each tip, to adhere to various substrates underwater [1,2]. The adhesive plaque comprises a variety of mussel foot proteins (mfps), which contain a catecholic amino acid (3,4-dihydroxyphenylalanine, DOPA) mediating strong underwater adhesion [3,4]. DOPA residues are generated upon post-translational modification of tyrosine residues catalyzed by the tyrosine hydroxylase (cresolase) activity of polyphenol oxidase (PPO) [3,5,6]. In O<sub>2</sub> saturated and alkaline seawater (pH ~ 8.0), DOPA exhibits high auto-oxidation tendency to Dopaquinone (DQ), which shows poor adhesion but good cohesion [3,7,8]. However, marine mussels are able to achieve strong adhesion forces, and obviously a tight and complex regulation of DOPA chemistry exists.

The incipient acidic (pH ~ 3.0) secretion of mfps [9] as well as the strong reducing environment [8,10] therein protect DOPA from auto-oxidation to begin with [3]. Previously, two reducing pathways were detected mediated by thiol-rich mfp-6 [8,10] as well as DQ

tautomerization [11,12]. Along with mfp-3 and mfp-5, mfp-6 is secreted at the substratum's interface during plaque formation [13,14]. mfp-6 contains a great number of tyrosine residues (~20 mol %) with inefficient post-translational modification into DOPA (< 5 mol %), as well as 11 cysteine residues, 9 of which possessing presumably free thiols and 2 of which being disulfide bonded [13]. mfp-6 itself demonstrates poor adhesion properties, whereas it can effectively rescue the adhesive properties of other mfps, such as mfp-3 [8,10,15]. Approximately 9 free thiols and 4 DOPA residues with ~17 electrons per molecule of mfp-6 devote to the reservoir of reducing electrons, reducing ~8 DQ to DOPA per mfp-6 molecule (DQ + 2 Cys-SH → Cys-S-S-Cys + DOPA) [10]. Further, DQ reduces to α,β-dehydro-DOPA (Δ-DOPA) upon tautomerization at neutral to alkaline pH [11,12]. Presumably, the Δ-DOPA bestows electrons on the reducing reservoir to extend the lifetime of DOPA as well [3].

Here, a full-length PPO-like cDNA sequence of *Mytilus galloprovincialis* (*M. galloprovincialis*, PPOL) has been identified in a mussel foot cDNA library [5,16]. The PPOL comprises 15 cysteine residues, ~2 of which are disulfide bonded leaving ~13 endowed with free thiols. The

\* Corresponding author at: Lehrstuhl Biomaterialien, Universität Bayreuth, 95440 Bayreuth, Germany.

E-mail address: [thomas.scheibel@bm.uni-bayreuth.de](mailto:thomas.scheibel@bm.uni-bayreuth.de) (T. Scheibel).

<sup>1</sup> Present address: GmbH, AmKlopferspitz 19 im IZB, D-82152 Planegg, München, Germany.

<https://doi.org/10.1016/j.eurpolymj.2019.01.069>

Received 21 September 2018; Received in revised form 21 January 2019; Accepted 30 January 2019

Available online 31 January 2019

0014-3057/ © 2019 Elsevier Ltd. All rights reserved.

**Table 1**  
Result of tblastn search of the sequence AAZ66340 in MytiBase [19].

Accession	Sequence
<b>AAZ66340</b> 317	YIDYVWQLFRRKLRNRLGIDPARDYLGHGGPAHAPNAPLLGLIPGWRNVHGYSNVFTQRVYRY +ID VW +F R LR+R IDP DY+ H P + L P +N+ GYS+ F +Y Y
<b>MGC01495</b> 2	FIDAVWTVFCRQLRHR-NIDPQDDYVIVDNKMRPERYMDHLFP-MKNIDGYSDFANNIYSY

Alignment of the PPO of *P. fucata* (GenBank AAZ66340) with the MytiBase-Entry MGC01495. The consensus amino acids are shown between the sequences with “+” as conservative amino acid substitutions. Spaces in MGC01495 are introduced to optimize the alignment.

recombinant PPOL (rPPOL) was produced in *E. coli* and exhibited antioxidant activity in its reduced state restraining DOPA oxidation into DQ.

## 2. Materials and methods

### 2.1. Sequence screening

The first PPO sequence in bivalve was identified from pearl oyster *Pinctada fucata* (*P. fucata*, GenBank AAZ66340) [17]. A nucleotide BLAST of this sequence against the MytiBase, a database with 18,788 high-quality expressed sequence tags (ESTs) or 17 cDNA libraries of various tissues of *M. galloprovincialis* with 7112 non-redundant sequences [18], showed no significant homology at DNA level [19]. In contrast, a BLAST of the corresponding protein sequence with the translated database (tblastn-Algorithm) revealed a moderate match to cluster MGC01495 (Table 1) [19].

A subsequent BLAST of cluster MGC01495 against a non-redundant protein sequence database (National Center for Biotechnology Information, NCBI) showed additional homologies with PPOs or PPO-related proteins [19]. On the basis of cluster MGC01495, the extraction of PPOL from a mussel foot cDNA library of *M. galloprovincialis* [5,16] was performed by PCR amplification using the specific reverse primer (MGC01495\_rev, 5'-TTATCGTTACTGAGGAATAGAAGC-3') targeting open reading frames (ORFs) and the vector pDONR222 complementary forward primer (M13\_fwd, 5'-TGTAACGACGCCAGT-3') [19]. The amplified fragment was purified from agarose gels, ligated with vector pGEM and sequenced. This sequence screening approach, derived from a study on *P. fucata*, was therefore nominated as Pf-approach.

In parallel to the Pf-approach, the following sequence screening, nominated as Cu-approach, was carried out based on highly conserved copper-binding domains (CuA, CuB) in known PPOs [19]. Different degenerated PCR reverse primers generated by reverse translation of the conserved protein sequences in respective areas were designed and combined with the forward primer (M13\_fwd) (Table S1) [19]. To reduce the degree of degeneration, the codon usage was optimized based on that of *M. galloprovincialis* (Codon Usage Database, <http://www.kazusa.or.jp/codon/>) [19]. From defined bands, DNA was extracted, ligated with vector pGEM (pGEM-PPOL) and sequenced.

### 2.2. Plasmid construction

*Escherichia coli* (*E. coli*) DH10B (Novagen, USA) was used as a cloning strain. The PPOL gene was amplified by PCR amplification with a mixture of a template, two primers, and Phusion DNA polymerase (New England Biolabs (NEB)) (Table S2). To produce full-length as well as short rPPOL (with its C-terminal domain deleted), the respective genes were cloned into pET-Vector containing a sequence encoding a His-Sumo-TAG at the 5' end and pET28-Vector containing a sequence encoding His-TAG at the 5' end yielding four constructs, including pET-sumo-PPOL, pET28a-His-PPOL, pET-sumo-P319 and pET28a-His-P319 (Fig. 1, Table S2).

### 2.3. Recombinant production and protein purification

The plasmids were transformed into different *E. coli* strains, namely BL21-CodonPlus (DE3)-RIPL, BL21-Gold (DE3)-pLysS and Rosetta-gami2 (DE3)-pLysS (Novagen, Merck, Germany). Gene expression was induced at OD<sub>600</sub> = 30 using 1 mM isopropyl β-D-1-thiogalactopyranoside (IPTG), followed by further 3 h of fermentation in a BIOSTAT B plus bioreactor (Sartorius, Goettingen, Germany) in 5 L LB medium containing 35 μg mL<sup>-1</sup> kanamycin at 30 °C. After centrifugation, cell pellets were washed twice using lysis buffer (40 mM Tris/HCl, pH 8.0) and further resuspended in 5 mL of lysis buffer per gram of wet weight.

The harvested cells were incubated with 1 mg lysozyme per gram cells (wet weight), 1 vial Protease-Inhibitor Mix-HP (SERVA, Heidelberg, Germany) and 1 mM phenylmethylsulfonyl fluoride (PMSF) using gentle shaking for 30 min at 4 °C. The cells were further disrupted by Sonopuls HD3200/KE76 ultrasonicator (Bandelin, Berlin, Germany) using a 2 sec pulse and 1 sec cooling period with sonication energy of 0.1 kJ per mL cell solution, followed by centrifugation (10 000 rpm, 20 min, 4 °C). The cell lysate pellet was firstly washed four times using wash buffer (40 mM Tris/HCl, 100 mM NaCl, 1% Triton X-100, pH 8.0) with slight sonication and then washed three times with Millipore (MQ) water. The protein was extracted from the pellet using buffer A (8 M urea, 40 mM Tris/HCl, 5 mM dithiothreitol (DTT), 50 mM imidazole, pH 8.0) at 20 °C overnight. The extraction solution after centrifugation (10 000 rpm, 20 min, 20 °C) was loaded onto a buffer A pre-equilibrated Ni-NTA sepharose column (120 mL, GE Healthcare, Germany), which was subsequently washed with buffer A. The protein was eluted using buffer B (8 M urea, 40 mM Tris/HCl, 5 mM DTT, 500 mM imidazole, pH 8.0).

Recombinant production and purification were analyzed using sodium dodecyl sulfate (SDS) polyacrylamide gel electrophoresis (PAGE) and Western Blotting. In the presence of Laemmli buffer (60 mM Tris/HCl (pH 6.8), 10% glycerol, 2% SDS, 5% β-mercaptoethanol, and 0.01% bromophenol blue), the samples were heated for 8 min at 95 °C. Proteins were loaded onto 20% Tris/Glycine SDS-PAGE gels, followed by Coomassie Blue staining. After SDS-PAGE, Western Blotting was performed by transferring proteins onto a polyvinylidene fluoride (PVDF) membrane (GE Healthcare, Germany) for 50 min at 40 mA. The PVDF membrane was blocked with 0.5% alkali-soluble casein, incubated with a horseradish peroxidase-conjugated anti-hexahistidine (His-TAG) antibody (Novagen, Madison, WI, USA), followed by luminol-based enhanced chemiluminescence (ECL) detection (GE Healthcare, Germany).

### 2.4. Protein refolding

Refolding of rPPOL variants out of 8 M urea was analyzed as a function of pH by monitoring the turbidity as well as tryptophan fluorescence. The turbidity was recorded at a wavelength of 600 nm using a Varian Cary 50 UV-Vis spectrophotometer (Agilent Technologies). The purified rPPOL variants in 8 M urea were diluted upon addition of 150 mM citrate-phosphate buffer (buffering capacity

Recombinant PPOL variants	Schematic structure	Cysteine residues	MW (kDa)	Theoretical pI
rSumo-PPOL		15	76.2	8.0
rSumo-P319		5	51.4	6.8
rPPOL		15	65.1	8.7
rP319		5	40.3	8.4

**Fig. 1.** Schematic representation of analyzed rPPOL variants. H6 and Sumo refer to His- and Sumo-TAG, respectively. The short variants comprise 319 amino acids of PPOL with the C-terminal domain deleted and are therefore nominated as rSumo-P319 and rP319. The theoretical molecular weight (MW) and isoelectric point (pI) were calculated using the ProtParam tool (<http://web.expasy.org/protparam>).

from pH 2.2 to 8.0) at 20 °C. Each experiment was performed in triplicate.

The tryptophan fluorescence is sensitive to the environment, which makes it convenient to assay a protein's refolding process [20,21]. Tryptophan fluorescence was performed with an excitation wavelength of 295 nm, and emission spectra were taken between 300 and 420 nm using a Jasco FP-6500 spectrofluorometer. The rPPOL variants in 8 M urea were diluted upon addition of 150 mM citrate-phosphate buffer, pH 3.0.

### 2.5. Catalytic activity

The activity of rPPOL variants was assayed by spectrophotometrically measuring p-topaquinone formation at 485 nm, which is the major product of DOPA oxidation at pH 3.0 [22,23]. With L-tyrosine as substrate to determine tyrosinase activity of PPOL, the standard reaction mixture contained 128 μM L-tyrosine, 9 μM rPPOL variants or commercial mushroom tyrosinase (positive control) and 150 mM citrate-phosphate buffer, pH 3.0 (pH 7.0 for positive control). In case the following oxidation of produced DOPA was inhibited at pH 3.0, 256 μM NaIO<sub>4</sub> was added to the reaction mixture as a chemical oxidant [24]. The absorption spectra between 380 nm and 650 nm were recorded using a Varian Cary 50 UV-Vis spectrophotometer (Agilent Technologies) upon incubation at 20 °C for 30 min. In parallel, to determine catecholase activity of rPPOL variants, 128 μM L-DOPA was added as substrate instead of L-tyrosine to the reaction mixture.

To determine the catalytic activity at seawater level pH (pH 8.0), dopachrome formation was detected at 475 nm. After incubation with L-tyrosine or L-DOPA in the absence of NaIO<sub>4</sub> for 30 min at 20 °C, the reaction mixtures were centrifuged to remove the precipitate for the following measurement, and the other conditions were kept identical to the measurement at pH 3.0.

### 2.6. Alkylation of cysteine residues

Alkylation of cysteine residues in rPPOL variants was performed using N-Ethylmaleimide (NEM) [25,26]. Briefly, alkylation was carried out in 20 mM NEM and 92.1 μM rPPOL variants at pH 3.0 upon incubation for 2.5 h at 20 °C. Excess NEM was removed by sufficient dialysis against 20 mM citrate buffer, pH 3.0. To quantify free thiols before (rPPOL and rP319) and after reaction with NEM (designated as rPPOL-NEM and rP319-NEM), respectively, Ellman's Reagent (5,5'-dithiobis-(2-nitrobenzoic acid), DTNB) was used [27]. The rPPOL variants with and without alkylation were freeze-dried and resolved in reaction buffer (8 M urea, 1 mM ethylenediaminetetraacetic acid (EDTA), 0.1 M Tris/HCl, pH 8.0). The reaction mixtures included 5 μM DTNB solution as well as 90 μM of each rPPOL-NEM, rP319, rP319-NEM or 45 μM of rPPOL in reaction buffer and incubated at 20 °C for 15 min. The absorbance at 412 nm was measured using a Varian Cary 50 UV-Vis spectrophotometer (Agilent Technologies).

### 2.7. Antioxidant activity

At acidic pH, auto-oxidation of L-DOPA is negligible. NaIO<sub>4</sub> was taken as chemical oxidant to oxidize L-DOPA [24]. Then, the oxidation process of L-DOPA with NaIO<sub>4</sub> was determined in the presence of rPPOL variants as antioxidant by spectrophotometrically measuring p-topaquinone formation at 485 nm. The reaction mixture included 128 μM L-DOPA, 256 μM NaIO<sub>4</sub>, 9 μM rPPOL variants (with as well as without alkylation), and 150 mM citrate buffer, pH 3.0. The reaction without addition of rPPOL variants was taken as negative control. The absorbance kinetics of the reaction at 485 nm was measured using a Varian Cary 50 UV-Vis spectrophotometer (Agilent Technologies) at 20 °C.

To further analyze the antioxidant property of rPPOL variants, a modified 2,2-diphenyl-1-picrylhydrazyl (DPPH) assay was used [28,29]. DPPH shows strong absorption at 515 nm due to its free radicals, whereas the absorption at 515 nm disappears after scavenging by antioxidant [28]. The reaction mixture contained 3.5 μM rPPOL variants (with as well as without alkylation) or ascorbic acid (control antioxidant), 100 μM freshly prepared DPPH, 0.3% (v/v) Tween 20 and 150 mM citrate-phosphate buffer, pH 3.0. The absorbance reduction at 515 nm was monitored over 500 min using a Varian Cary 50 UV-Vis spectrophotometer (Agilent Technologies) at 20 °C. To eliminate the self-reduction influence of DPPH, the absorbance reduction at 515 nm was normalized to the reaction without addition of antioxidant. Each experiment was performed in triplicate, and the shown graphs represent mean values ± s.d. Data were fitted using a biphasic exponential decay function  $y = y_0 + A_1 * \exp(-x/t_1) + A_2 * \exp(-x/t_2)$ . To get the half-maximal effective concentration (EC<sub>50</sub>), DPPH assays of rPPOL at concentrations of 14, 7, 5.25, 3.5, 2.6, 1.75, 0.88, 0.22 and 0.073 μM as well as rP319 at concentrations of 14, 10.5, 7, 5.25, 3.5, 1.75, 0.44, and 0.15 μM were performed. Then, the reaction kinetics of rPPOL as well as rP319 were plotted at different concentrations. The percentage of remaining DPPH radicals were determined at steady state, which was plotted as a function of molar ratio of rPPOL (rP319) to DPPH.

To determine the antioxidant property at seawater level pH, DPPH assay was detected at 515 nm at pH 8.0 as well. After incubation of 1 min, 15 min and 60 min, the reaction mixtures were centrifuged to remove the precipitate for the following measurement, and the other conditions were kept identical to the measurement at pH 3.0.

## 3. Results and discussion

### 3.1. Full-length gene and protein sequence of PPOL

Given the known PPO sequence (GenBank [AAZ66340](#)) of *P. fucata* [17], the tblastn search in MytiBase identified the cluster MGC01495 [19]. Fishing in a mussel foot cDNA library of *M. galloprovincialis* [5,16], based on the sequence of cluster

MGC01495 (Pf-approach), generated a ~1.6 kb fragment (Fig. 2A)

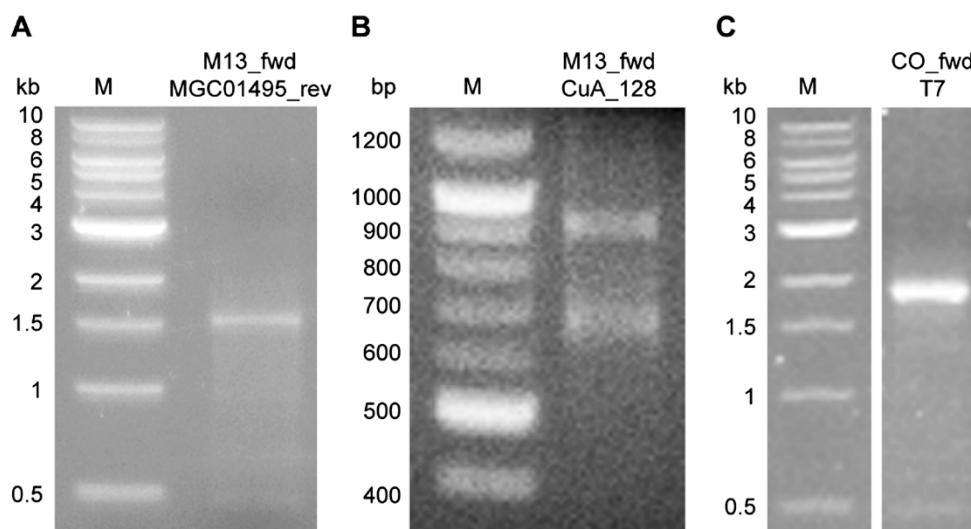


**Fig. 2.** PCR amplification results of the identified PPOL from *M. galloprovincialis* [19]. (A) *P. fucata* derived sequence screening approach (Pf-approach) using primers MGC01495\_rev and M13\_fwd. M: 1 kb marker. (B) Copper-binding domain derived sequence screening approach (Cu-approach) using primers CuA\_128 and M13\_fwd. M: 100 bp marker. (C) Continued Cu-approach: PCR using primers CO\_fwd and T7. M: 1 kb marker.

[19]. Sequencing showed a high homology to PPOs. In addition to the Pf-approach, a Cu-approach based on the conserved copper binding domains (CuA, CuB) in PPOs generated two bands with ~650 and ~950 bp, respectively (Fig. 2B) [19]. The resulting ~650 bp sequence showed a high homology to the PPO of *P. fucata*, and was assumed to be a 5' terminal sequence of PPOL [19]. To obtain the full-length PPOL, PCR was performed using a specific forward primer (CO\_fwd, 5'-ATG AAACCTACATTACAACACTACTGCTATTG-3'), targeting this short ~650 bp sequence, as well as a reverse complementary T7 primer [19]. The PCR reaction generated a ~1.8 kb band (Fig. 2C). Sequencing showed that the ~1.8 kb sequence (GenBank MG975894) obtained by the Cu-approach was identical to the sequence obtained by the Pf-approach, but it differed in length [19]. Sequence alignments showed a deletion of 62 nucleotides in sequences achieved by the Pf-approach, leading to a reading frame shift that resulted in a premature stop codon (Fig. S1A) [19].

A potential secretory signal peptide was identified with a cleavage site between amino acid residues C21 and D22 (SignalP 3.0 Server, neuronal network method) (Fig. S1B) [19,30]. The protein thus has 540 amino acid residues with a molecular weight of 62.7 kDa and a theoretical isoelectric point (pI) of 8.6 (calculated using ProtParam) [19]. The BLAST against NCBI revealed numerous homologous sequences of PPO or PPO-related proteins (Fig. 3) [19]. The PPOL, in particular, shows high homology to the tyrosinase 2 of green mussel *Perna viridis* (GenBank KF318705.1, identity = 59%) and both contain several cysteine residues (Fig. S2) [31]. Within the sequence of PPOL, the catalytic site (two copper-binding sites, CuA and CuB) comprising all essential amino acid residues shows a maximum homology to other PPOs in particular concerning the six copper coordinating histidine residues (Fig. 3) [19]. It is noteworthy that the third histidine residue of the CuA-binding site shows a WHK motif instead of the conserved WHR motif (Fig. 3) [19]. A homology-based model of PPOL was generated using the Phyre2 server, which shows an ensemble of  $\alpha$ -helices connected by long unstructured loops (Fig. S3) [19]. A recent transcriptome analysis of *Mytilus californianus* did not show PPO-like sequences, but in general its byssus sequences, except Mcfp-10, showed no significant homology with those of other species [32].

### 3.2. Recombinant production of PPOL

The full-length rPPOL variants (rSumo-PPOL, rPPOL) as well as

short variants (rSumo-P319, rP319) with the C-terminal domain (containing 10 cysteine residues) deleted were produced in different *E. coli* hosts (Figs. 1, 4). As shown in Fig. 4A and B, all rPPOL variants were produced at the highest expression level in BL21-CodonPlus (DE3)-RIPL and were mainly found in insoluble inclusion bodies (IBs). Even the presence of a Sumo-TAG did not increase the solubility. Therefore, the rPPOL variants without Sumo-TAG (rPPOL, rP319) were chosen for further purifications and analysis.

Refolding of rPPOL and rP319 was investigated after denaturation and purification from IBs (Fig. 4C). Protein precipitation along refolding was analyzed by turbidity measurements at different buffer conditions within the pH range from 3.0 to 8.0 (Fig. 5A). At pH 3.0, a large amount of carboxyl groups of rPPOL and rP319 was protonated, which charged the protein positively and kept it in a soluble state (Figs. 1, 5A). Notably, an abrupt increase in turbidity was observed upon a pH jump from pH 4.0 to 8.0 with deprotonation of the carboxyl groups and therefore a decreasing net charge. In other words, rPPOL and rP319 displayed the highest solubility at pH 3.0 and started to precipitate at higher pH. As shown in Fig. 5B, the tryptophan fluorescence blue shifted upon refolding. To keep the proteins in a soluble state, rPPOL and rP319 were dialyzed against 20 mM citrate buffer, pH 3.0, coincident with the mussel secretion pH.

### 3.3. Catalytic activity

PPOs catalyze two types of reaction: hydroxylation of monophenols to o-diphenols (tyrosinase / cresolase activity) and oxidation of o-diphenols to o-quinones (catecholase activity). These reactions can be spectrophotometrically studied by recording the increase of absorbance at 485 nm owing to p-topaquinone formation at pH 3.0. Based on the high solubility of rPPOL variants at pH 3.0 (reflecting the pH of secretion), the following catalytic and antioxidant activity measurements were mainly investigated at pH 3.0. Tyrosinase activity was not detected using L-tyrosine as substrate, even when using NaIO<sub>4</sub> as additional oxidant to oxidize the hypothetical intermediate product DOPA at pH 3.0 (Fig. S4).

Next, catecholase activity of rPPOL and rP319 was assayed using L-DOPA as substrate at pH 3.0. There was no detectable absorption at 485 nm, except for the positive control with commercially available mushroom tyrosinase (Fig. 6A). In the presence of NaIO<sub>4</sub> as chemical oxidant, L-DOPA oxidized and exhibited absorption at 485 nm (Fig. 6A,

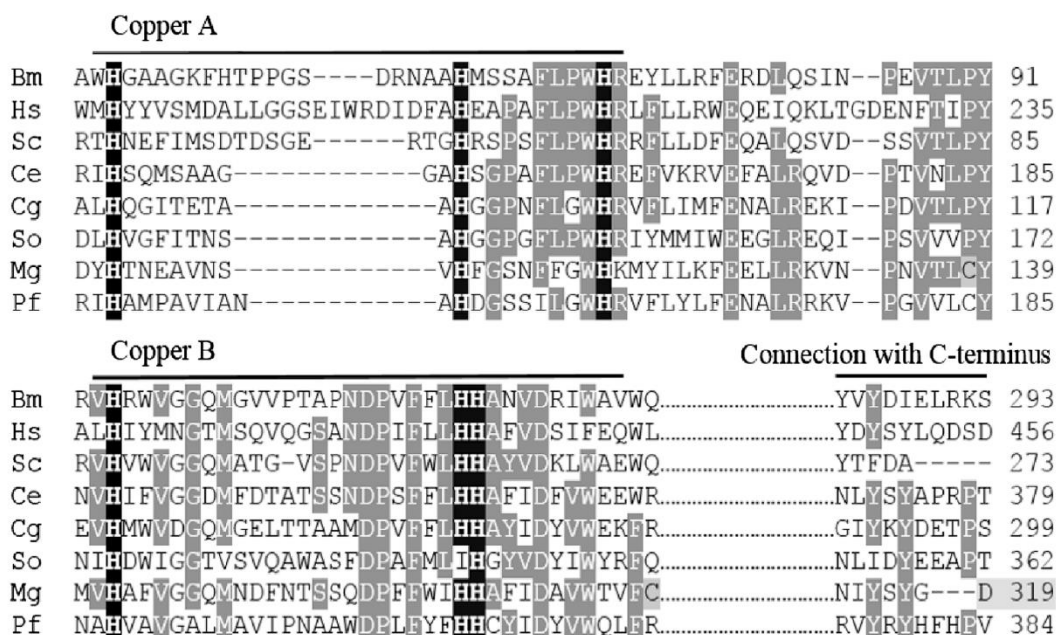


**Fig. 3.** Multiple amino acid sequences alignment of the two conserved copper-binding sites of PPOs from different species [19]. Six highly conserved histidine residues (H) are indicated with black shading, and other conserved residues with gray shading. Position 319 (D) within the connecting region with the C-terminal domain in PPOL is marked by light gray shading. Gaps ( ) are introduced to optimize the alignment. Suspension points (...) represent omitted amino acids. Abbreviations of species are used as follows: Bm, *Bacillus megaterium*; Hs, *Homo sapiens*; Sc, *Streptomyces castaneoglobosporus*; Ce, *Caenorhabditis elegans*; Cg, *Crassostrea gigas*; So, *Sepia officinalis*; Mg, *Mytilus galloprovincialis*; Pf, *Pinctada fucata*.

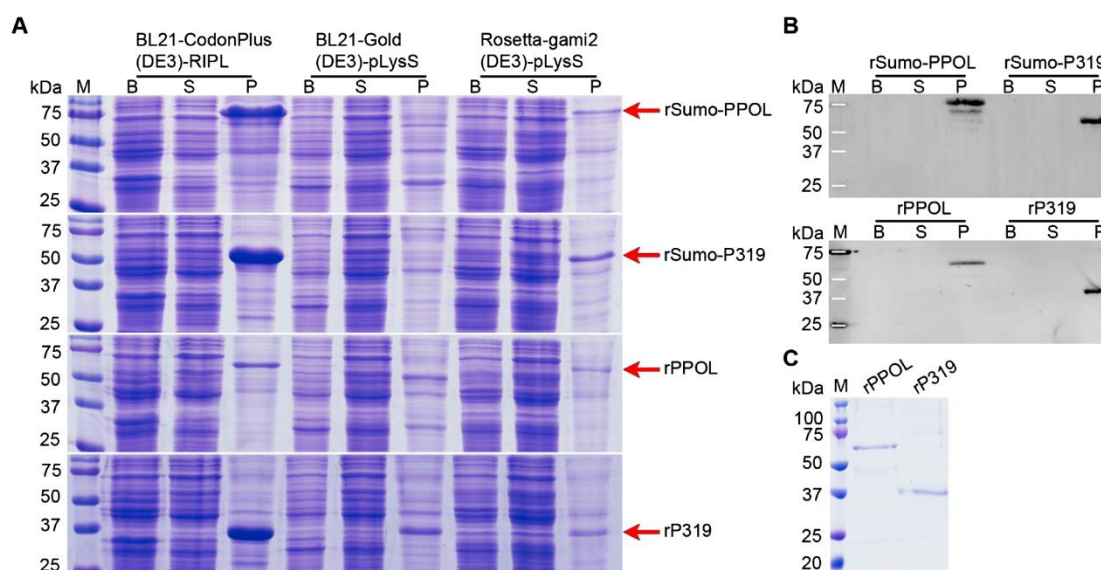


**Fig. 4.** Recombinant production of PPOL variants using *E. coli*. (A) SDS-PAGE and (B) Western Blotting analysis of four rPPOL variants produced in *E. coli* strains BL21-CodonPlus(DE3)-RIPL, BL21-Gold(DE3)-pLysS and Rosetta-gami2(DE3)-pLysS. M, protein marker; B, cell components before induction; S, soluble supernatant fraction after cell lysis; P, insoluble cell debris fraction after cell lysis. (C) SDS-PAGE analysis of purified rPPOL and rP319 after Ni-NTA column purification.

control). Strikingly,  $\text{NaIO}_4$ -induced oxidation of L-DOPA was suppressed to some extent upon addition of rPPOL and rP319 (Fig. 6A). This phenomenon was further analyzed using absorption kinetics at 485 nm (Fig. 6B). Oxidation of L-DOPA was inhibited in the presence of rPPOL (Fig. 6B). rP319, with 10 cysteine residues less than rPPOL, showed a similar inhibition behavior, but it was less effective (Fig. 6B). In order to test the contribution of free thiols deriving from reduced cysteine residues to this phenomenon, rPPOL and rP319 were alkylated

using NEM to block free thiols yielding rPPOL-NEM and rP319-NEM. Both alkylated variants showed comparatively weak inhibition of L-DOPA oxidation (Fig. 6B). The detected behavior suggests that rPPOL presumably acts as antioxidant as long as free thiols are available. Though rPPOL variants precipitated at pH 8.0 (seawater pH), the catalytic activity was assayed at pH 8.0 as well, but no absorption was detectable at 475 nm indicating no dopachrome formation (Figs. S4B, S5).

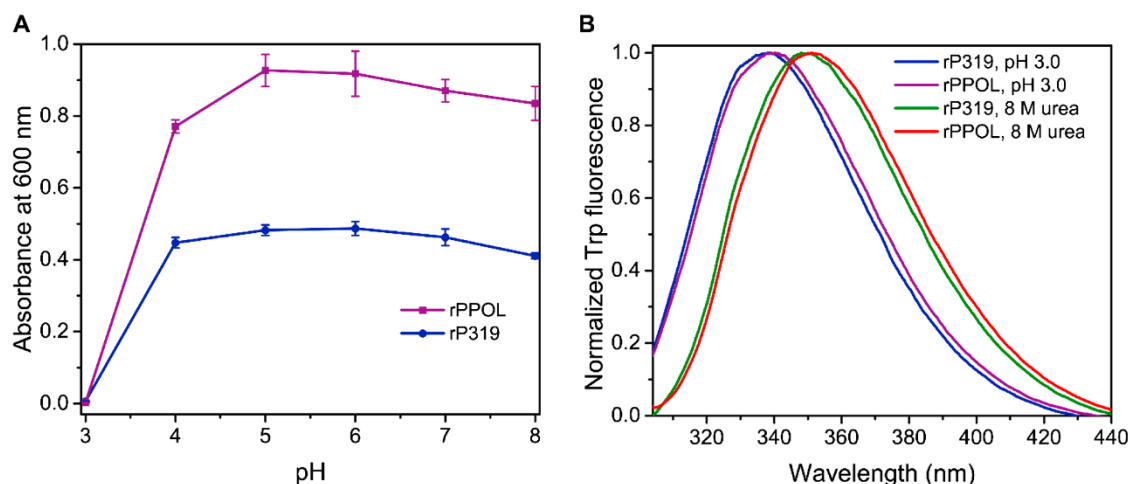


**Fig. 5.** Refolding of rPPOL variants. (A) Turbidity analysis of rPPOL and rP319 at different pH values. Vis absorption of 7.7  $\mu$ M rPPOL and rP319 was measured at 600 nm. Error bars indicate the standard deviation ( $n = 3$ ). (B) Tryptophan fluorescence analysis of rPPOL and rP319 in refolded (pH 3.0) as well as denatured (8 M urea) states. Tryptophan fluorescence spectra were recorded using an excitation wavelength of 295 nm.

It could be shown that little copper was bound to rPPOL as well as rP319 using Zincon [33], probably due to the decreasing copper coordination of the conserved histidine copper-binding sites at pH 3.0 (Fig. S6). Presumably, rPPOL and rP319 need a metallochaperone to accommodate two copper ions within the catalytic center at acidic conditions [34] and/or additional so far unidentified activation processes as reported for other PPOs [35–37]. Another possibility is that rPPOL and rP319 do not possess polyphenol oxidase activity.

#### 3.4. Antioxidant activity

An optimized standard DPPH radical quenching assay was used to determine the relative antioxidant activity of rPPOL variants [29]. Free radicals of DPPH have maximum absorption at 515 nm, which disappears upon reduction by antioxidant [28]. Time course measurements of DPPH radical quenching upon addition of 3.5  $\mu$ M antioxidants were recorded for 500 min (Fig. 7A). In the presence of rPPOL variants, the DPPH radicals were significantly reduced taking  $\sim$ 500 min to reach the steady state, whereas in the presence of ascorbic acid, the DPPH

radicals were less reduced taking less than 1 min to reach the steady state (Fig. 7A). Since free thiols play an important role in antioxidant activity [8,39], the number of free thiols was quantified using Ellman's reagent (Table S3). A relation of the rate of initial decay, the reductive capacity and the free thiol quantity could be deduced (Fig. 7A, Table S3). The rPPOL with the most thiols (in comparison to rP319-NEM, which is mostly deficient in thiols), showed the fastest (slowest) initial decay and the maximum (minimum) reductive capacity (Fig. 7A, Table S3). Alkylated rPPOL variants, especially rPPOL-NEM, still exhibited reductive capacity, which presumably came from the incomplete alkylation with NEM (Fig. 7A). However, there could be also other so far unidentified reductive groups of rPPOL involved in this activity at all.

The antioxidant activity of rPPOL and rP319 was clearly protein concentration dependent (Fig. S7). The  $EC_{50}$  for rPPOL as well as rP319 were determined upon plotting the data and evaluating the antiradical power (ARP,  $1/EC_{50}$ ), stoichiometric value ( $2^*EC_{50}$ ) and the number of reduced DPPH by one mole antioxidant ( $1/\text{stoichiometric value}$ ) as previously described in Ref. [38] (Fig. 7B, inlet table). The higher the ARP, the higher the antioxidant activity [38]. Obviously, rPPOL

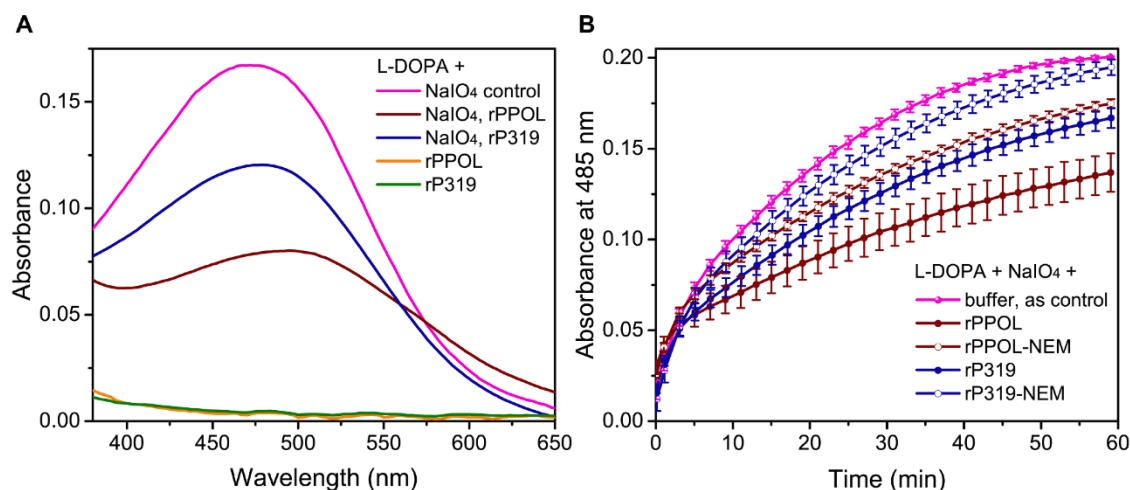


**Fig. 6.** Characterization of catecholase activity of rPPOL variants at pH 3.0. (A) Vis absorption of L-DOPA in the presence of rPPOL as well as rP319 with or without NaIO<sub>4</sub> after 30 min incubation. L-DOPA with NaIO<sub>4</sub> was taken as positive control. (B) Absorption kinetics of L-DOPA at 485 nm in the presence of NaIO<sub>4</sub> with additional rPPOL, rP319, rPPOL-NEM, rP319-NEM, respectively. NEM indicates that the protein has been partially alkylated using N-Ethylmaleimide.

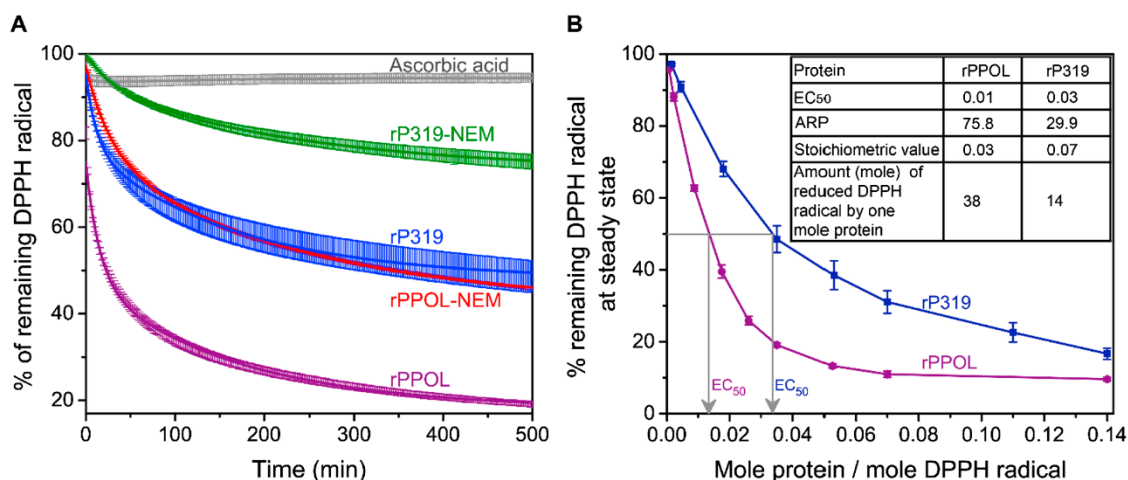


**Fig. 7.** Radical scavenging of rPPOL variants using the DPPH assay. (A) Time course of DPPH radical (100  $\mu\text{M}$ ) quenching (%) by rPPOL and rP319 as well as alkylated rPPOL-NEM and rP319-NEM at identical molar concentrations (3.5  $\mu\text{M}$ ) at pH 3.0. Ascorbic acid (3.5  $\mu\text{M}$ ) was taken as a positive control. Data (rPPOL, rP319, rPPOL-NEM and rP319-NEM) were fitted using an exponential decay function  $y = A1 * \exp(-x/t1) + A2 * \exp(-x/t2) + y0$ . (B) Extrapolated fraction of remaining DPPH radical (%) at steady state (500 min, Fig. S7) at various concentrations of rPPOL and rP319.  $EC_{50}$  values (half-maximal effective concentration) were calculated from the fitted curves and represent molar ratios of protein to DPPH radical with 50% DPPH radical scavenged. The inset table shows the calculated  $EC_{50}$ , ARP (antiradical power,  $1/EC_{50}$ ), stoichiometric value ( $2*EC_{50}$ ) and the number of reduced DPPH radical by one mole protein ( $1/\text{stoichiometric value}$ ) at steady state (upon 500 min incubation) [38]. Error bars indicate the standard deviation ( $n = 3$ ).

(ARP  $\sim 75.8$ ) exhibited a  $\sim 2.5$  times higher antioxidant activity than rP319 (ARP  $\sim 29.9$ ) and a  $\sim 6$  times higher activity than gallic acid (ARP  $\sim 12.5$ ), which showed the highest ARP among the described antioxidants in Ref. [38] (Fig. 7B). Accordingly, rPPOL (rP319) reduced  $\sim 38$  ( $\sim 14$ ) DPPH radical molecules per molecule despite the fact that it only comprises  $\sim 13$  ( $\sim 3$ ) free thiols per molecule. This further indicated that besides free thiols, there might be other reactive groups contributing to the antioxidant activity. The antioxidant activity was assayed at pH 8.0 (seawater pH) as well, showing limited antioxidant activity (Table S4), which might be due to the precipitation at pH 8.0.

#### 4. Conclusions

DOPA in mussel foot protein is the key substrate to achieve underwater adhesion to various substrates mainly through multiple bidentate H-bonds [3,4,14]. The auto-oxidation tendency of DOPA to DQ in alkaline and oxidizing seawater lead to partial elimination of adhesion and acquisition of cohesion [3,7,8]. The full-length PPOL cDNA sequence (GenBank MG975894) from *M. galloprovincialis* has been identified after screening a mussel foot cDNA library [5,16] using different degenerated PCR primers. The cDNA of PPOL was generated from mussel foot tissue [5,16] and the recombinant protein was produced in *E. coli*. It is, however, unresolved where the PPOL is located, e.g. within the mussel byssus comprising the protective cuticle, fibrous core or adhesive plaque. Due to its potential antioxidant activity inhibiting DOPA oxidation at pH 8.0, the free thiol-enriched PPOL probably functions at the plaque-substrate interface; however, verification of this hypothesis requires further investigation. Upon alkylation of free thiols within PPOL, the antioxidant activity decreases, but still exists, which indicates that the free thiols in cysteine residues as well as some other active groups bestow the antioxidant property to PPOL. Taken together, the thiol-dependent antioxidant property is the basis of a proper redox modulation of DOPA chemistry in marine mussels. However, the applied in vitro antioxidant substrate of PPOL was L-DOPA. Therefore, it has to be determined whether the antioxidant activity of PPOL also applies to mfps and how the antioxidant property of PPOL might interplay with the recently discovered coacervation of mfps [40,41].

#### 5. Notes

The authors declare no competing financial interest.

#### Author contributions

J.W., M.S. and T.S., conceptualization; J.W. and M.S., investigation; J.W., writing (original draft); T.S., writing (review and editing); J.W., visualization; T.S., supervision.

#### Acknowledgments

We would like to thank Martin Neuenfeldt for giving advice on cloning and Dr Anja Hagenau for providing the cDNA library of mussel foot tissue. Jia Wang thanks the China Scholarship Council (CSC, 201406630012) for awarding a fellowship for carrying out her PhD in Germany in the lab of Prof. Dr. Thomas Scheibel.

[The raw/processed data required to reproduce these findings cannot be shared at this time as the data also forms part of an ongoing study.]

#### Appendix A. Supplementary material

Supplementary data to this article can be found online at <https://doi.org/10.1016/j.eurpolymj.2019.01.069>.

Extended experimental section, Degenerated primers used for PCR amplifications of a potential PPOL (Table S1); Primers used for plasmid construction (Table S2); Modification of cysteine residues in rPPOL and rP319 (Table S3); Radical scavenging of rPPOL variants using DPPH assay at pH 8.0 (Table S4); Complete cDNA sequence and translated protein sequence of PPOL from *M. galloprovincialis* (Fig. S1); Amino acid sequence alignment of PPOL (Mg\_PPOL) and tyrosinase 2 from *Perna viridis* (PV\_Tyr2) (Fig. S2); Homology-based structural fit of the putative PPOL from *M. galloprovincialis* (Fig. S3); Vis-spectroscopy characterization of tyrosinase activity of rPPOL variants (Fig. S4); Catecholate activity of rPPOL variants at pH 8.0 (Fig. S5); Absorption spectra of Zincon- $\text{Cu}^{2+}$  (Fig. S6); Time course experiments of DPPH (100  $\mu\text{M}$ ) radical reduction in the presence of different concentrations of rPPOL and rP319 at pH 3.0 (Fig. S7).

## References

- [1] J.H. Waite, Nature's underwater adhesive specialist, *Int. J. Adhes. Adhes.* 7 (1) (1987) 9–14.
- [2] H.G. Silverman, F.F. Roberto, Understanding marine mussel adhesion, *Mar. Biotechnol.* 9 (6) (2007) 661–681.
- [3] J.H. Waite, Mussel adhesion-essential footwork, *J. Exp. Biol.* 220 (4) (2017) 517–530.
- [4] H. Lee, N.F. Scherer, P.B. Messersmith, Single-molecule mechanics of mussel adhesion, *Proc. Natl. Acad. Sci. USA* 103 (35) (2006) 12999–13003.
- [5] A. Hagenau, M.H. Suhre, T.R. Scheibel, Nature as a blueprint for polymer material concepts: protein fiber-reinforced composites as holdfasts of mussels, *Prog. Polym. Sci.* 39 (8) (2014) 1564–1583.
- [6] J. Wang, T. Scheibel, Recombinant production of mussel byssus inspired proteins, *Biotechnol. J.* 13 (2018) 1800146.
- [7] J. Yu, W. Wei, E. Danner, J.N. Israelachvili, J.H. Waite, Effects of interfacial redox in mussel adhesive protein films on mica, *Adv. Mater.* 23 (20) (2011) 2362–2366.
- [8] J. Yu, W. Wei, E. Danner, R.K. Ashley, J.N. Israelachvili, J.H. Waite, Mussel protein adhesion depends on interprotein thiol-mediated redox modulation, *Nat. Chem. Biol.* 7 (9) (2011) 588.
- [9] N.R. Martinez Rodriguez, S. Das, Y. Kaufman, J.N. Israelachvili, J.H. Waite, Interfacial pH during mussel adhesive plaque formation, *Biofouling* 31 (2) (2015) 221–227.
- [10] S.C. Nicklisch, J.E. Spahn, H. Zhou, C.M. Gruian, J.H. Waite, Redox capacity of an extracellular matrix protein associated with adhesion in *Mytilus californianus*, *Biochemistry* 55 (13) (2016) 2022–2030.
- [11] L.M. Rzepecki, T. Nagafuchi, J.H. Waite,  $\alpha$ ,  $\beta$ -Dehydro-3, 4-dihydroxyphenylalanine derivatives: potential sclerotization intermediates in natural composite materials, *Arch. Biochem. Biophys.* 285 (1) (1991) 17–26.
- [12] R. Mirshafian, W. Wei, J.N. Israelachvili, J.H. Waite,  $\alpha$ ,  $\beta$ -Dehydro-Dopa: a hidden participant in mussel adhesion, *Biochemistry* 55 (5) (2016) 743–750.
- [13] H. Zhao, J.H. Waite, Linking adhesive and structural proteins in the attachment plaque of *Mytilus californianus*, *J. Biol. Chem.* 281 (36) (2006) 26150–26158.
- [14] V.V. Papov, T.V. Diamond, K. Biemann, J.H. Waite, Hydroxyarginine-containing polyphenolic proteins in the adhesive plaques of the marine mussel *Mytilus edulis*, *J. Biol. Chem.* 270 (34) (1995) 20183–20192.
- [15] S.C. Nicklisch, S. Das, N.R. Martinez Rodriguez, J.H. Waite, J.N. Israelachvili, Antioxidant efficacy and adhesion rescue by a recombinant mussel foot protein-6, *Biotechnol. Prog.* 29 (6) (2013) 1587–1593.
- [16] A. Hagenau, Analyse der Struktur-Funktionsbeziehungen natürlicher Muschelbyssusfäden der Miesmuschel *Mytilus galloprovincialis* [Dissertation], Lehrstuhl Biotechnologie, TU München, Germany, 2011.
- [17] C. Zhang, L. Xie, J. Huang, L. Chen, R. Zhang, A novel putative tyrosinase involved in periostracum formation from the pearl oyster (*Pinctada fucata*), *Biochem. Biophys. Res. Commun.* 342 (2) (2006) 632–639.
- [18] P. Venier, C. De Pittà, F. Bernante, L. Varotto, B. De Nardi, G. Bovo, P. Roch, B. Novoa, A. Figueras, A. Pallavicini, G. Lanfranchi, MytiBase: a knowledgebase of mussel (*M. galloprovincialis*) transcribed sequences, *BMC Genom.* 10 (1) (2009) 72.
- [19] M. Suhre, Struktur-/Funktionsbeziehung rekombinant hergestellter Proteine aus dem Byssusfaden der Miesmuschel *Mytilus galloprovincialis* [DSci Dissertation], Universität Bayreuth, Germany, Lehrstuhl Biomaterialien, 2013.
- [20] J.T. Vivian, P.R. Callis, Mechanisms of tryptophan fluorescence shifts in proteins, *Biophys. J.* 80 (5) (2001) 2093–2109.
- [21] C.A. Royer, Probing protein folding and conformational transitions with fluorescence, *Chem. Rev.* 106 (5) (2006) 1769–1784.
- [22] F. García-Cánovas, F. García-Carmona, J. Vera-Sánchez, J.L. Iborra-Pastor, J.A. Lozano-Teruel, The role of pH in the melanin biosynthesis pathway, *J. Biol. Chem.* 257 (1982) 8738–8744.
- [23] D.G. Graham, P.W. Jeffs, The role of 2,4,5-trihydroxyphenylalanine in melanin biosynthesis, *J. Biol. Chem.* 252 (1977) 5729–5734.
- [24] L.M. Rzepecki, J.H. Waite,  $\alpha$ ,  $\beta$ -Dehydro-3,4-dihydroxyphenylalanine derivatives: rate and mechanism of formation, *Arch. Biochem. Biophys.* 285 (1) (1991) 27–36.
- [25] J.R. Winther, C. Thorpe, Quantification of thiols and disulfides, *Biochim. Biophys. Acta, Gen. Subj.* 1840 (2) (2014) 838–846.
- [26] J.F. Riordan, B.L. Vallee, [36] Reactions with N-ethylmaleimide and p-mercuribenzoate, *Methods Enzymol.* 25 (1972) 449–456.
- [27] G.L. Ellman, Tissue sulfhydryl groups, *Arch. Biochem. Biophys.* 82 (1) (1959) 70–77.
- [28] M.S. Blois, Antioxidant determinations by the use of a stable free radical, *Nature* 181 (4617) (1958) 1199–1200.
- [29] S.C. Nicklisch, J.H. Waite, Optimized DPPH assay in a detergent-based buffer system for measuring antioxidant activity of proteins, *MethodsX* 1 (2014) 233–238.
- [30] J.D. Bendtsen, H. Nielsen, G.V. Hejlskov, S. Brunak, Improved, prediction of signal peptides: signalp 3.0, *J. Mol. Biol.* 340 (4) (2004) 783–795.
- [31] P.A. Guerette, S. Hoon, Y. Seow, M. Raida, A. Masic, F.T. Wong, V.H.B. Ho, K.W. Kong, M.C. Demirel, A. Pena-Francesch, S. Amini, G.Z. Tay, D. Ding, A. Miserez, Accelerating the design of biomimetic materials by integrating RNA-seq with proteomics and materials science, *Nat. Biotechnol.* 31 (10) (2013) 908–915.
- [32] D.G. DeMartini, J.M. Errico, S. Sjoestrom, A. Fenster, J.H. Waite, A cohort of new adhesive proteins identified from transcriptomic analysis of mussel foot glands, *J. R. Soc. Interface* 14 (2017) 20170151.
- [33] C.E. Säbel, J.M. Neureuther, S. Siemann, A spectrophotometric method for the determination of zinc, copper, and cobalt ions in metalloproteins using Zincon, *Anal. Biochem.* 397 (2010) 218–226.
- [34] Y. Matoba, N. Bando, K. Oda, M. Noda, F. Higashikawa, T. Kumagai, M. Sugiyama, A molecular mechanism for copper transportation to tyrosinase that is assisted by a metallochaperone, caddie, *J. Biol. Chem.* 286 (34) (2011) 30219–30231.
- [35] N. Liu, T. Zhang, Y. Wang, Y. Huang, J. Ou, P. Shen, A heat inducible tyrosinase with distinct properties from *Bacillus thuringiensis*, *Lett. Appl. Microbiol.* 39 (5) (2004) 407–412.
- [36] E. Selinheimo, M. Saloheimo, E. Ahola, A. Westerholm-Parvinen, N. Kalkkinen, J. Buchert, K. Kruus, Production and characterization of a secreted, C-terminally processed tyrosinase from the filamentous fungus *Trichoderma reesei*, *FEBS J.* 273 (18) (2006) 4322–4335.
- [37] M. Fairhead, L. Thöny-Meyer, Role of the C-terminal extension in a bacterial tyrosinase, *FEBS J.* 277 (9) (2010) 2083–2095.
- [38] W. Brand-Williams, M.E. Cuvelier, C. Berset, Use of a free radical method to evaluate antioxidant activity, *LWT-Food Sci. Technol.* 28 (1) (1995) 25–30.
- [39] S.M. Deneke, Thiol-based antioxidants, *Curr. Top. Cell. Regul.* 36 (2001) 151–180.
- [40] W. Wei, Y. Tan, N.R. Martinez Rodriguez, J. Yu, J.N. Israelachvili, J.H. Waite, A mussel-derived one component adhesive coacervate, *Acta Biomater.* 10 (4) (2014) 1663–1670.
- [41] J. Wang, T. Scheibel, Coacervation of the recombinant *Mytilus galloprovincialis* foot protein-3b, *Biomacromolecules* 19 (9) (2018) 3612–3619.

***A mussel polyphenol oxidase-like protein shows thiol-mediated antioxidant activity***

*European Polymer Journal* 2019, 113, 305–312

DOI: 10.1016/j.europolymj.2019.01.069

Jia Wang<sup>a</sup>, Michael H. Suhre<sup>a,1</sup>, Thomas Scheibel<sup>a,b,c,d,e,f,\*</sup>

<sup>a</sup>Lehrstuhl Biomaterialien, <sup>b</sup>Forschungszentrum für Bio-Makromoleküle (BIOmac), <sup>c</sup>Bayreuther Zentrum für Kolloide und Grenzflächen (BZKG), <sup>d</sup>Bayreuther Materialzentrum (BayMat), <sup>e</sup>Bayreuther Zentrum für Molekulare Biowissenschaften (BZMB), <sup>f</sup>Bayrisches Polymerinstitut (BPI), Universität Bayreuth, 95440 Bayreuth, Germany

<sup>1</sup>Present address: GmbH, AmKlopferspitz 19 im IZB, D-82152 Planegg, München, Germany.

**Table S1.** Degenerated primers used for PCR amplifications of a potential PPOL [1].

Name	Sequence (5' - 3')	Origin and aimed sequence	Result
CuA_65536	ARGWAYNSNCKRTGCCANCCNARRA	alignment of nine different tyrosinase sequences  CuA,WHR-motive	no PCR product
CuA_2048	AGGWAYWCYCKATGCCAYCCWARRAWRCT	<i>P. fucata</i> tyrosinase Sequence (GenBank AAZ66340, BAF74507)  CuA,WHR-motive	multiple PCR products with wrong sequences
CuA_1536	ARRAANACYCTRTRGCCAWCCHARRAT	<i>P. fucata</i> tyrosinase sequence (GenBank AAZ66340, BAF74507)  CuA,WHR-motive	multiple PCR products with wrong sequences
CuA_1024	CCTGGRAGRWAATCWAWSGTSGARTCCCARTRCA	<i>P. fucata</i> tyrosinase (GenBank AAZ66340, BAF74507)  CuA, conserved upstream region of WHR-motive	no PCR product
<b>CuA_128</b>	<b>GRMCCSWSRTGMGCGT</b>	<b><i>P. fucata</i> tyrosinase</b>  <b>CuA, conserved downstream region of WHR-motive</b>	<b>two defined PCR bands (see text)</b>
CuB_36863	TGRTGVARMHWRAQANANNGGRTC	alignment of nine different tyrosinase sequences  CuB, region of the third histidine residue	no PCR product
CuB_576	TGRTGRAADGTRAAHARRGGRTC	<i>P. fucata</i> tyrosinase sequence (GenBank AAZ66340, BAF74507)  CuB, region of the third histidine residue	no PCR product
CuB_128	ATGRTGRAAAWAGAAWASWGGRTC	<i>P. fucata</i> tyrosinase sequence (GenBank AAZ66340, BAF74507)  CuB, region of the third histidine residue	multiple PCR products with wrong sequences

The degeneration degree of each primer is included in the names of oligonucleotides. The third histidine residue of the CuA binding site in all known type 3 copper proteins comprises the Trp-His-Arg tripeptide (WHR).

**Table S2.** Primers used for plasmid construction.

PCR amplification		Primer	Sequence (5' - 3')
Outcome	Template		
pET-sumo-PPOL	pGEM-PPOL	PPOL_Bam_fwd	ATAATGGATCCGATGTCATAACTGACCAGTATCCTGC
		PPOL_Not_rev	TAATTGCGGCCGCTTAATAGCAAAGGAACGCC
pET28a-His-PPOL	pGEM-PPOL	PPOL_Nhe_fwd	ATAATGCTAGCGATGTCATAACTGACCAGTATCCTGC
		PPOL_Not_rev	TAATTGCGGCCGCTTAATAGCAAAGGAACGCC
pET-sumo-P319	pET-sumo-PPOL	PPOL_Nco_fwd	TAAGAAGGAGATATACCATGGGCAGCAG
		P319_Xho_rev	ATCGCTCGAGTTATTAATCACCATATGAAT
pET28a-His-P319	pET28a-His-PPOL	PPOL_Nco_fwd	TAAGAAGGAGATATACCATGGGCAGCAG
		P319_Xho_rev	ATCGCTCGAGTTATTAATCACCATATGAAT

**Table S3.** Modification of cysteine residues in rPPOL and rP319.

		rPPOL	rPPOL-NEM	rP319	rP319-NEM
Molar concentration ( $\mu$ M)	Protein	92.1	92.1	92.1	92.1
	Free thiols detected	1230 $\pm$ 12.2	105 $\pm$ 2.33	374 $\pm$ 8.28	63.5 $\pm$ 0.45
Numbers of different cysteine derivatives per protein molecule	Free thiols ( free thiols moles / protein moles)	~ 13	~ 1	~ 3	~ 1
	Cystine (disulfide bond)	1	1	1	1
	Alkylated cysteine	~ 0	~ 12	~ 0	~ 2

Cysteine residues of rPPOL, rP319 and alkylated rPPOL-NEM, rP319-NEM are shown in molarity (M) and number. Measurements are means  $\pm$  standard deviation (n = 3).

**Table S4.** Radical scavenging of rPPOL variants using DPPH assay at pH 8.0.

	% of remaining DPPH radical		
	1 min	15 min	60 min
rPPOL	90.31 $\pm$ 1.33	85.91 $\pm$ 0.44	85.11 $\pm$ 0.27
rP319	95.4 $\pm$ 0.56	93.74 $\pm$ 0.28	91.99 $\pm$ 0.1

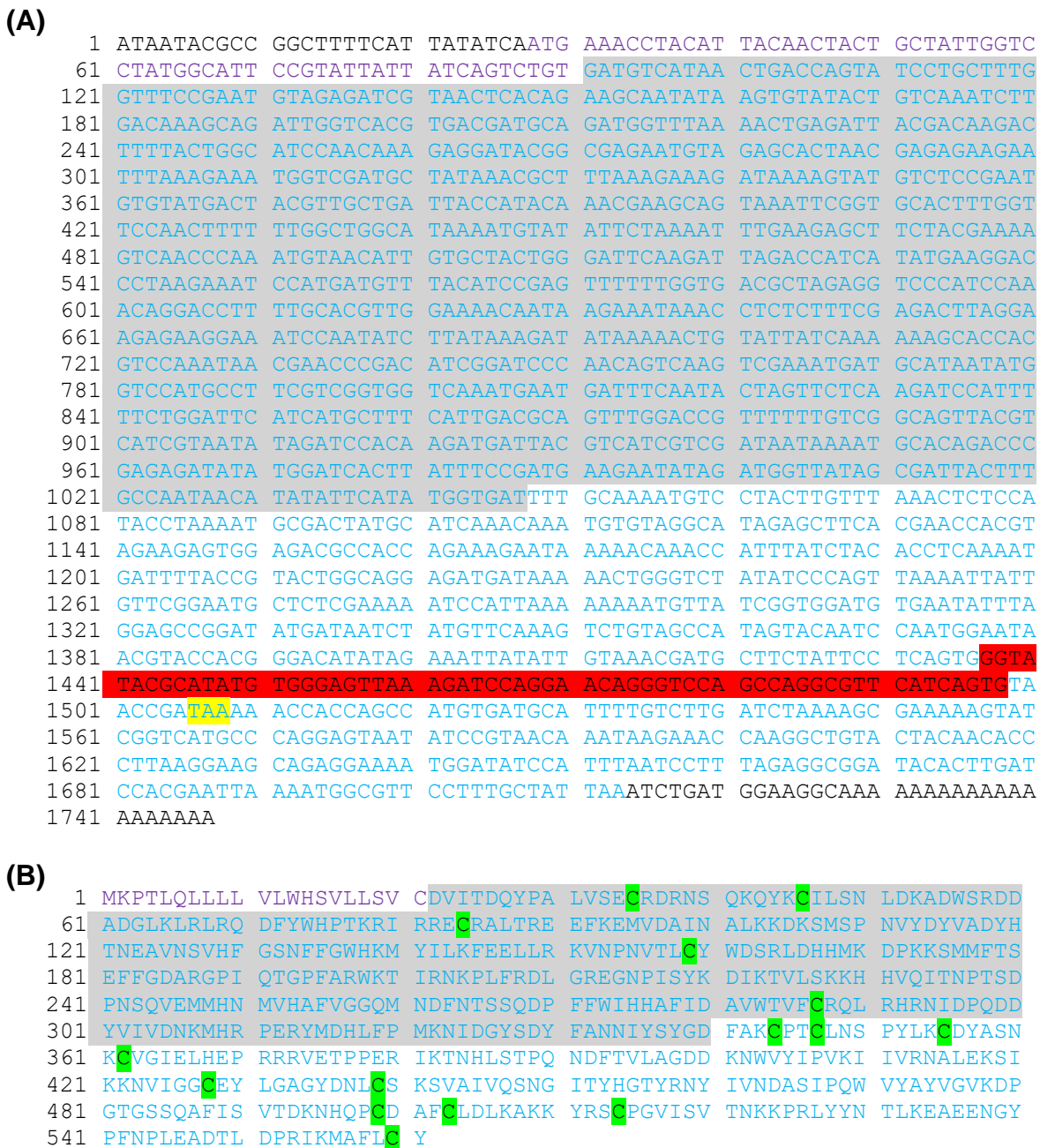


**Figure S1.** (A) Complete cDNA sequence of PPOL from *M. galloprovincialis* [1]. The 5' and 3' untranslated regions are shown in black, the deleted sequence in the Pf-approach is indicated by a red shading and the corresponding artificial stop codon, which results in premature chain termination, is highlighted by yellow shading. The 5' terminal purple sequence is responsible for signal peptide translation (SignalP 3.0 Server, neuronal network method), the full-length PPOL cDNA sequence used for plasmid construction is shown in blue, and the short sequence construct is indicated by grey shading. (B) Translated protein sequence of PPOL. The corresponding signal peptide, full-length and short sequence of PPOL are shown in purple, blue and grey shading, respectively. The cysteine residues are highlighted by green shading.



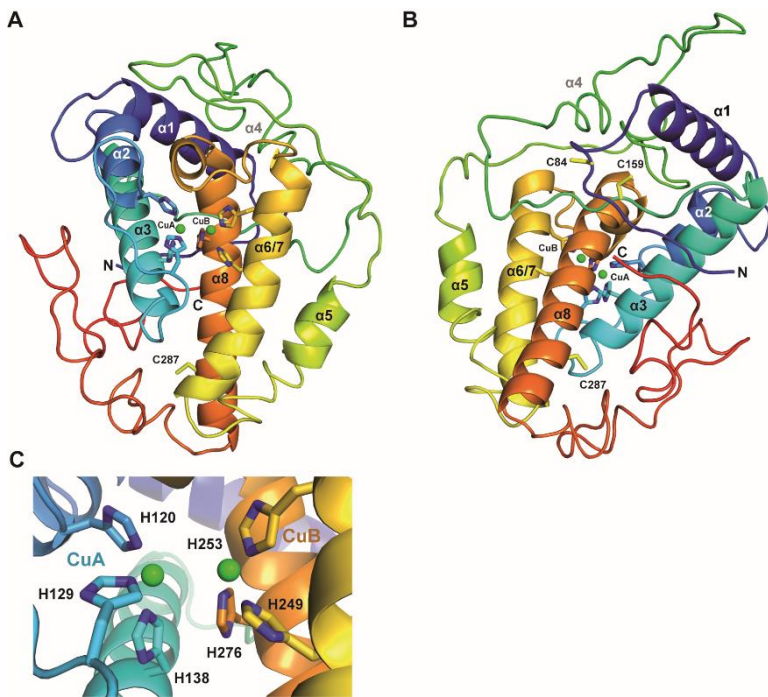


**Figure S3.** Homology-based structural model of the putative PPOL from *M. galloprovincialis* [1]. Homology model of the catalytic domain of PPOL obtained from Phyre<sup>2</sup> in (A) front and (B) rear view, based on the high sequence homology with four known crystal structures. Blue: amino terminus; Red: carboxyl terminus. The numbering of  $\alpha$ -helices is indicated by the established PPO crystal structure [3]. Helix 4 (gray letter) is missing and helices 6 and 7 are united here. Both modeled copper ions are represented as green spheres. Six histidine residues (H) and three cysteine residues located in the catalytic domain are shown as a stick model. (C) Detailed view of the potential copper binding site with six histidine residues (H) annotated. The established crystal structures or SCOP entries of PPO used here were tyrosinase from *Bacillus megaterium* (PDB ID 3NPY) and *Streptomyces castaneoglobisporus* (PDB ID 1wx2), hemocyanin from *Octopus dofleini* (PDB ID 1JS8) and *Rapana thomasiana* (PDB ID 1LNL).

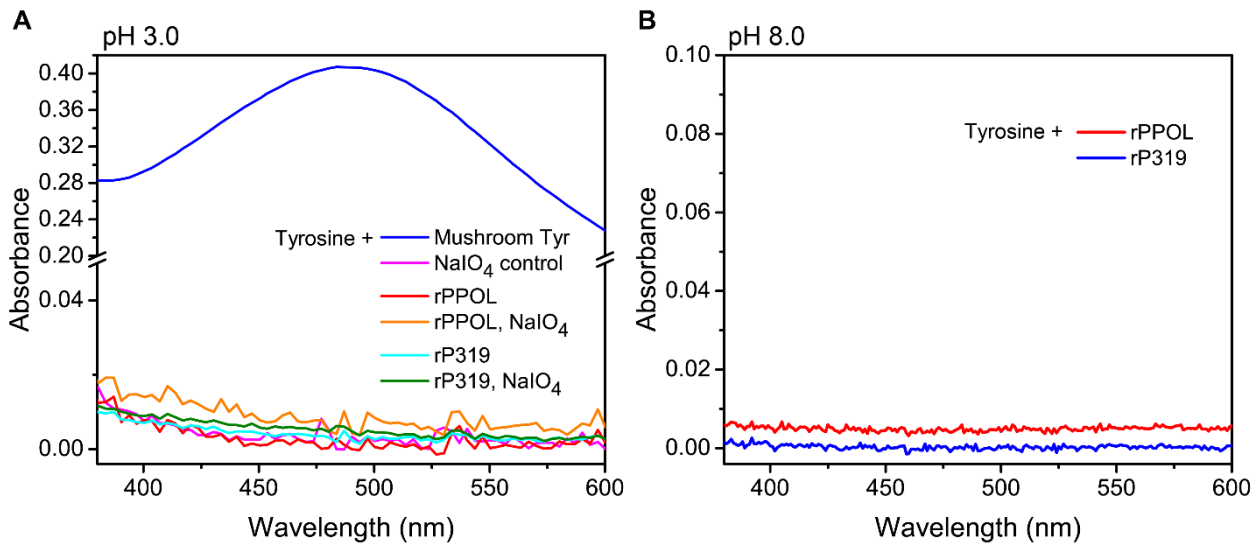


**Figure S4.** Tyrosinase activity of rPPOL variants. Vis absorption of rPPOL as well as rP319 using L-tyrosine as substrate upon 30 min incubation at pH 3.0 (A) and pH 8.0 (B). The samples with mushroom tyrosinase (Tyr, at pH 7.0) and NaIO<sub>4</sub> were taken as controls with tyrosinase activity and chemical oxidation ability, respectively.

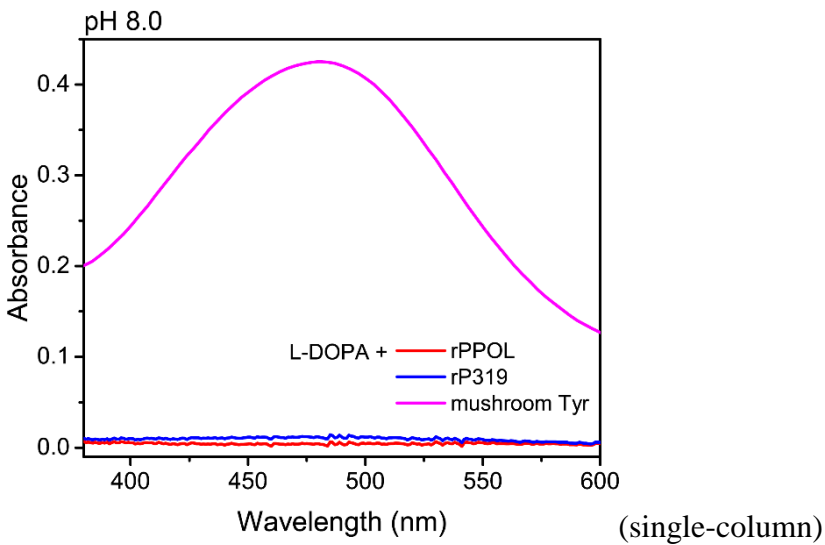


**Figure S5.** Catecholase activity of rPPOL variants at pH 8.0. Vis absorption of L-DOPA in the presence of rPPOL as well as rP319 after 30 min incubation. L-DOPA with mushroom tyrosinase (Tyr) was taken as positive control.

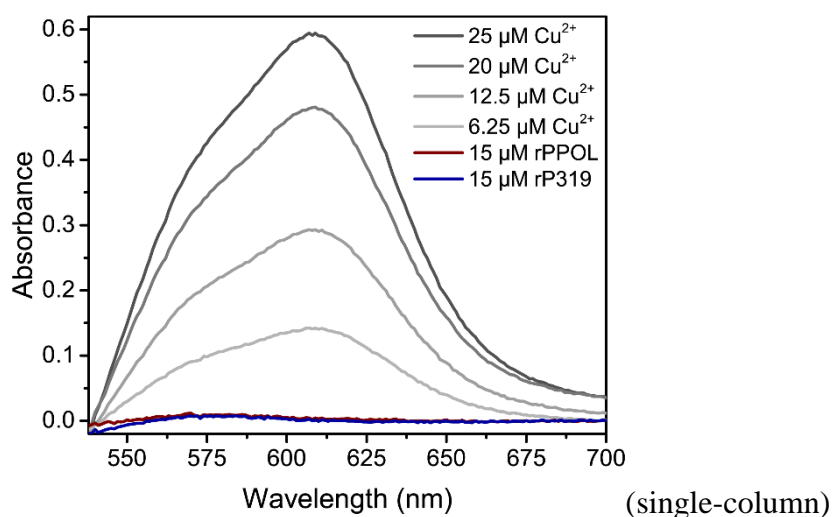


**Figure S6.** Absorption spectra of Zincon-Cu<sup>2+</sup>. All spectra were recorded in 8 M urea, 50 mM borate buffer (pH 9.0), 40 μM Zincon (2-Carboxy-2-hydroxy-5-sulfoformazylbenzene) and different concentrations of Cu<sup>2+</sup> at 20 °C [4]. The Zincon-Cu<sup>2+</sup> complex showed  $\lambda_{\text{max}}$  at 610 nm ( $\epsilon_{\text{max}} = 23,640 \text{ M}^{-1}\text{cm}^{-1}$ ). rPPOL and rP319 at a concentration of 15 μM were able to bind 30 μM Cu<sup>2+</sup> in theory, which was in the range of the detection.

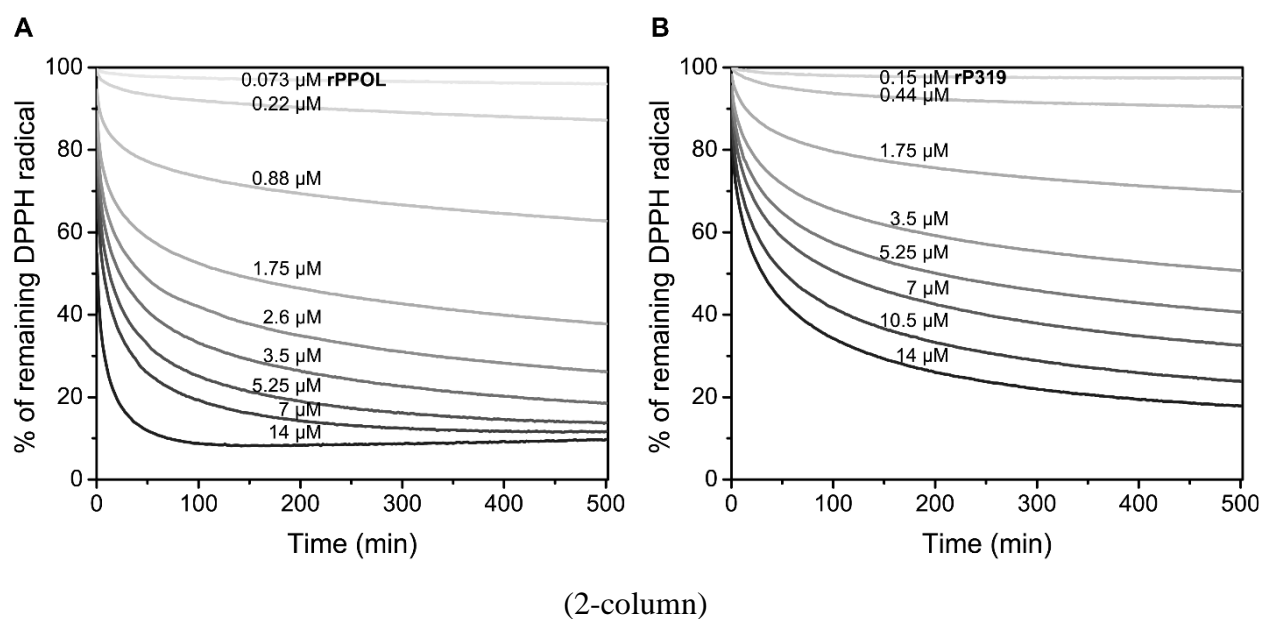


**Figure S7.** Time course of DPPH (100 μM) radical reduction in the presence of different concentrations of rPPOL (A) and rP319 (B) at pH 3.0.

## References

- [1] M. Suhre. Struktur-/Funktionsbeziehung rekombinant hergestellter Proteine aus dem Bysusfaden der Miesmuschel *Mytilus galloprovincialis* [DSci Dissertation], Lehrstuhl Biomaterialien, Universität Bayreuth, Germany (2013) 210 pp.
- [2] P.A. Guerette, S. Hoon, Y. Seow, M. Raida, A. Masic, F.T. Wong, V.H.B. Ho, K. W. Kong, M. C. Demirel, A. Pena-Francesch, S. Amini, G.Z. Tay, D. Ding, A. Miserez, Accelerating the design of biomimetic materials by integrating RNA-seq with proteomics and materials science, *Nat. Biotechnol.* 31 (10) (2013) 908-915.
- [3] M. Sendovski, M. Kanteev, V.S. Ben-Yosef, N. Adir, A. Fishman, First structures of an active bacterial tyrosinase reveal copper plasticity, *J. Mol. Biol.* 405 (1) (2011) 227-237.
- [4] C.E. Säbel, J.M. Neureuther, S. Siemann, A spectrophotometric method for the determination of zinc, copper, and cobalt ions in metalloproteins using Zincon, *Anal. Biochem.* 397 (2010) 218-226.

## Acknowledgements

First and foremost, I would like to thank my supervisor Prof. Dr. Thomas Scheibel for taking me as a PhD student in the fantastic Fiberlab as well as the opportunity to work on such a great and interesting project. I enjoy the tremendous benefit of his excellent supervision throughout the topic selection, resolution of research problems, result analyses, academic presentation & writing skills and so on, which is valuable in my future career.

Many thanks to Prof. Dr. Ruth Freitag and Prof. Dr. Hans-Werner Schmidt, who agreed to be my mentors. I will cherish their great guidance. I would also like to thank my PhD committee members Prof. Dr. Thomas Scheibel, Prof. Dr. Dirk Schüler, Prof. Dr. Birte Höcker and Prof. Dr. Schmidt, who gave me valuable advice at key milestones.

I gratefully acknowledge the scholarship from China Scholarship Council (CSC) and the following one-year scholarship from University of Bayreuth. Thanks to Prof. Dr. Thomas Scheibel and my former supervisor Prof. Dr. Qing Meng during master study for their input in supporting me to get the scholarship.

I appreciate so much to work with so many lovely colleagues here. We have really spend great and fun-loving time, which is a priceless memory. The open discussions no matter in seminar or anywhere else broadened my horizon and promoted the process on my project. I greatly appreciate the assist from the technical assistants as well as the secretaries, who supported the lab and office work nicely every day. Especially Johannes Diehl and Andreas Schmidt helped me for the quiet frequent fermentation: thank you for your helpful hand. A special thanks to Dr. Martin Humenik, Dr. Martin Neuenfeldt and Dr. Joschka Bauer, who helped me a lot at the beginning to get into my topic. Great thanks to my senior and cooperation partner Dr. Michael H. Suhre for great job and I can therefore continue his work. Thanks Dr. Hendrik Bargel and Claudia Stemmann for the perfect SEM images and Andreas Schmidt for the execution of MALDI-TOF analyses.

I would also like to thank my office-mates, both those from the past and the current, Dr. Joschka Bauer, Dr. Christopher Thamm, Dr. Christian B. Borkner, Heike Herold, Tamara Aigner, Dr. Sushma Kumari, and Carolin Grill. Besides scientific part, we also made a lot of fun in office in spare time, which relaxed the stressful laboratory work. An especially thanks to Dr. Sushma Kumari for helping me solving my experimental problems and many academic issues.

Last but not least, I would like to sincerely thank my family and friends, who always encourage me to realize my dreams. Without their moral support and encouraging, I could never finish my PhD study.

## **(Eidesstattliche) Versicherungen und Erklärungen**

(§ 9 Satz 2 Nr. 3 PromO BayNAT)

*Hiermit versichere ich eidesstattlich, dass ich die Arbeit selbstständig verfasst und keine anderen als die von mir angegebenen Quellen und Hilfsmittel benutzt habe (vgl. Art. 64 Abs. 1 Satz 6 BayHSchG).*

(§ 9 Satz 2 Nr. 3 PromO BayNAT)

*Hiermit erkläre ich, dass ich die Dissertation nicht bereits zur Erlangung eines akademischen Grades eingereicht habe und dass ich nicht bereits diese oder eine gleichartige Doktorprüfung endgültig nicht bestanden habe.*

(§ 9 Satz 2 Nr. 4 PromO BayNAT)

*Hiermit erkläre ich, dass ich Hilfe von gewerblichen Promotionsberatern bzw. -vermittlern oder ähnlichen Dienstleistern weder bisher in Anspruch genommen habe noch künftig in Anspruch nehmen werde.*

(§ 9 Satz 2 Nr. 7 PromO BayNAT)

*Hiermit erkläre ich mein Einverständnis, dass die elektronische Fassung meiner Dissertation unter Wahrung meiner Urheberrechte und des Datenschutzes einer gesonderten Überprüfung unterzogen werden kann.*

(§ 9 Satz 2 Nr. 8 PromO BayNAT)

*Hiermit erkläre ich mein Einverständnis, dass bei Verdacht wissenschaftlichen Fehlverhaltens Ermittlungen durch universitätsinterne Organe der wissenschaftlichen Selbstkontrolle stattfinden können.*

Bayreuth, 10.02.2020, \_\_\_\_\_

Ort, Datum, Unterschrift